Exotic Seismic Sources: Nearly Identically Repeating Events and

Non-Double-Couple Earthquakes

by

Dennise Christine Templeton

B.A. (Rice University) 1999

M.S. (University of California, Berkeley) 2004

A dissertation submitted in partial satisfaction of the

requirements for the degree of

Doctor of Philosophy

in

Geophysics

in the

Graduate Division

of the

University of California, Berkeley

Committee in charge:

Professor Roland Bürgmann, Chair
Professor Douglas Dreger
Professor Steven Glaser

Spring 2007

The dissertation of Dennise Christine Templeton is approved:

Chair   _____   Date   _____

             _____   Date   _____

             _____   Date   _____

University of California, Berkeley

Spring 2007

Exotic Seismic Sources: Nearly Identically Repeating Events and

Non-Double-Couple Earthquakes

Abstract

Exotic Seismic Sources: Nearly Identically Repeating Events and
Non-Double-Couple Earthquakes

by

Dennise Christine Templeton

Doctor of Philosophy in Geophysics

University of California, Berkeley

Professor Roland Bürgmann, Chair

This dissertation investigates two exotic seismic sources: non-double-couple
earthquakes and nearly identically repeating events. Using non-double-couple
earthquakes, I aim to better understand the connection between earthquake production
and geothermal/magmatic systems. I focus on a 100-km-wide circular area centered at
the Long Valley caldera and comprehensively search for events greater than M3.5
since 1993 with significant coseismic volume changes. Using three-component
broadband digital waveforms at regional distances, I solve for four different source
models: DC, deviatoric (DC+CLVD), DC+isotropic, and full moment tensor
(DC+CLVD+isotropic). Using the F test as a statistical aid, the best model is
determined for each event. I then conduct stability tests to determine the robustness of

the focal mechanism solutions and isotropic components. The results show that fluid-influenced earthquakes in the magnitude range studied are quite rare in the Long Valley volcanic region. Of 33 high quality events, 28 are best characterized by a simple DC source model, four by a DC+isotropic source model, and one by a full moment tensor model.

Nearly identically repeating events, or repeating earthquakes (REs), are sequences of events that have nearly identical waveforms and are interpreted to represent fault asperities driven to failure by loading from aseismic creep on the surrounding fault surface at depth. REs are identified using a combination of cross-correlation and spectral coherence techniques. I investigate the location of these REs along faults in central California to determine which faults exhibit creep and to examine the spatio-temporal distribution of this creep.

Between March 1984 and May 2005, I investigate the occurrence of REs at both the juncture of the San Andreas and southern Calaveras-Paicines faults and west of the creeping section of the San Andreas fault within the Coast Range. REs in these areas reflect a heterogeneous creep distribution along the fault plane with significant variations in time. Creep at depth appears to mimic the behaviors seen of creep on the surface in that evidence of steady slip, triggered slip, and episodic slip phenomena are also observed in the RE sequences. Additionally, REs are sometimes observed to occur in bursts, suggesting that these REs are not produced by steady aseismic creep of the surrounding fault surface.

I also investigate RE sequences on the central Calaveras fault to investigate postseismic deformation after the 1984 M6.2 Morgan Hill earthquake. Both the

accelerated slip transients due to the earthquake as well as the return to interseismic background creep rates can be imaged from our dataset. A comparison between the regions of the fault that ruptured coseismically and the locations of the REs show that the REs preferentially occur in areas adjacent to the coseismic rupture. A mechanical forward model of the subsurface slip distribution 6 months after the mainshock is compared with the observed surface electronic distance meter (EDM) line length changes between stations near the Morgan Hill rupture area. Our modeling shows that RE data consistently underpredict the observed line-length changes, possibly due to the lack of REs, and thus RE-derived slip information, below the seismogenic zone and within the velocity strengthening portions of the fault.

_____

Professor Roland Bürgmann

Dissertation Committee Chair

To my husband.

Table of Contents

Acknowledgments

This dissertation would not have been possible without the aid and guidance of my advisors Roland Bürgmann and Douglas Dreger. Thank you for your support and for sharing in my enthusiasm for seismology and geodesy. I would also like to thank Bob Nadeau for sharing his knowledge and time, and for being my unofficial third advisor. I would like to thank Steven Glaser for being a member of my dissertation committee and for reading the manuscripts. Many thanks to the BSL students, faculty, and administrative staff, both current and former, for their help throughout the years.

Finally, I would like to thank my husband and parents for supporting me and for standing by me throughout these years from beginning to end. You are truly wonderful.

Chapter 1

Introduction

In this dissertation, I investigate two naturally occurring exotic seismic sources to better understand the tectonic environment that they are found in. Specifically, I use non-double-couple events as an indicator of fluid influenced faulting in geothermal and magmatic systems and nearly identically repeating earthquakes to determine creep at depth.

In Chapter 2, I search for non-double-couple (non-DC) earthquakes greater than M3.5 in the Long Valley volcanic region to better understand the connection between volumetric earthquakes and fluid flow at depth. Non-DC earthquakes can be characterized using compensated-linear-vector-dipole (CLVD) components, which suggest either fluid flow or complex shear failure as the faulting mechanism, and/or isotropic components, which describe volume changes in the source region. Using three-component broadband digital waveforms at regional distances, I solve for four different source models: DC, deviatoric (DC+CLVD), DC+isotropic, and full moment tensor (DC+CLVD+isotropic). Using the F test as a statistical aid, I determine which of the four models is most appropriate for each event. Stability tests are then

conducted to determine the robustness of the focal mechanism solutions and isotropic components. The results show that fluid-influenced earthquakes in the magnitude range studied are quite rare in the Long Valley volcanic region. Of 33 high quality events, 28 are best characterized by a simple DC source model, four by a DC+isotropic source model, and one by a full moment tensor model. The small number of non-DC events in this magnitude range is surprising and may indicate an inability of individual high-pressure reservoirs to sustain pressurization for events of this size during the faulting process as the crack or fault grows larger.

In Chapter 3, I investigate the occurrence of repeating earthquakes (REs) along faults in central California to determine which faults exhibit creep and the spatio-temporal distribution of this creep. REs are sequences of events that have nearly identical waveforms and are interpreted to represent fault asperities driven to failure by loading from aseismic creep on the surrounding fault surface at depth. At the juncture of the San Andreas and southern Calaveras-Paicines faults, both faults as well as a smaller secondary fault, the Quien Sabe fault zone, are observed to produce REs over the observation period of March 1984 – May 2005. REs in this area reflect a heterogeneous creep distribution along the fault plane with significant variations in time. Cumulative slip over the observation period at individual sequence locations is determined to range from 5.5 – 58.2 cm on the San Andreas fault, 4.8 – 14.1 cm on the southern Calaveras-Paicines fault, and 4.9 – 24.8 cm on the Quien Sabe fault. Creep at depth appears to mimic the behaviors seen of creep on the surface in that evidence of steady slip, triggered slip, and episodic slip phenomena are also observed in the RE sequences. For comparison, we investigate the occurrence of REs west of the San

Andreas fault within the southern Coast Range Salinian block. Events within these RE sequences tend to occur close in time to one another and the sequences themselves were only active for a short period of time. This suggests that REs in this area are not produced by steady aseismic creep of the surrounding fault surface and that creep itself may be hindered in environments where granitic rocks occur on both sides of the fault.

In Chapter 4, I determine slip at repeating earthquake (RE) sequence locations on the central Calaveras fault to investigate postseismic deformation after the 1984 M6.2 Morgan Hill earthquake. REs are identified using a combination of cross-correlation and spectral coherence techniques. Both the accelerated slip transients due to the earthquake as well as the return to interseismic background creep rates can be imaged from the dataset. The slow decrease of slip rates through time over the study area shows that the Morgan Hill earthquake influenced the recurrence times of REs until at least 1989. Forward models are developed using RE-derived subsurface slip distributions at 6 and 18 months after the mainshock which allow us to compare the observed and predicted surface electronic distance meter (EDM) line length changes between stations near the Morgan Hill rupture area. The modeling shows that RE data alone consistently under predict the observed line length changes possibly due to the lack of REs below the rupture zone within the velocity strengthening portions of the fault. These results show that when investigating fault interactions beyond coseismic static stress increases, it is important to consider the effects due to the deeper fault relaxation beneath the seismogenic zone.

Chapter 2

Non-Double-Couple Earthquakes in the Long Valley Volcanic Region

2.1 Introduction

In volcanic areas, deviations from the usual double-couple (DC) model of shear faulting may be able to illuminate a link between the source process of an earthquake and fluids associated with the geothermal or magmatic system. These non-double-couple (non-DC) earthquakes have mechanisms vastly different from simple shear along a linear fault plane and are characterized by a compensated-linear-vector-dipole (CLVD) component, suggesting either fluid involvement or complex shear failure, and/or an isotropic component which describes volume changes in the source region. Many possible physical mechanisms have been proposed to account for these two non-DC components however, the details of these physical source processes are still not well understood (Julian et al., 1998).

Non-DC events with significant volumetric components have been observed in various volcanic and geothermal areas such as The Geysers geothermal area, California, Aso Volcano, Japan, and Mt. Etna and Campi Flegrei, Italy, (Ross et al.,

1999 ; Legrand et al., 2000 ; Saraò et al., 2001 ; Guidarelli et al., 2002). These studies have shown that the percentage of events with isotropic components and the strength of the isotropic component can vary with location. These differences appear to be due to different underlying physical mechanisms. Four non-DC events have also been previously identified in the Long Valley caldera, California (Dreger et al., 2000). In this paper, we consider the Long Valley caldera along with the Mono-Inyo craters and the seismically active Sierra Nevada block to be part of the Long Valley volcanic region located in eastern California within the Sierra Nevada frontal fault system (Figure 2.1).

Since the installation of geophysical monitoring equipment, Long Valley caldera has displayed periods of unrest characterized by increased seismicity, ground deformation, localized increases in volcanic gas emissions and subsurface magma movement. The most recent episode of unrest within the caldera began in 1997 with progressively increasing deformation rates across the resurgent dome followed by an increase in the rate of earthquake production in the south moat of the caldera (Hill et al., 2003). Well water-level changes due to local large earthquakes associated with this swarm have been attributed to the upward migration of high temperature fluids beneath the south moat of the caldera (Roeloffs et al., 2003). Surface deformation within the caldera over this time period has been modeled using two deep magmatic inflation sources, one 6 – 7 km below the resurgent dome and another 10 – 20 km below the south moat of the caldera combined with right-lateral slip on a steeply dipping plane in the south moat (Langbein, 2003). This modeling is consistent with previous seismic studies using S-to-P amplitude ratios, teleseismic P-wave
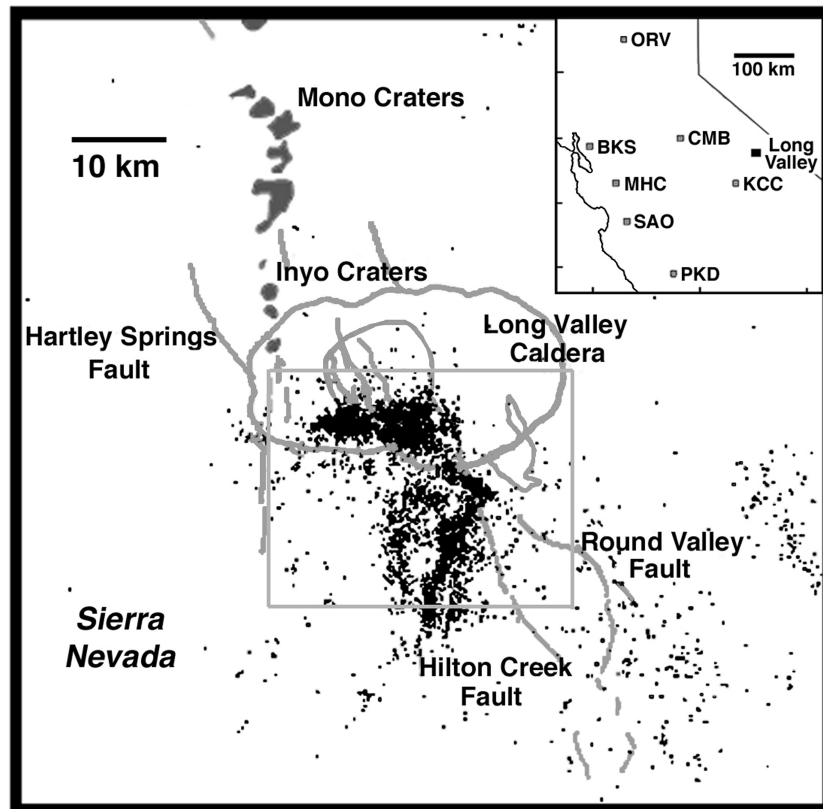
Figure 2.1: Area map showing location of the Long Valley caldera, Mono-Inyo volcanic chain and major Sierra Nevada frontal faults. NCSN catalog seismicity between 1980-2000 shown as small gray dots. Inset map of California shows the distribution of stations used in this study. Rectangle delineates area plotted in Figure 2.2.

polarizations and PS converted waves which have mapped an anomalous region 7-12 km below the resurgent dome indicating a high temperature region containing an area with a significant percentage of melt and the top of the offset central magma body (Steck and Prothero, 1994 ; Sanders and Nixon, 1995). At these depths below the resurgent dome, geologic studies have suggested that this area is congealed magma overlying a partially molten magma chamber contained within the Sierran basement (Bailey, 1989).

Equivocal evidence for fluids has also been identified south of the caldera in the seismically active Sierra Nevada block. Three large events, a M5.8 October 4, 1978 Wheeler Crest earthquake along with two M6 May 1980 events, were best described using a combination of DC and CLVD components (Julian and Sipkin, 1985). Unlike the 1978 event, the 1980 earthquakes were part of a larger earthquake swarm which extended up into the Long Valley caldera. The CLVD components were thought to be due to water or low-viscosity magma involvement in the source process. However, there has been much controversy surrounding this solution since these events can also be modeled using a complex DC source involving multiple rupture planes (Wallace,1985). Unfortunately, the exact source model cannot be resolved with the available data and this controversy continues. Additionally, in August 1998, during a minor earthquake sequence without a clear mainshock, three microearthquakes displayed strikingly harmonic spectral signatures which were hypothesized to have been caused by a magmatic fluid controlled source process (Hough et al., 2000). Possible magma bodies have also been identified in the Sierra Nevada block from early S-wave shadowing studies (Ryall and Ryall, 1984). In contrast to the caldera and the Sierra Nevada block, the Mono-Inyo volcanic chain to the north has exhibited little seismicity even though the most recent volcanic eruption occurred in this region (Sieh, 1984).

In this study, we investigated the source kinematics of events greater than M3.5 occurring between 1993 – 2003 within a 100 km wide circular area centered at the Long Valley caldera to identify events with significant coseismic volume changes. In this active geothermal and magmatic area, we treat coseismic volume changes as an

indicator of fluid involvement at the source. Our results show that events with significant volumetric components in this magnitude range were fairly rare over the observation period. Of 33 high quality events, 28 are best characterized by a simple DC source model and only five have coseismic volume increases.

2.2 Data and Methodology

In this study we solved for four different source models: DC, deviatoric (DC+CLVD), DC+isotropic and the full moment tensor model. In our analysis, the full moment tensor solution is decomposed into deviatoric and volumetric components. The deviatoric portion is then further decomposed into DC and CLVD components by assuming that the same principal stresses produced both components (Minson and Dreger, in prep.), thus allowing for the inclusion of DC, CLVD and volumetric forces in the source process. This model can characterize source processes involving a combination of tensile and shear faulting (Julian et al., 1998). The deviatoric moment tensor solution a priori sets the volumetric component to zero, and solves only for the DC and CLVD components. This model describes volume conserving source processes which deviate from a simple DC mechanism. DC+isotropic source mechanisms have been used to describe combinations of near-simultaneous faulting near an underground explosion source (Massé, 1981 ; Dreger and Woods, 2002). The pure DC model assumes that the earthquake source is best modeled as shear along a linear fault plane and a priori sets the CLVD and volumetric components to zero.

For the DC and DC+isotropic models, a grid search method iterating over strike, dip, rake, DC moment and isotropic moment, which is equal to zero in the pure DC case, was used to find the solution which best fit the observed three-component waveforms bandpass filtered between 0.02 and 0.05 Hz. Since the grid search method finely searched over the entire model space, we feel confident that although the method iterates over non-linear equations it does not suffer from local minima complications such as those common in linearized approaches. For the deviatoric and full moment tensor models, the second rank symmetric seismic moment tensor is solved by linearly inverting complete three-component filtered broadband seismograms in the time domain using a weighted least squares approach. The percent isotropic for these models is determined by dividing the isotropic moment, one-third the trace of the diagonalized moment tensor, by the total moment. The deviation of the source from a DC is determined by $\varepsilon = |\lambda_{min} / \lambda_{max}|$ where λ_{min} and λ_{max} refer to the smallest and largest eigenvalue, in an absolute sense. The percent DC and CLVD of the deviatoric portion of the moment tensor is then $(1 - 2\varepsilon) * 100\%$ and $(2\varepsilon) * 100\%$, respectively. Green's functions for all four models were computed utilizing a frequency wave-number integration method and the SoCal velocity model (Dreger and Helmberger, 1993) for source depths every 3 km between 2 – 17 km. A set of seven Berkeley Digital Seismic Network stations (BKS, CMB, KCC, MHC, ORV, PKD, and SAO) providing the best azimuthal coverage and data quality are used in this investigation. In practice, however, a solution would usually have a subset of these stations depending on station availability and data quality issues.

The variance reduction is the goodness-of-fit parameter between the data and synthetics and is computed using

$$VR = \left(1 - \frac{\int (d-s)^2\, dt}{\int d^2\, dt}\right) * 100\% \qquad (2.1)$$

where d refers to the data and s to the synthetics, with implied time dependence. A variance reduction of 100% would indicate an exact match between the data and synthetics. This measure was used to assess the quality of each of the solutions. Best depths were determined by choosing the solution with the highest variance reduction in the range of possible depths determined by the extensive Northern California Seismic Network.

When testing more complex source models, the variance reduction usually increased with increasing complexity. F test statistics were performed to determine if the additional CLVD and/or volumetric components represented a true aspect of the source mechanism or if they were simply added non-physical parameters in the inversion. To do this we computed the prediction error, e_i,

$$e_i = \left(d_i - s_i\right) \qquad (2.2)$$

where d and s are the data and synthetics at a particular time i, to estimate the variance, σ^2,

$$\sigma^2 = \frac{\sum e_i}{(N-M)} \qquad (2.3)$$

of each model where N and M are the number of observations and model parameters. For the DC, deviatoric, DC+isotropic and full moment tensor (FMT) models there are 4, 5, 5 and 6 independent model parameters, respectively. The number of observations are the number of uncorrelated data points per waveform multiplied by the number of waveforms used in the inversion. For waveforms bandpass filtered between 0.02 and 0.05 Hz, the number of uncorrelated data points for a 200 sec waveform is set to 10 assuming one sample/sec and a 20 sec width for the lowpass filter corner. The F test statistic is determined by taking the ratio of the variances

$$F \ ratio \ 1 = \frac{\sigma^2_{dc}}{\sigma^2_{dev}} \tag{2.4}$$

$$F \ ratio \ 2 = \frac{\sigma^2_{dc+isotropic}}{\sigma^2_{FMT}} \tag{2.5}$$

$$F \ ratio \ 3 = \frac{\sigma^2_{dc}}{\sigma^2_{dc+isotropic}} \tag{2.6}$$

$$F \ ratio \ 4 = \frac{\sigma^2_{dev}}{\sigma^2_{FMT}} \tag{2.7}$$

and comparing these values with known statistical tables. The degrees of freedom for each model is equal to $N - M - 1$ (Menke, 1989). In this way we tested if the more complex model fit the data significantly better than the simpler model. We determined that the more complex model was appropriate if the improvement in fit to the data was at or above the 95% confidence level as dictated by the F test. By taking all four F

ratios into account it becomes clear if any, either or both non-DC components are significant.

2.3 Results

Within the chosen space and time constraints, 33 high quality events are identified that have solutions with three or more stations in their inversion (Table 2.1). Of these 33 events, 28 are best characterized using a simple DC model. Synthetic waveforms produced using the more complex source models do not fit the data significantly better. This is quantitatively determined using the four statistical tests which show that the deviatoric, DC+isotropic and full moment tensor model waveforms do not significantly improve the solution at or above the 95% confidence level using an F test. Table 2.2 gives the derived focal mechanism solutions for these 28 DC events.

The remaining five events all have statistically significant positive volumetric components. The two statistical tests which determine the significance of the volumetric components, F ratios 3 and 4, show that source models containing isotropic components fit the data significantly better than source models which do not. For these five events, we use F ratio 2 to determine if the CLVD component is also significant. This test shows that only one of the five, Event 10, also has a statistically significant CLVD component. Tables 2.3 and 2.4 show the mechanisms for the DC+isotropic and full moment tensor events, respectively. The variance reduction values in Table 2.5 show how well each model fits the waveforms of the non-DC events. Table 2.6 gives the results of the F tests for the five events with significant volumetric components.

Event	UTC Date	UTC Time	Latitude North	Longitude West	NCSN Mag.	Depth (km)
1	1993/08/11	05:48:20.94	37.5262	-118.8835	4.3	5.13+/-1.01
2	1995/03/05	00:07:03.12	37.5975	-118.8325	4.2	10.34+/-0.55
3	1995/03/05	02:48:47.42	37.5928	-118.8325	4.0	10.56+/-0.54
4	1996/02/17	01:03:48.29	37.6240	-118.8758	3.6	8.73+/-0.37
5	1996/03/29	18:14:49.42	37.6293	-118.8530	3.9	8.92+/-0.43
6	1996/03/30	23:15:18.50	37.6282	-118.8657	4.0	7.54+/-0.36
7	1996/04/01	04:13:36.49	37.6178	-118.8568	3.9	9.78+/-0.38
8	1996/04/02	01:50:07.61	37.6243	-118.8610	4.2	7.98+/-0.37
9	1997/02/10	23:26:28.88	37.5648	-118.8605	4.2	9.76+/-0.85
10	1997/11/22	12:06:55.98	37.6352	-118.9175	4.5	8.38+/-0.35
11	1997/11/22	17:20:35.14	37.6363	-118.9360	4.8	7.66+/-0.38
12	1997/11/22	18:00:37.44	37.6445	-118.9492	3.5	7.96+/-0.73
13	1997/11/22	18:10:59.45	37.6340	-118.9507	4.7	8.20+/-0.34
14	1997/11/30	21:17:05.42	37.6343	-118.9462	4.8	7.10+/-0.45
15	1997/12/31	20:36:47.34	37.6312	-118.8697	4.8	6.59+/-0.32
16	1998/01/05	14:11:12.89	37.6338	-118.8712	4.1	6.43+/-0.35
17	1998/06/08	03:55:14.43	37.5893	-118.7975	4.0	6.66+/-0.50
18	1998/06/09	05:24:40.16	37.5887	-118.7955	5.1	6.75+/-0.48
19	1998/06/11	06:33:29.08	37.5842	-118.7843	4.3	8.26+/-0.53
20	1998/06/26	20:07:41.85	37.5925	-118.8070	4.3	6.21+/-0.46
21	1998/07/15	04:53:19.25	37.5635	-118.8063	5.1	6.22+/-0.55
22	1998/07/15	06:50:56.89	37.6440	-118.9123	3.7	7.14+/-0.32
23	1998/08/01	06:01:43.96	37.5693	-118.7935	4.3	5.93+/-0.73
24	1998/08/02	14:45:45.47	37.5725	-118.7972	4.3	6.79+/-0.51
25	1998/09/11	14:38:42.66	37.3880	-118.6893	3.9	12.30+/-0.93
26	1998/12/14	04:14:02.94	37.5262	-118.7958	3.8	7.96+/-2.29
27	1999/05/15	13:22:10.66	37.5298	-118.8172	5.6	5.59+/-0.56
28	1999/05/15	17:54:08.77	37.5093	-118.8310	4.7	7.33+/-0.80
29	1999/05/17	06:37:19.15	37.5118	-118.8263	4.3	3.27+/-0.81
30	1999/05/26	03:53:53.45	37.5558	-118.8035	4.2	4.47+/-0.65
31	1999/05/26	18:04:07.21	37.5455	-118.8062	4.2	4.09+/-0.70
32	1999/06/03	21:36:27.74	37.5375	-118.8052	4.4	3.29+/-0.87
33	2003/03/08	15:35:01.71	37.5705	-118.8848	4.0	5.46+/-0.34

Table 2.1: List of events. UTC event date (YYYY/MM/DD) and time (HH:MM:SS). NCSN location, magnitude, and depths, including formal vertical errors.

Assuming that both F ratio 3 and 4 determine that an event does not have a statistically significant isotropic component, F ratio 1 can determine if a deviatoric source model is preferred over a DC source model. However, none of the 33 events are best characterized by a deviatoric source model. At this point, it is important to remember

Event	Stations	MT Depth	Strike	Rake	Dip	M_0	M_W
2	BCO	11	105	-159	78	2.05E+22	4.2
3	BCS	11	357	-24	78	1.16E+22	4.0
4	BCK	8	306	-147	48	6.46E+21	3.8
5	BCKO	8	291	-147	57	8.20E+21	3.9
6	BCKO	8	204	-39	84	3.08E+22	4.3
7	CKO	8	201	-36	42	1.30E+22	4.0
8	BCKO	8	300	-174	54	4.31E+22	4.4
9	COP	8	54	24	78	2.05E+22	4.2
12	BCK	8	279	-174	45	5.33E+21	3.8
15	BCMOPS	5	288	177	51	1.78E+23	4.8
16	BCOP	5	29	27	68	2.07E+22	4.2
17	CKO	8	201	-27	81	3.61E+21	3.7
18	BKMOPS	5	300	177	54	2.85E+23	4.9
19	BCO	8	114	-150	72	8.20E+21	3.9
20	BCO	5	33	9	69	1.03E+22	4.0
21	BCKMOPS	5	165	-87	45	3.08E+23	5.0
22	BCK	8	270	-171	42	5.13E+21	3.8
23	BCOP	5	123	-156	81	1.78E+22	4.1
24	CKOP	5	324	-129	42	1.46E+22	4.1
25	BOPS	14	69	6	78	6.65E+21	3.9
26	CKO	5	120	-174	72	6.46E+21	3.8
27	BMOPS	5	294	-171	72	2.32E+24	5.5
28	BKOP	8	291	-177	57	1.05E+23	4.7
29	CKO	2	327	-129	51	8.61E+21	3.9
30	BMOPS	5	15	-18	63	9.90E+21	4.0
31	CKO	5	105	-159	78	5.38E+21	3.8
32	BKO	2	6	-18	42	3.61E+22	4.3
33	BCKMO	5	3	-39	54	1.44E+22	4.1

Table 2.2: Table of DC solutions. Station code is B=BKS, C=CMB, K=KCC, M=MHC, O=ORV, P=PKD and S=SAO.

Event	Stations	MT Depth	Strike	Rake	Dip	DC M_0	ISO M_0	M_W
1	BCO	5	108	156	48	1.91E+22	1.76E+22	4.2
11	BCMOPS	8	24	48	63	2.49E+23	1.32E+23	4.9
13	BCMOS	8	342	18	75	6.67E+22	3.84E+22	4.5
14	BCKMOS	8	18	27	60	2.41E+23	9.50E+22	4.9

Table 2.3: Table of DC + isotropic solutions. Station code is B=BKS, C=CMB, K=KCC, M=MHC, O=ORV, P=PKD and S=SAO.

that the applied statistics can only determine which of the four source models is most

appropriate for each earthquake, but place no guarantee on the physical mechanism

14

Event	Stations	MT Depth	M_{XX}	M_{XY}	M_{XZ}	M_{YY}	M_{YZ}	M_{ZZ}	M_W
10	BCMOS	8	4.7567	3.9713	-5.1655	4.0490	-4.7136	6.3743	4.5

Table 2.4: Table of full moment tensor solutions. Moment tensor components have units of 10^{22} dyne cm. Station code is B=BKS, C=CMB, K=KCC, M=MHC, O=ORV, P=PKD and S=SAO.

Event	DC VR	Deviatoric VR	DC+Iso VR	FMT VR
1	88.2%	88.5%	92.4%	93.4%
10	79.3%	83.2%	85.5%	89.1%
11	83.1%	86.3%	90.8%	92.0%
13	82.1%	88.4%	91.2%	91.8%
14	84.8%	85.9%	89.0%	91.0%

Table 2.5: Variance reduction of all four source models for non-DC events. VR, variance reduction; DC+iso, DC+isotropic; FMT, full moment tensor.

behind these non-DC events. All non-DC events are located either in the south moat of the caldera or in the Sierra Nevada block (Figure 2.2). We were not able to analyze the source process of earthquakes in or near the vicinity of the Mono-Inyo volcanic chain or Mammoth Mountain because events greater than M3.5 were not recorded during the time interval investigated by this study.

The first event with a significant volumetric component, Event 1, occurred on August 11, 1993 in the Sierra Nevada block during an intense earthquake swarm. The six day Red Slate Mountain earthquake swarm started on August 10 and produced the largest earthquake and the greatest number of events associated with a single earthquake swarm in the Long Valley volcanic region in 1993. As seen in Table 2.6, F ratios 3 and 4 determine that this event has a statistically significant isotropic component at the 95% confidence level. F ratio 2 determines that adding the CLVD component to the inversion does not significantly improve the solution. Hence, the

Event	F ratio 1 DC v Dev	F ratio 2 DC+Iso v FMT	F ratio3 DC v DC+Iso	F ratio 4 Dev v FMT	Best Mechanism
1	-	-	95%	95%	DC+iso
10	-	95%	95%	99%	FMT
11	-	-	99%	99%	DC+iso
13	99%	-	99%	95%	DC+iso
14	-	-	95%	99%	DC+iso

Table 2.6: Greater than 95% significance levels for non-DC events. F ratios 1 and 2 test for significant CLVD components. F ratios 3 and 4 test for significant isotropic components. Dev, deviatoric; DC+iso, DC+isotropic; FMT, full moment tensor.

best source model for this event is the DC+isotropic model. The isotropic component of this event contributes 48% of the total moment release.

The next four events with coseismic volume increases (Events 10, 11, 13, and 14) occurred in the south moat of the Long Valley caldera during a period of unrest at the peak of a large earthquake swarm which spanned July 1997 though January 1998. These events had been previously identified as having significant volumetric components by Dreger et al. (2000) however, the current study investigates a wider range of possible source mechanisms. Thus, the results presented here update the solutions of the previous investigation. We will first discuss Event 10. Both F ratios 3 and 4 indicate that this event has a significant isotropic component. We then utilized F ratio 2, since it a priori assumes that the event in question has a significant isotropic component, to determine if the CLVD component is also significant. The results of this test indicate that the addition of the CLVD component significantly improves the fit to the data. As such, Event 10 is best described using the full moment tensor model. The CLVD component of this event contributes a large 57% to the total moment release while the isotropic component contributes 42%. Interestingly, the DC component is only 1% of the total moment suggesting that shear along a fault plane
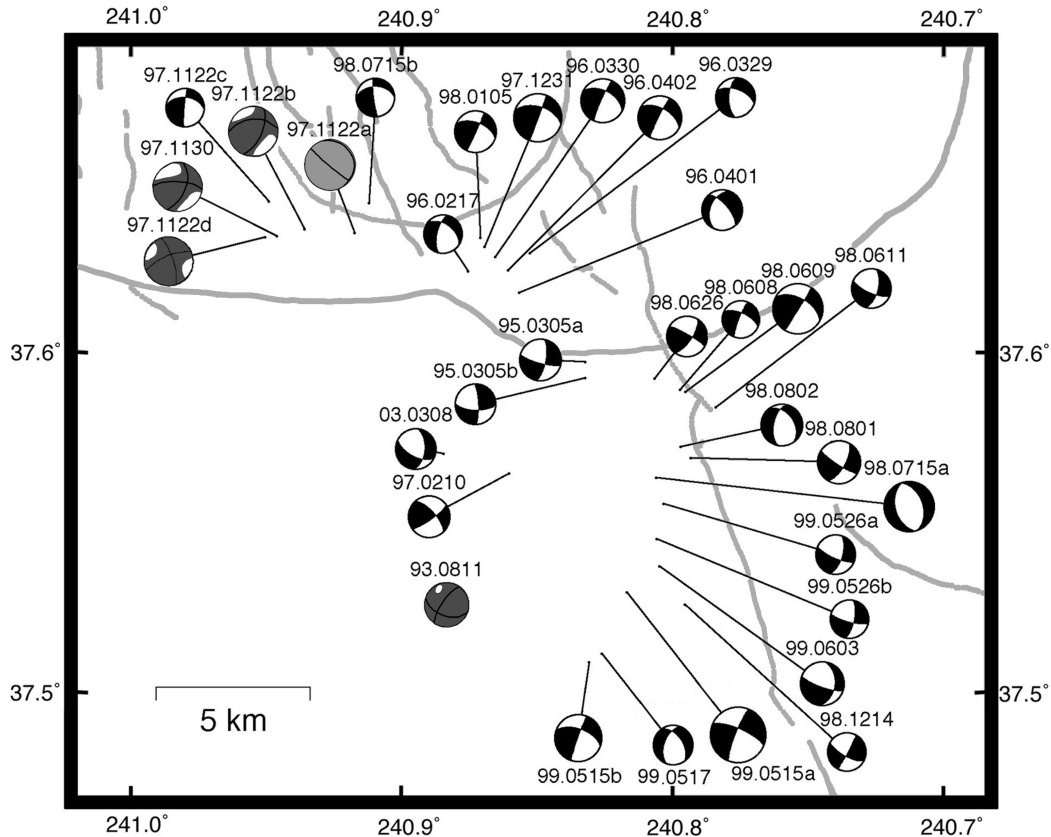
Figure 2.2: Graphical moment tensor results. DC solutions shown in black. DC+isotropic solutions shown as dark gray. Full moment tensor solutions shown as light gray. Date of event shown as YY.MMDD.

was not an important part of the earthquake process and implying that the mechanism for this event resembled an opening tensile fault.

For Event 11, both F ratio 3 and 4 indicate that this earthquake has a significant isotropic component at the 99% confidence level. The results of F ratio 2 indicate that the CLVD component is statistically insignificant. Hence, this event is best described using the DC+isotropic model. This solution revealed that the isotropic component produced 35% of the total moment release for this event. As an example of how the different sources can influence the waveforms, Figure 2.3 compares the
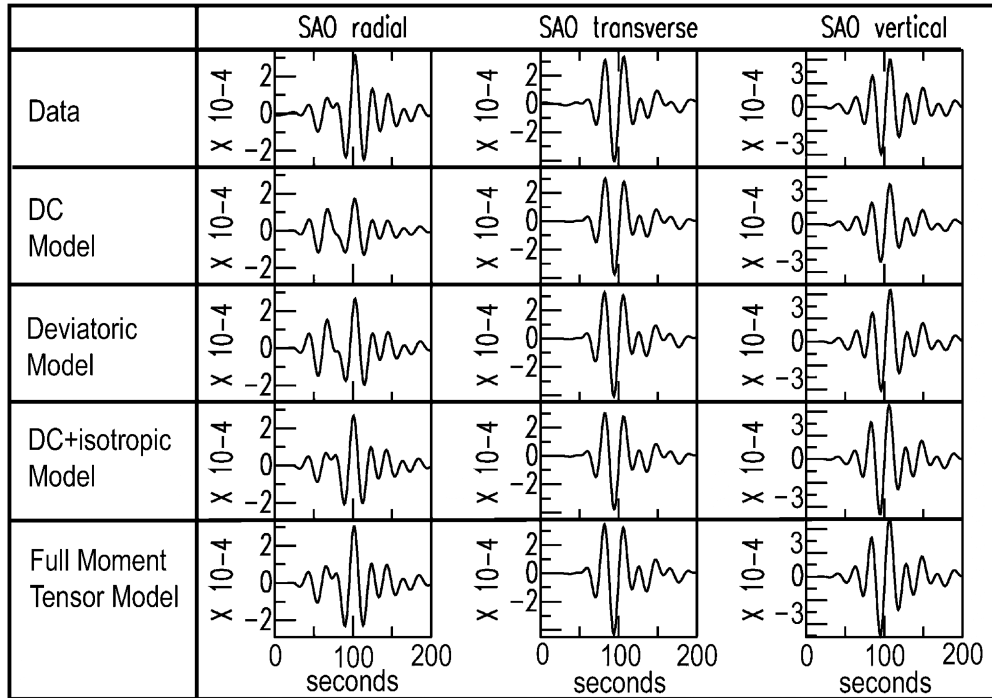
Figure 2.3: Data, DC model synthetics, deviatoric model synthetics, DC+isotropic model synthetics and full moment tensor model synthetics filtered between 0.02 - 0.05 Hz for all three components at station SAO for DC+isotropic Event 11 in units of centimeters.

filtered data observed at station SAO with synthetic waveforms computed using the

four different source models. In this example, the most notable differences can be seen

in the radial component. Figure 2.4 compares the observed data at all stations for

Event 11 with the DC+isotropic source synthetic waveforms.

For Event 13, F tests 3 and 4 also indicate that this event has a significant

isotropic component while F ratio 2 determines that this event has a statistically

insignificant CLVD component. Thus, this event is also best modeled using the

DC+isotropic solution. The results of this inversion indicate that the isotropic

component of this event contributes 27% of the total moment release.
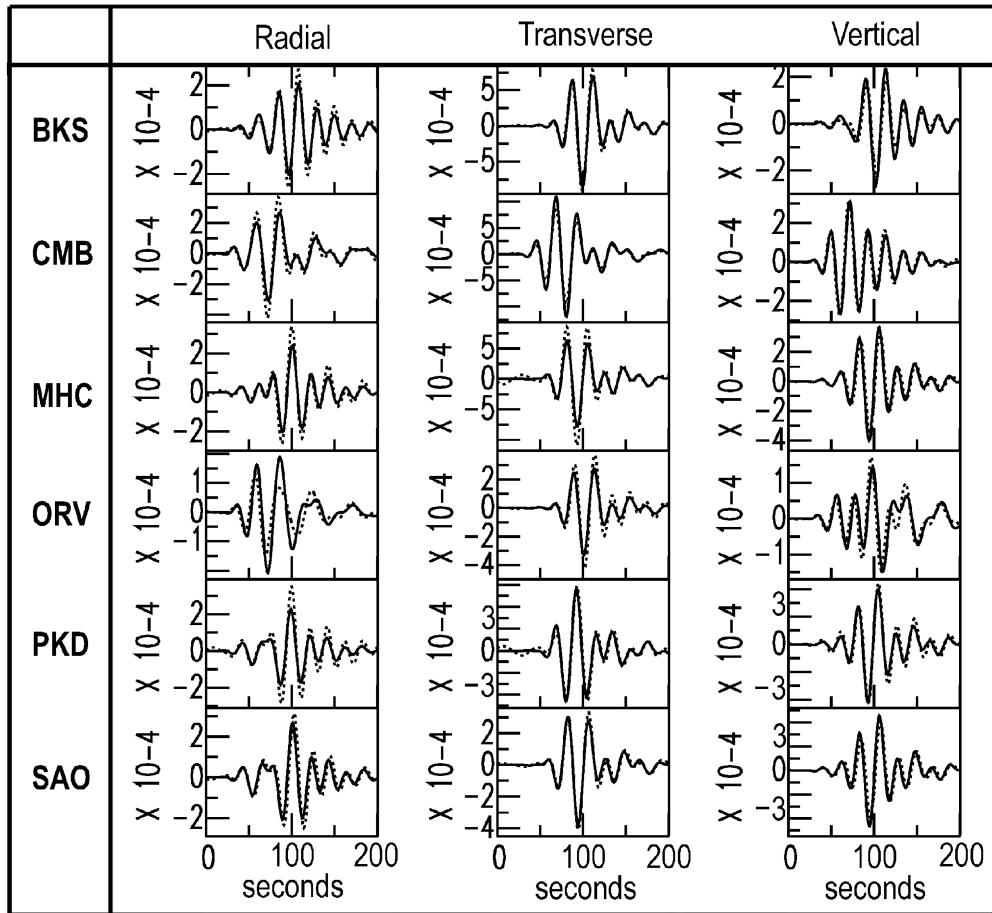
Figure 2.4: Best solution for Event 11 showing data in dotted black lines and DC+isotropic model synthetics in solid black lines in units of centimeters.

For the remaining event, Event 14, F tests 3 and 4 again indicate that it has a significant isotropic component. As seen in Table 2.6, F ratio 2 indicates that this event does not have a significant CLVD component. As such, this event is best modeled using the DC+isotropic source model. The isotropic component of Event 14 contributes 35% of the total moment.

Pure DC events sometimes occurred close in space and time to events with significant non-DC components (Figure 2.2). For example, DC Event 12 occurred 10 minutes before non-DC Event 13 and was located just a few kilometers away from all

four south moat non-DC events.   In some cases, DC events determined by this study were located near previously identified fluid influenced microseismicity structures. For example, Events 15 and 16 occurred close in space to a microseismicity trend inferred to be a compensated tensile failure plane (Foulger et al., 2004). Thus, it appears that the factors necessary to produce isotropic components only coalesce and trigger non-DC events within a relatively small physical and temporal window in the Long Valley volcanic region.

2.4 Stability of Focal Mechanism Solutions

To test the stability of the focal mechanism solution, we performed Jackknife tests on three events: DC Event 15, DC+isotropic Event 11, and full moment tensor Event 10. We solved for all combinations of three, four, and five station combinations and compared these results with the original solution for each event. In Figure 2.5, we show a representative set of focal mechanisms showing the distribution of calculated solutions. DC and DC+isotropic solutions are remarkably stable for all station combinations of three or more. The full moment tensor event shows that the P-wave radiation pattern is stable with at least four stations in the inversion but that the orientation of the faulting planes is unstable regardless of the number of stations used. However it is important to note that the DC component of this event produced only 1% of the total moment release and that the CLVD and isotropic components dominate the inversion, hence the instability of the faulting planes is not surprising.
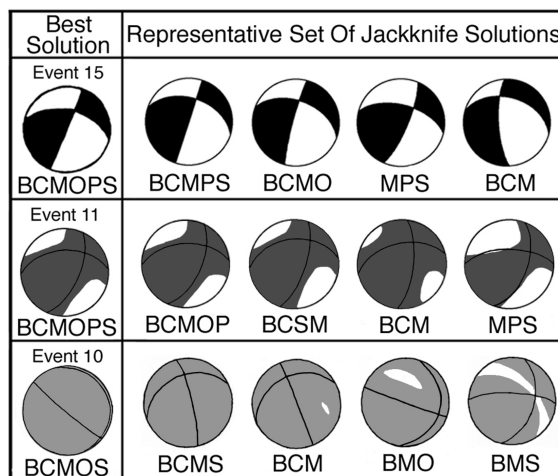
Figure 2.5: A representative set of focal mechanism solutions of Jackknife test results for DC Event 15, DC+isotropic Event 11, and full moment tensor Event 10. Station code is B=BKS, C=CMB, M=MHC, O=ORV, P=PKD and S=SAO.

Most of the three station inversions produced similar radiation patterns to solutions using more stations however, there were a few exceptions (Figure 2.5). Thus, focal mechanism solutions with as few as three stations can be treated with confidence. This is consistent with previous stability studies in other volcanic areas (Šílený et al., 1996 ; Panza and Saraò, 2000).

2.5 Stability of Isotropic Component

Previous studies of synthetic and real data recorded at local distances have investigated how noise, hypocenter mislocation and velocity model inaccuracies affect the resolution of the isotropic component, taking into account the distribution of seismic stations (Šílený et al., 1996 ; Panza and Saraò, 2000). The studies using synthetic data have shown that the isotropic component can be correctly recovered even with poor station configurations when as few as three three-component local

stations are used. These synthetic tests have also shown that errors in the hypocenter and velocity model are small compared to errors due to high noise levels.

In this study, we conduct a detailed investigation of 33 events with low noise levels. With respect to the velocity model, at the passband used in this study, the SoCal model has been shown to not produce statistically significant isotropic components due to unmodeled near-source velocity structure in the Long Valley caldera (Panning et al., 2001). To determine the stability of the isotropic component with station configuration for data recorded at regional distances, we first performed Jackknife tests on the four events with significant isotropic components that had four or more stations in their solution to determine the likelihood of non-DC events incorrectly being identified as DC events. Thus, for each event, for all station combinations of three or more, we determined the statistical significance of the volumetric component. For the event with the significant CLVD component, Event 10, we compared the deviatoric and full moment tensor solutions. For events without significant CLVD components, we compared the DC and DC+isotropic solutions. Statistically significant isotropic components were determined if the improvement in fit to the data was at or above the 95% significance level as determined by using the F test statistic. Unfortunately Event 1 had only three stations with good quality data and thus Jackknife tests were not performed on this event. For Events 10 and 13, there were 5 four station solutions and 10 three station solutions. For Events 11 and 14, there were 6 five station solutions, 15 four station solutions, and 20 three station solutions.

All 52 combinations of four or more stations recovered the statistically significant isotropic component. For solutions with three stations, six iterations out of 60 failed to recover the isotropic component. It is reasonable to assume that significant isotropic components can be recovered with as few as three, but preferably with at least four, stations in the solution.

We also investigated the possibility of obtaining a spurious isotropic component due to poor data coverage. For this test, we took three high quality DC solutions (Events 15, 18, and 21) and performed Jackknife tests to see if any combination of three or more stations would result in a statistically significant isotropic component at or above the 95% significance level. For this test we compared the DC and DC+isotropic solutions for all three events. For their best solutions, Events 15 and 18 originally had six stations in their solutions while Event 21 had seven stations.

Of 75 three station solutions, one returned a false positive. Of 65 four station solutions, three incorrectly determined that the event had a significant isotropic component. Five and six station solutions did not return false positives. Thus, we feel confident that the isotropic components of our non-DC events with at least five stations in their inversion are not due to poor data coverage. This test, however, casts a small amount of doubt as to the validity of non-DC Event 1 which has only three stations in its solution.

2.6 Discussion

Earthquakes greater than M3.5 with significant non-DC components are not common in the Long Valley volcanic region. Only five such events occurred between 1993 and 2004. Four occurred in the Long Valley caldera during the peak of a large earthquake swarm in November 1997. The remaining event occurred in the seismically active Sierra Nevada block in August of 1993 during the largest earthquake swarm which occurred in the area that year. All five had significant isotropic components, indicating that fluids were involved in the source process of these events. No earthquakes occurred in or near the vicinity of the Mono-Inyo craters during the time interval investigated by this study even though the most recent eruption in the region occurred along this volcanic chain and it is the expected location of the next eruption within the Long Valley volcanic region (Hill et al., 1985).

Of the events that occurred within the caldera, Events 11, 13, and 14 are best characterized using a DC+isotropic model while Event 10 is best described using a full moment tensor model which solves for DC, CLVD, and isotropic components. The isotropic components of all four events indicate that there was a coseismic volume increase in the source region. These events occurred during a period of unrest that also affected the geothermal system. Water-level changes at wells within the caldera were attributed to upward migration of hydrothermal fluids (Roeloffs et al., 2003). An examination of relocated seismicity on the day that the four non-DC events occurred revealed a cloud of seismicity that began to migrate at approximately the same time as the first non-DC event occurred (Prejean, 2002a). This cloud of seismicity started at approximately 9 km depth and fanned out upward and westward over an approximately 1 km wide near vertical fault zone traveling at about 0.05 m/s

for 23 hours to achieve depths as shallow as 4.5 km. This migration is most probably

indicative of fluid circulation, which when combined with pre-existing tectonic

stresses could have initiated the events with significant isotropic components. In light

of the fact that the Long Valley caldera has a known active geothermal system, it is

not unexpected to find events with large isotropic components in this area.

Sierra Nevada Block Event 1 also has a significant non-DC component

however, our solution stability analysis indicated that events with only three stations in

their solution have a small chance of producing spurious isotropic components. This

study determined that Event 1 is best characterized by a DC+isotropic model whose

sign indicated a coseismic volume increase in the source region. Since the strike-slip

faults in the Sierra Nevada block do not appear to intersect the ring fracture system of

the Long Valley caldera (Prejean et al., 2002b), we speculate that the source of the

fluids influencing Event 1 were not geothermal fluids originating from within the

caldera that migrated into the Sierra Nevada block via these conduits. Although there

has been equivocal evidence of magma or magmatic fluids present in this area from

early S-wave shadowing studies (Ryall and Ryall, 1984) and from the analysis of three

microearthquakes observed during an August 1998 earthquake sequence (Hough et al.,

2000), the locations of these potential sources of fluids were not near Event 1. The

most likely potential fluid source would be fluids associated with the local

hydrothermal system. Previously, the only non-DC events to occur in this area were a

1978 M5.8 event and two M6 1980 events (Julian and Sipkin, 1985). Event 1,

however, did not occur along the same fault planes as these earlier events (Prejean et

al., 2002b). Additionally, the full six-component moment tensor solution can not be

computed for the three earlier events with the available data and thus it is not known if the non-DC components were due to fluid involvement or complex shear faulting. In this study, we specifically solved for the full moment tensor and hence can conclusively rule out complex coseismic shear faulting as a possible mechanism for the five events with significant isotropic components.

The increase of broadband seismometers in geothermal and volcanic areas has facilitated the world-wide exploration for non-DC earthquake source mechanisms. These studies have shown that the percentage of events with isotropic components and the strength of the isotropic component can vary with location. At Aso Volcano, Japan, inversions of near-field broadband signals of long-period tremors and phreatic eruptions has shown primarily isotropic mechanisms, greater than 95% of the total moment released, for dozens of events over a one year period (Legrand et al., 2000). Other volcanos such as Mt. Etna produced only two microearthquakes out of 28 events with M ≥ 2.0 with significant volumetric components over a 16 month period preceding the 1991-1993 eruption (Saraò et al., 2001). These volumetric components were between 17-47% of the total moment released for each event. A study of 18 microearthquakes occurring during a period of intense seismicity in 1984 at Campi Flegrei showed that less than half of these events had large volumetric components up to 93% of the total moment release (Guidarelli et al., 2002). These differences are most probably due to different underlying physical mechanisms. The Long Valley volcanic area is more similar to the Mt. Etna region in terms of the scarcity and strength of the isotropic components. In this study, out of 33 events investigated, only

five have significant non-DC mechanisms whose isotropic components are between 27-48% of the total moment released for each event.

A previous full moment tensor study using a dense temporary seismic network operating during the summer of 1997 showed that most of 26 microearthquakes less than M3.1 were characterized by positive CLVD and isotropic components (Foulger et al., 2004). These events, all between 0 - 6 km, were located in the south moat of the caldera, near the southwestern rim of the resurgent dome and under Mammoth Mountain. Foulger et al. (2004) determined that the solutions for these microearthquakes were consistent with a combined shear and tensile faulting model with rapid fluid flow into the opening crack. The small magnitude of these events suggests that the fluid involved was probably not magmatic but rather water, steam or CO_2. Interestingly, five events in that study were equivocally characterized by small volume decreases indicating a closing of cracks or voids. The difference in the total number of isotropic events in the two magnitude ranges studied in the Long Valley caldera suggests that conditions are scale dependent, possibly in terms of the ability of individual high pressure reservoirs to sustain pressurization during the faulting process as the crack or fault grows larger. It is interesting to note that events larger than M3.5 did not occur near the southwestern rim of the resurgent dome or under Mammoth Mountain. Unfortunately, this meant that events in these areas could not be investigated using our method.

The world-wide diversity apparent in the strength and production of isotropic components should be closely studied, ultimately to determine if there is a predictive relationship between these events and changes to the geothermal or magmatic system.

To achieve this goal, future studies should strive to combine non-seismic as well as seismic data when determining the source kinematics, the properties of the fluid involved, and the feasibility and physics behind the different possible physical mechanisms.

2.7 Data Sources

Broadband Berkeley Digital Seismic Network (BDSN) waveform data used in this study was collected by the Berkeley Seismological Laboratory (BSL) at the University of California, Berkeley. This data is freely available from the Northern California Earthquake Data Center (www.ncedc.org).

Chapter 3

Behavior of Repeating Earthquake Sequences in Central California and the Implications for Subsurface Fault Creep

3.1 Introduction

Repeating earthquakes (REs) are nearly identically repeating events that have similar magnitudes and hypocenters. They can be identified by their extremely similar waveforms and have either aperiodic or quasi-periodic recurrence intervals. To date, they have been observed in both transform and convergent plate boundaries (Vidale et al., 1994 ; Nadeau et al., 1995 ; Schaff et al., 1998 ; Igarashi et al., 2003 ; Uchida et al., 2003). Nadeau and McEvilly (1999) suggested that the congruent waveforms result from stuck patches in an otherwise creeping fault which repeatedly rupture the same asperity. Other proposed physical models for REs include weak asperities at the border between larger locked and creeping patches on the fault plane (Sammis and Rice, 2001), inner asperities embedded within a creeping patch within an otherwise locked fault plane (Anooshehpoor and Brune, 2001), or creeping patches that strain harden until they fail seismically (Beeler et al., 2001). In each of these proposed

physical models, creep adjacent to the asperity plays an important role in cyclically loading the RE sequence location to failure. Thus, even the simple detection of a RE sequence along a fault plane would imply that the fault is creeping. Of course, the absence of REs along a fault plane does not necessarily mean that creep is not occurring. Recently, burst type REs, sequences of nearly identically repeating events which have extremely short recurrence intervals and are active only for a short period of time, have been identified in subduction zones, both on the plate boundary itself and off the actual subduction interface (Kimura et al., 2006 ; Igarashi et al., 2003). Kimura et al. (2006) hypothesized that they are triggered by a local increase in stress due to the occurrence of large nearby earthquakes and do not reflect the background creep rate of the fault.

Although the mechanism for creep is not known, several hypotheses have been proposed as to what may initiate or facilitate aseismic fault creep. These include the presence of weak minerals or ductile materials within the fault gouge, which could lower the frictional strength of the fault, or high fluid pressures within the fault zone, which could lower the effective normal stress (Moore et al., 1997 ; Irwin and Barns, 1975). The geometry of the fault zone itself has also been suggested to influence aseismic creep (Moore and Byerlee, 1992). Furthermore, surface creep can be affected by non-tectonic environmental factors, such as rainfall and yearly seasonal variations (Roeloffs, 2001).

Faults that creep aseismically may also produce major earthquakes. Identifying which areas of the fault are locked and accumulating strain to be released during a future earthquake and which areas are slowly releasing, at least a portion, of this strain

through aseismic creep is essential when evaluating seismic potential and hazard. Determining the distribution of displacement over these actively creeping fault planes can be aided by the ability to calculate slip at specific points at depth on a fault from RE seismic data. This information can complement slip results from geodetic measurements of surface deformation (Schmidt et al., 2005). Additionally, since surface geodetic measurements can have difficulty resolving slip in the mid- to lower seismogenic zone (Bos and Spakmann, 2003), even areas with excellent surface geodetic data could benefit from RE data points which can extend down to the bottom of the seismogenic zone. Additionally, in areas where surface geodetic data is poor or non-existent, the identification of REs becomes crucial when investigating the occurrence, magnitude and distribution of fault creep.

In this study, we compare the occurrence and behavior of REs within and between two different areas in central California to determine which faults are slipping aseismically and the magnitude of this subsurface creep using the method and model of Nadeau and McEvilly (1999).

3.2 Study Regions

The first study area focuses on the juncture between the San Andreas and southern Calaveras-Paicines faults (Box A, Figure 3.1). This juncture region marks a transition of the behavior of the Pacific-North American plate boundary fault system. North of the juncture region, the plate boundary forms an intricate network of parallel, predominately right-lateral strike-slip faults. To the south, it becomes a relatively
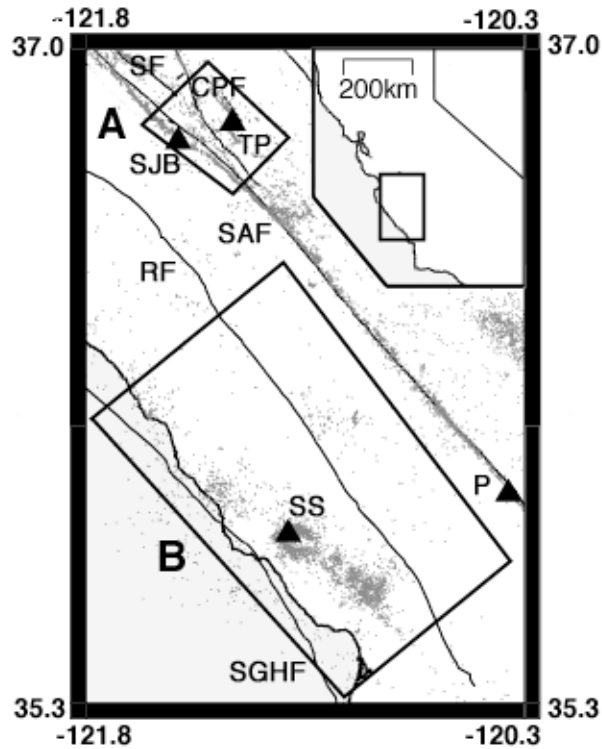
Figure 3.1: Map of central California. Box A delineates the San Andreas and southern Calaveras fault juncture study area while Box B delineates the southern Coast Ranges study area. Seismicity as small grey dots and faults as black lines. Fault labels are SAF = San Andreas fault, CPF = Southern Calaveras-Paicines fault, SF = Sargent fault, RF = Rinconada Fault, and SGHF = San Gregorio-Hosgri fault. Triangles are locations of large earthquakes considered in the discussion: SJB = Mw 5.1 1998 San Juan Bautista earthquake, TP = Ml 5.5 1986 Tres Piños earthquake, SS = Mw6.5 2003 San Simeon earthquake, and P = Mw6.0 2004 Parkfield earthquake. Inset map is of California with box representing zoomed in area.

simple single fault strand that accommodates the majority of the motion between the

two plates. The juncture area also marks the transition between the creeping section of

the San Andreas fault to the south and a locked portion of the fault that slipped in the

Mw7.9 1906 San Francisco earthquake. The San Andreas fault in this region separates

the granitic and metamorphic rocks of the Salinian block to the west from the Great

Valley Sequence, Franciscan Complex, and Coast Range ophiolite to the east

(Wallace, 1990).

Geodetic data has shown that surface creep within the juncture region appears to be influenced not only by larger earthquakes, such as the Mw6.9 1989 Loma Prieta earthquake, which occurred north of our study area (Breckenridge and Simpson, 1997), and the Ml 5.5 1986 Tres Piños earthquake (Simpson et al., 1988), but also by slow earthquakes such as the 1992, 1996, and 1998 San Andreas fault slow earthquakes which had equivalent moments equal to M4.8, M4.9 and M5.0, respectively (Linde et al., 1996 ; Johnston et al., 1996 ; Gwyther et al., 2000). Additionally, an inversion of GPS and InSAR data has shown that between 1995 – 2000, the subsurface creep along the San Andreas fault in this juncture region generally increased from north to south but also included two asperities large enough to nucleate moderate sized earthquakes (Johanson and Bürgmann, 2005).

The second study area is located within the southern Coast Ranges, west of the creeping section of the San Andreas fault and directly to the south of the previously mentioned San Andreas-southern Calaveras fault juncture (Box B, Figure 3.1). Faults within the southern Coast Ranges are composed of both right-lateral strike slip faults, associated with the transform tectonic regime related to the San Andreas fault, and thrust faults, which are thought to accommodate a small component of fault-normal compression (Clark et al., 1994). As opposed to the juncture region previously described, this area is primarily composed of granitic and metamorphic rocks of the Salinian block. However, a narrow region of coastal Franciscan rocks is also present within the Coast Ranges consisting of relatively coherent, low P-T metamorphosed graywackes (Clark et al., 1994 ; McLaughlin et al., 1982 ; Ernst 1971 ; Platt 1986).

The Mw6.5 2003 San Simeon earthquake is thought to have occurred within this complex (Hauksson et al., 2004).

3.3 Data and Methodology

3.3.1 Sequence Identification

We identify RE sequences by first cross-correlating local unfiltered waveform data collected by the Northern California Seismic Network (NCSN) and archived at the Northern California Earthquake Data Center (NCEDC). The cross correlation was performed over a 5 second window beginning with the P-phase arrival in the frequency domain for all pairs of events with epicenters within 10 km of each other. This distance is greater than twice the formal catalog-location uncertainties for more than 90% of the events studied.

Once the cross-correlations are performed, we identify RE sequences via a two-step process. The first step is to identify a pair of events, which we call a master-pair, that are nearly identical and thus repeating. The second step is to identify all earthquakes that are also nearly identical to at least one of the master-pair of events.

To determine if a particular master-pair of events are nearly identical, we first determine that its cross correlation coefficient averaged over all vertical component NCSN stations within 50 km is greater then 0.95. Next we calculate the coherence of their phase and amplitude spectra in the complex domain. To do this we compute the RMS amplitudes of the first 5 sec of the two events at a station and normalize the waveform amplitudes. We then compute the complex spectra of the normalized waveforms and determine the complex unit vectors, ν_1 and ν_2, from the spectra

$$v_1 = \frac{a_1(f) + ib_1(f)}{\sqrt{(a_1(f))^2 + (ib_1(f))^2}} \qquad (3.1)$$

$$v_2 = \frac{a_2(f) + ib_2(f)}{\sqrt{(a_2(f))^2 + (ib_2(f))^2}} \qquad (3.2)$$

between 8 – 20 Hz in 0.2 Hz increments. We then determine the angle θ between the

vectors and use this to calculate the phase coherence, C_P,

$$C_P = \cos(\theta) \qquad (3.3)$$

for each frequency increment. The phase coherence between the two earthquakes is

then determined by averaging the coherence over all frequency increments and

stations. To find the maximum phase coherence between the master-pair, this process

is then repeated after shifting the waveforms up to +/- 5 samples in increments of 1/25

of a sample. A phase coherence value of 1 would indicate an exact match between the

two waveforms.

Next, we perform two tests to determine the coherence of the amplitude spectra

of the events under consideration. First, we calculate the difference in the amplitude

spectra, α_1 - α_2, of the normalized waveforms between 8 – 20 Hz in 0.2 Hz

increments. We then determine the amplitude coherence, C_{A1}, between the two

waveforms using

$$C_{A1} = 1 - \frac{\sum(|\alpha_1 - \alpha_2|)}{N_f} \qquad (3.4)$$

where N_f are the number of frequency increments. An amplitude coherence value of 1

would then indicate an exact match between the two spectra. The second amplitude

coherence method we use involves cross-correlating the amplitude spectra between 8 –

20 Hz. A cross correlation value of 1 would indicate an exact match between the amplitude spectra using this method.

The master-pair under consideration is identified as a repeating earthquake if the average of the three above mentioned methods of determining the amplitude and phase coherence is greater than 0.85. If this is the case, the amplitude and phase spectra coherency is then also determined in the same manner for all other events that have cross correlation coefficients greater than 0.85 when compared to one of the original master-pair of events. These additional earthquakes are included within the repeating earthquake sequence if the average of the three amplitude and phase coherence measures is greater than 0.85. Lastly, we visually inspect the RE groups to assure quality. A previous study of RE sequences on the San Andreas fault using both surface and borehole seismometers suggested that nearby RE sites with average magnitudes less than ~M1.3, which were clearly separate using the borehole data, are not clearly separated when using only NCSN surface data (Nadeau and McEvilly, 2004). Therefore, we include only RE sequences with average magnitudes greater than this value in our analysis.

This method of determining RE sequences was applied to the waveforms of the over 5,000 events occurring between 1 March 1984 and 1 May 2005 at the juncture of the San Andreas and southern Calaveras faults (Box A, Figure 3.1). This region also includes portions of the San Andreas fault that contained previously identified RE sequences (Nadeau and McEvilly, 2004). For these REs, we extended the time series of each sequence to include repeats occurring until 1 May 2005. Locations of RE

sequences within this juncture region are plotted using a hypoDD-relocated earthquake catalog of northern California (Ellsworth *et al.*, 2000).

We also applied our RE sequence identification technique to the area west of the San Andreas fault within the southern Coast Ranges (Box B, Figure 3.1). Waveforms for over 7,000 events occurring between 1 March 1984 and 1 May 2005, which included the aftershock sequence of the Mw6.5 2003 San Simeon earthquake, were obtained from NCSN stations up to 50 km away and compared to identify RE sequences. Approximately 5,500 events in this study area are located within the San Simeon aftershock zone. RE sequences in this area are plotted using locations obtained from the NCSN catalog.

3.3.2 Slip Rates From REs

We use the method of Nadeau and McEvilly (1999) to determine the amount of slip at specific asperities along the fault plane. This approach assumes that a RE is a stuck patch in an otherwise creeping fault which "catches up" with the adjacent creeping fault when it fails seismically. The total amount of slip in centimeters, D_{tot}, at a RE location can be determined by the empirical relationship

$$D_{tot} = \left(10^{0.255(M-0.15)+0.377}\right) \times n \qquad (3.5)$$

where M is the average NCSN preferred catalog magnitude of the RE sequence and n the number of times the earthquake repeats. This empirical relationship, originally determined by calibrating geodetic creep and RE data along the creeping section of the San Andreas fault at Parkfield, estimates the amount of creep surrounding a RE location between each repeat within a sequence and multiplies it by the number of

times the earthquake repeats over the observation period to compute the cumulative amount of slip at each sequence location. Incorporating additional assumptions, the empirical relationship can be used to infer the mechanical properties of rupture on these asperities, such as stress drop, but for the purposes of determining subsurface slip these additional assumptions are not required.

Although the empirical relation in Equation 3.5 was calibrated on the Parkfield segment of the San Andreas fault, it has also been employed in a subduction zone setting where the RE derived spatial and temporal distribution of slip along the plate boundary was shown to be consistent with independently determined geodetic interpretations of the plate coupling behavior (Igarashi et al., 2003 ; Uchida et al., 2003). Additionally, other studies on the Chihshang fault in Taiwan and on the Hayward fault in California have shown that creep rates determined from REs compare well with results from measurements taken at the surface (Chen and Rau, 2003 ; Bürgmann et al., 2000). This surprising observational result suggests that the strength of asperities that produce repeating earthquakes does not vary significantly between these locations and that these asperities rupture under essentially the same critical stress conditions in each of these diverse tectonic regimes.

3.3.3 Background on Empirical Method

Here we review the assumptions and method of Nadeau and McEvilly (1999) to determine an empirical relationship between slip on a RE patch and the size of the RE after RE sequences have already been identified. To compute the slip at RE locations using this method, we must first assume V_g, the average long-term tectonic

loading rate based on geodetic data for the region under consideration. On the

Parkfield segment of the San Andreas fault, this value is assumed to be

$$V_g = 2.3 cm/yr.$$
(3.6)

After identifying the REs within a sequence, we can then determine the recurrence

interval, T_r, between events within sequences. Using the recurrence intervals and the

assumed tectonic loading rate, T_r and V_g, we can determine d_i, the average tectonic

load on the asperity prior to rupture (i.e. the surrounding aseismic fault creep that

loads a RE asperity to failure during the time interval between events) by assuming

that

$$V_G \propto \frac{1}{T_r}$$
(3.7)

and specifically using the equation

$$d_i = V_g \times T_r.$$
(3.8)

After determining d_i, we can plot $\log(d_i,)$ versus the $\log(M_0)$ for all events to

determine the empirical equation necessary to be able to transfer this relationship to

other areas, assuming that the strength of asperities is the same as that at Parkfield.

The average M_0 of a sequence can be determined from the average magnitude

of all events within a sequence using the relationship of Hanks and Kanamori (1979):

$$\log M_0 = 1.5M + 16.1.$$
(3.9)

If HRSN borehole seismometer data is used then

$$M = M_w.$$
(3.10)

If NCSN surface seismological data is used then

$$M = M_P - 0.15$$
(3.11)

where M_p is the NCSN preferred magnitude. The Hanks and Kanamori relationship is based on the Gutenberg-Richter relation between the wave energy, E_S, and M_S (Gutenberg and Ricter, 1956)

$$\log E_S = 1.5 M_S + 11.8,$$
(3.12)

the relationship between E_S and M_0 by Kanamori (1977)

$$E_S = \frac{\Delta\sigma}{2\mu} M_0,$$
(3.13)

and assumes that the ratio between stress drop, $\Delta\sigma$, and twice the rigidity, μ, is equal to

$$\frac{\Delta\sigma}{2\mu} = \frac{1}{2 \times 10^4}.$$
(3.14)

As a side note, holding the rigidity constant, an increase in the assumed stress drop would have the effect of lowering the 16.1 y-intercept value in the Hanks and Kanamori (1979) relationship, which in turn would cause an overprediction of M_p at smaller depths. Should the rigidity also increase, this value could still be valid. Although the values required for the ratio to hold for stress drops determined using the Nadeau and McEvilly (1999) method are non-traditional, the Hanks and Kanamori (1979) relationship which uses this ratio appears to give meaningful results when applied to the Nadeau and McEvilly (1999) method.

Returning to the $\log(d_i)$ versus $\log(M_0)$ plot, the best least squares fit to the data could be plotted as a straight line with slope β, intercept α and in the form

$$d_i = 10^\alpha M_0^\beta.$$
(3.15)

Using the assumed tectonic loading rate and the observed recurrence intervals, the best fit values determined at the Parkfield segment of the San Andreas fault were $\alpha = -2.36$

and β=0.17, which we have exported to the San Andreas fault juncture area and which others have exported to other tectonic regions (Igarashi et al., 2003 ; Uchida et al., 2003 ; Chen and Rau, 2003 ; Bürgmann et al., 2000) with different slip rates. This is possible since the above equation for d_i, is divorced from recurrence intervals. It simply depends on the amount of load that a particular size RE asperity can sustain before it ruptures, which is assumed to be the same at all locations.

For this empirical method to be valid, we assume that REs occur on the same asperity each time, that the rupture threshold is constant through time (i.e. after a given load, the RE will always rupture), and that the slip on an asperity keeps pace with the tectonic slip. This relationship does not automatically assume that the seismic slip is equal to the assumed tectonic loading rate, the two need only be proportional. The relationship makes no assumptions about the tectonic environment or geology, only that the strength properties at the RE asperities be essentially the same.

3.3.4 Implications Concerning Stress Drop and Earthquake Scaling

While the empirical relationship does not directly use stress drop to determine slip at RE patches, it does have some surprising implications concerning this quantity and earthquake scaling.

The scaling between earthquake size and stress drop is an issue that is currently being debated. It has been a long held theory that stress drop is constant (Hanks, 1977) and has been supported by many observational studies. Some of the most recent ones looked at stress drop from the spectra of earthquakes using borehole seismometers and saw a roughly constant value of stress drop with earthquake size down to $M_W 0$,

41

although a proportionally larger increase of stress drop with increasing size at the lower magnitude ranges could not be excluded (Abercrombie and Leary, 1993 ; Abercrombie, 1995). Other studies have suggested an increase of stress drop with size of the earthquake, but could not for certain determine if this was real or an artifact caused by the attenuation of higher frequencies within the crust (Hardebeck and Hauksson,). Thus to date, different studies have shown constant stress drop with earthquake size (the majority), as well as both increasing or decreasing stress drop with earthquake size (the minority).

Considering the method of Nadeau and McEvilly (1999), assuming a circular fault and a constant rigidity μ, the relationship between the static stress drop $\Delta\sigma$ and the size of the earthquake rupture can be determined by

$$\Delta\sigma = \frac{7\pi}{16}\mu\frac{d}{\sqrt{A/\pi}} \tag{3.16}$$

(Kanamori and Anderson, 1975). The value of d was previously calculated and the area of the fault, A, that slipped during the earthquake can be determined using

$$M_0 = \mu A d \tag{3.17}$$

The plot of $\log(\Delta\sigma)$ versus $\log(M_0)$ using this method clearly shows an increasing stress drop with decreasing M_0, or size of the REs. This is opposed to most the previous earthquake scaling studies that show stress drop as being roughly constant over all earthquake sizes. Traditional stress drops have been observed in the $0.01 - 60$ bar range (Abercrombie, 1995 ; Hanks and McGuire, 1981) while the Nadeau and McEvilly method can have kilobar-level stress drops for the smallest earthquakes (M1 to lower M2 range) (Nadeau and Johnson, 1998).

Interestingly, if we combine moment magnitude relationship of Hanks and Kanamori (1979) with

$$M_0 = \mu A d \tag{3.18}$$

and the stress drop relationship of (Kanamori and Anderson, 1975) we can obtain

$$d = \frac{10^{(1.5M_w + 16.05)}\Delta\sigma^2}{\mu^3\pi^3 d^2 (7/16)^2} \tag{3.19}$$

$$d = \frac{\Delta\sigma^{2/3} 10^{0.5M_w} \sqrt[3]{\dfrac{10^{16.05}}{(7/16)^2}}}{\mu} \tag{3.20}$$

$$\log(d) = \log\left(\frac{\Delta\sigma^{2/3}}{\mu}\right) + 0.5M_w + 5.092. \tag{3.21}$$

A comparison between slip values, d, determined from the Nadeau and McEvilly (1999) relationship and slip values determined from the above derived relationship can be shown to match if stress drop increases with decreasing magnitude.

3.4 Results

The range of ~22-year cumulative slip amounts calculated at individual patches along the fault plane using RE data on the San Andreas, southern Calaveras-Paicines, and Quien Sabe faults is determined to be between $5.5 - 58.2$ cm, $4.8 - 14.1$ cm, and $4.9 - 24.8$ cm, respectively (Figure 3.2). This corresponds to a range of average slip
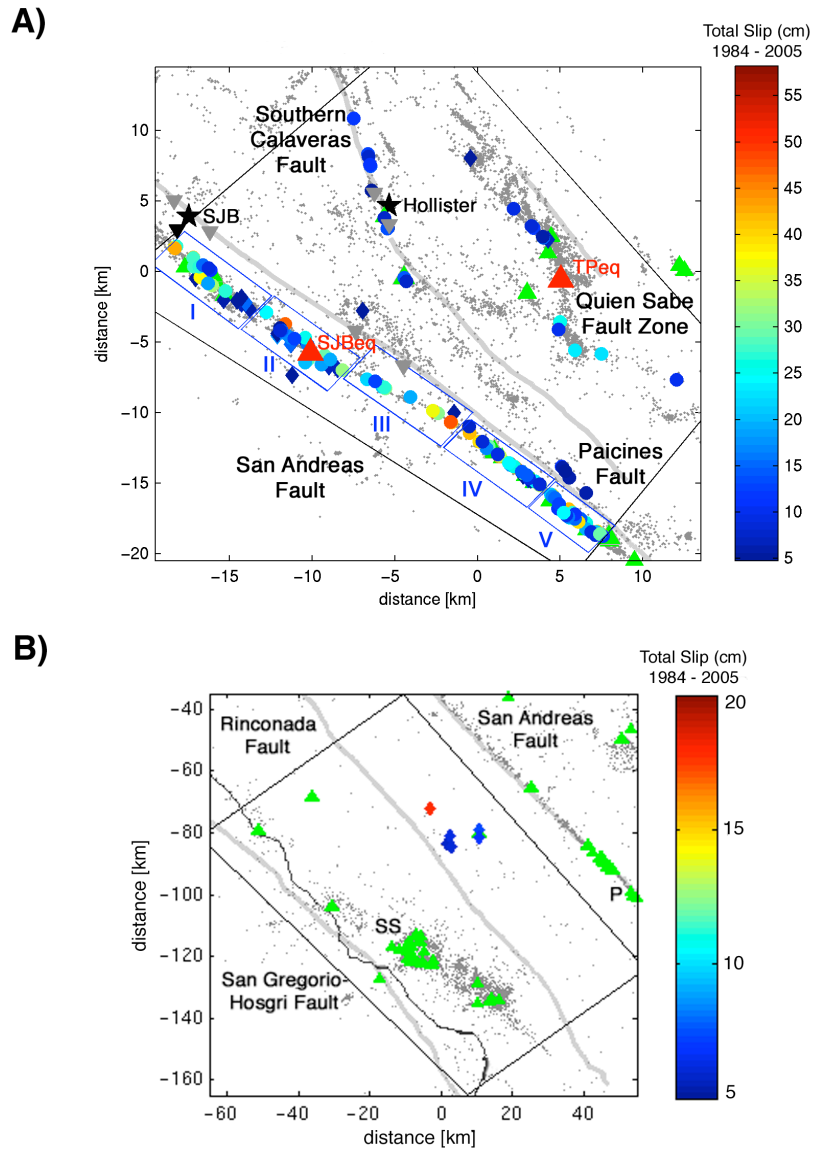
Figure 3.2: A) Map of the juncture of the San Andreas and Calaveras faults. Extent of study area indicated by black box. Blue boxes indicate subsections I – V on the San Andreas fault discussed within the text. RE locations as large colored circles, burst type REs as colored diamonds, and fault traces as thick grey lines. Background seismicity relocated by Ellsworth et al. (2000) as small grey dots, earthquakes larger than M4.0 as green triangles, green triangles with grey outline indicate catalog locations of earthquakes greater than M4.0 that were not included in the relocated catalog. Two largest earthquakes to occur in the study area are indicated by large red triangles labeled TPeq, for the Ml 5.5 1986 Tres Piños earthquake, and SJBeq, for the Mw 5.1 1989 San Juan Bautista earthquake. Creepmeters are indicated by inverted grey triangles and strainmeter by the inverted black triangle. Cities are indicated by black stars and labeled SJB, for the city of San Juan Bautista, and Hollister, for the city of Hollister.

44

rates between 2.5 – 26.7 mm/yr, 2.2 – 6.5 mm/yr, and 2.2 – 11.4 mm/yr, respectively, if we divide D_{tot}, by the time of the observation window, 21.83 yrs. Histogram distributions of the cumulative slip on these three faults can be seen in Figure 3.3 where the number of RE sequences with similar cumulative slip amounts are sorted into 6 cm bins. The repeating earthquake sequences in this dataset have average magnitudes between M1.3 and M3.2. We document all RE event information and slip estimates determined in this study in Table 3.1.

Although we present slip rates for the San Andreas, southern Calaveras-Paicines and Quien Sabe faults, we will primarily focus on cumulative slip amounts when comparing the magnitude of slip between faults in this study since slip rates on two of our target faults are low and vary in time. This can be seen in the fact that the majority of RE sequences along the Quien Sabe and southern Calaveras-Paicines faults repeat only two or three times over the observation period. This is illustrated graphically in Figures 3.4 and 3.5 which show the occurrence and timing of events within individual sequences on these two faults throughout the observation period. Conversely, sequences on the San Andreas fault are seen to repeat up to 10 times (Figure 3.6). Here the repeat interval between events is short enough with respect to the observation window that a reasonably accurate estimate of the creep rate on the fault is possible since several cycles of loading and rupture are observed.

3.4.1 San Andreas Fault Repeating REs
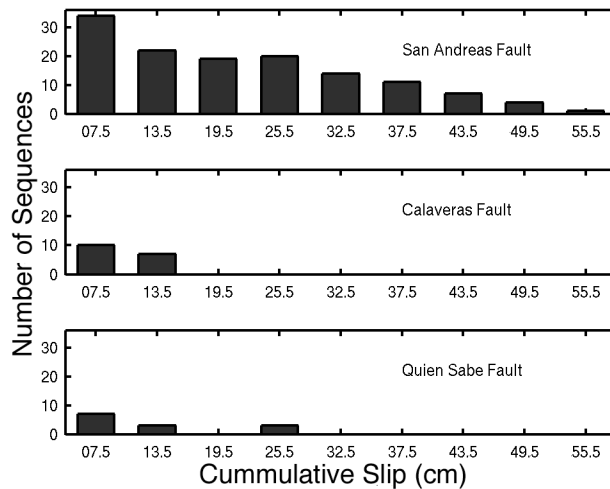
Figure 3.3: Histogram plots showing the number of RE sequences on each of the three faults in the San Andreas-southern Calaveras study area sorted into 6 cm cumulative slip bins. X label indicates the median slip value of the bins.

On the San Andreas fault, RE sequences occur on the fault throughout the seismogenic zone between approximately 1 – 15 km depths, sometimes on horizontal linear streaks of seismicity (Figure 3.7). As seen in previous studies (Breckenridge et al., 1997 ; Schaff et al., 1998 ; Nadeau and McEvilly, 2004), the Mw6.9 1989 Loma Prieta earthquake, which occurred approximately 30 km to the north of our study area, produced a strong increase in creep rate along the San Andreas fault. This increase in creep was strongest in the northwestern portion of the San Andreas fault studied and weaker in the southeastern portion. This can be seen in terms of RE inferred deep creep in Figure 3.6 by comparing the recurrence intervals and timing of events between Sections I and V before and after the Loma Prieta earthquake. In Section I, RE sequences were seen to start or to increase their frequency after the Loma Prieta earthquake while in Section V, sequences did not appear to be strongly influenced by
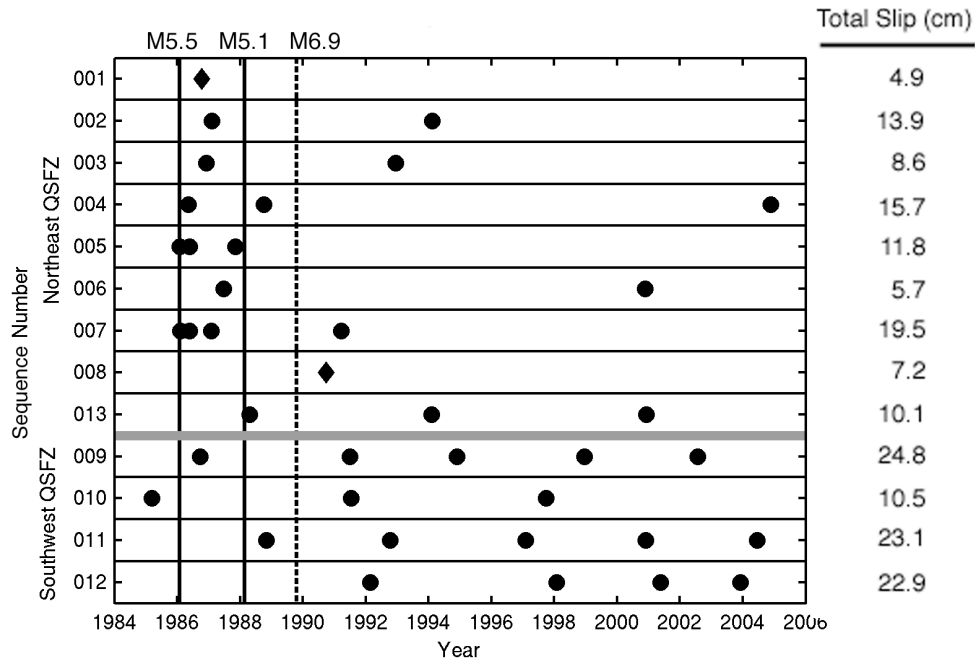
Figure 3.4: Occurrence of REs though time for all RE sequences located on the Quien Sabe fault zone. Cumulative total slip at a sequence location over the observation period is shown in centimeters. Time is in years. Thick grey horizontal line separates sequences found on the northeastern segment of the fault (top) from those found on the southwestern segment (bottom). Dashed vertical line indicates the time of the Mw6.9 1989 Loma Prieta earthquake. Solid vertical black lines indicate the time of nearby earthquakes larger than M4.7. Magnitudes of the large nearby earthquakes indicated at top of plot.

the earthquake (Figure 3.6). Section II shows a disrupted creep zone, an area with

significantly fewer REs, that had been previously identified by Nadeau and McEvilly

(2004) to be a locked segment of the San Andreas fault which ruptured as the Mw5.1

12 August 1998 San Juan Bautista event. Consequently, directly after the Loma Prieta

earthquake, an increase in the amount of creep was not observed in this area.

However, a clear and immediate effect on the San Andreas RE sequences in

Section II occurred after the 1998 Mw5.1 San Juan Bautista event (Uhrhammer et al.,
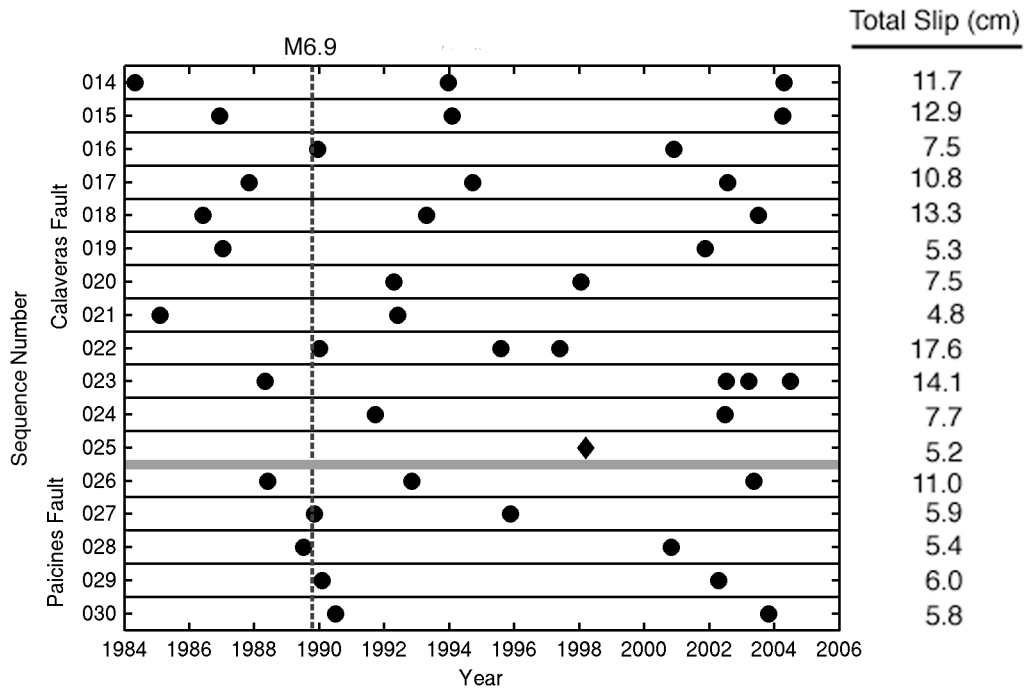
Figure 3.5: Occurrence of REs though time for all RE sequences located on the Calaveras-Paicines fault. Cumulative total slip at a sequence location over the observation period is shown in centimeters and time is in years. Thick grey horizontal line separates sequences found on the southern Calaveras fault from those found on the Paicines fault. Dashed vertical line indicates the time of the Mw6.9 1989 Loma Prieta earthquake. Solid vertical black lines indicate the time of nearby earthquakes larger than M4.7. Magnitudes of the large nearby earthquakes indicated at top of plot.

1999) (Figure 3.6). It increased the frequency of RE repeat times of sequences up to 3.5 km away.

The largest event to occur within our study area during the observation period was the Ml 5.5 Tres Piños earthquake that occurred on 26 January 1986 on the Quien Sabe fault zone. This event also had a M4.0 aftershock a few hours after the mainshock on the northeast segment of the Quien Sabe fault zone. Although this event produced up to ~5 mm of creep at the surface of the San Andreas fault (Simpson et al.,

Total Slip (cm)

M4.7   M6.9   M5.1

		Total Slip (cm)
Section I	032	37.2
	033	42.3
	034	41.4
	036	27.7
Section II	053	17.2
	140	5.5
	141	7.4
	063	22.1
Section III	072	47.9
	073	46.9
	084	45.0
	087	17.6
Section V	124	21.3
	126	29.6
	128	39.5
	129	11.1

Sequence Number

1984 1986 1988 1990 1992 1994 1996 1998 2000 2002 2004 2006
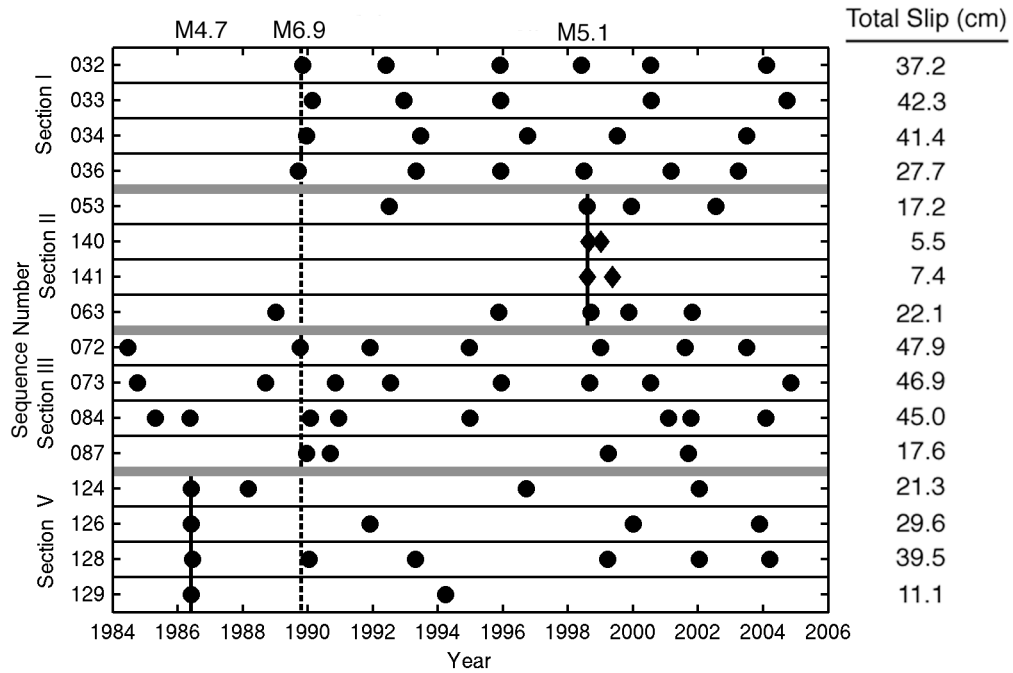
Year

Table 3.6: Occurrence of REs though time for a subset of RE sequences located on the San Andreas fault. Cumulative total slip at a sequence location over the observation period is shown in centimeters. Time is in years. Thick grey horizontal lines separate four different subsections of the fault with Section I as the northernmost section within the study area and Section V as the southernmost. Sequence numbers are the numerical label names associated with each RE sequence. Dashed vertical line indicates the time of the Mw6.9 1989 Loma Prieta earthquake. Solid vertical black lines indicate the time of nearby earthquakes larger than M4.7. Magnitudes of the large nearby earthquakes indicated at top of plot.

1988), there is no clear indication of a change in the rate of creep at depth on the San

Andreas from the RE data.

Additionally, a M4.7 event occurred on 31 May 1986 just south of our study

area on the San Andreas fault. This event appears to influence the timing of 5 RE

sequences up to 1.5 km away (Section V of Figure 3.6). Another M4.7 event that

occurred on 28 December 2001 on the study area's southern boundary on the San

Andreas fault, did not produce a clear and consistent effect upon the timing of nearby

RE sequences.
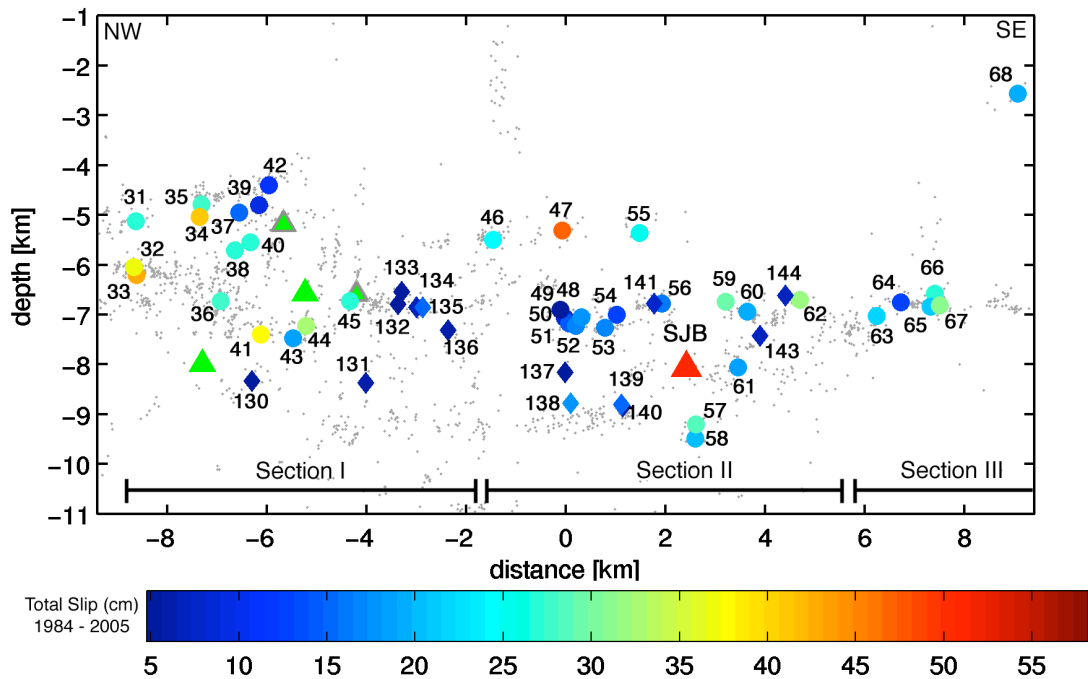
Figure 3.7: Cross-section map of northern portion of San Andreas Fault studied. REs as colored circles and labels are individual sequence names for reference. Sequence label numbers increase from northwest to southeast. Burst type REs are colored triangles and labels are individual sequence names for reference. Burst type RE sequence label numbers increase from northwest to southeast. Color indicates the cumulative amount of slip at each sequence location over the observation period. Small dots are background seismicity from the hypoDD-relocated catalog of Ellsworth et al. (2000). Triangles indicate earthquakes larger than M4.0 and green triangles with grey outline indicate catalog locations of earthquakes greater than M4.0 that were not included in the relocated catalog. Red triangle labeled SJB is the Mw5.1 1998 San Juan Bautista event.

3.4.2 Calaveras-Paicines Fault REs

On the Calaveras-Paicines fault, RE sequences occur between 3 – 9 km depth sometimes on short subhorizontal linear streaks of seismicity (Figure 3.S4). Several fault strands are seismically active in the general location of the Calaveras fault zone in this area (Figure 3.2A); nonetheless RE sequences can only confirm that one structure is actively creeping at depth throughout the observation period. Interestingly,

50

RE sequences are not found in the transition zone between the southern Calaveras and Paicines faults, 5 km south of Hollister. The Paicines fault does not appear to merge with the San Andreas fault at depth as the repeating sequences delineate two creeping fault strands 1.6 km apart at 4.5 - 5 km depth (Figures 3.2A and 3.S6). The background seismicity is extremely sparse along the Paicines fault, but it also appears to suggest that the Paicines and San Andreas faults are separate down to 11 km (Figure 3.S6).

It is unclear if nearby larger events on other faults, such as the Mw6.9 Loma Prieta and the Mw5.1 San Juan Bautista earthquakes on the San Andreas fault, affect the timing of RE sequences on the southern Calaveras-Paicines fault (Figure 3.5). Additionally, two events larger than M4.0 occurred on the Calaveras fault during our observation period; however for both events, a M4.2 event in 1997 and a M4.3 event in 2003, it was unclear if they influenced the timing of RE sequences since an obvious response from nearby RE sequences was not observed (Figure 3.5).

3.4.3 Quien Sabe Fault REs

The smaller Quien Sabe fault zone is more structurally complex than the more mature San Andreas and southern Calaveras-Paicines faults and does not appear to have any linear streaks of seismicity, suggesting that streaks and a relatively simple fault geometry are not a requirement for deep fault creep or for the production of REs (Figures 3.2A and 3.S1). RE sequences occur between 3 – 10 km depth and delineate two planar structures on the Quien Sabe fault zone. The northeast segment is a slightly west-dipping fault plane that is connected to an east dipping fault plane by a

seismically active fault structure that was ruptured by the Ml 5.5 Tres Piños earthquake.

The timing of REs on the northeast segment of the Quien Sabe fault zone was clearly affected by the 26 January 1986 Tres Piños earthquake (Figure 3.4). Two repeating clusters on the northeast segment, sequences 5 and 7, just over 4.5 km away from the mainshock began within two weeks of this event and had repeat intervals that increased with time from the mainshock. The majority of the remaining sequences on the northeast segment produced an earthquake within a year or two of the mainshock, repeated before the mid-1990s, and have been aseismic since. Total slip at individual sequence locations on this segment was determined to be between 5.7 - 15.7 cm. During the observation period, the total slip averaged over all sequences on this segment was 11.0 cm. This is in contrast to RE sequences found on the southwest segment where the total slip at sequence locations was between 10.5 – 24.8 cm with an averaged total slip of 20.3 cm over all sequences on this segment. It is unclear if creep on the southwest segment was initiated or influenced by the Tres Piños mainshock since the pre-mainshock time period is very limited. Interestingly, these sequences occur with quasi-periodic recurrence intervals unlike the strikingly aperiodic recurrence intervals of the northeast segment, suggesting that this fault plane has been steadily creeping over the entire observation period (Figure 3.4).

Neither the Loma Prieta earthquake nor the San Juan Bautista earthquake produced a notable effect on the timing of RE sequences on the Quien Sabe fault zone. Additionally, two other earthquakes greater than M4.0, a 1987 M4.1 event and a 1988 M5.1 event, which also occurred on the Quien Sabe fault zone during our observation

52

period, produced no obvious effect on the timing of events within RE sequences. This was surprising since the M4.1 event occurred a few kilometers below several of the RE sequences on the northeast segment and the closest RE sequence to the M5.1 event was just over 2.5 km away. However, it is important to note that any influence that these smaller events may have exerted on the RE sequences may be indistinguishable from the influence of the larger Tres Piños event.

3.4.4 Burst Type REs

As described earlier, some repeating earthquake sequences involve events that recur within hours or days of each other. We refer to these as burst type REs. In the San Andreas fault juncture region, 24 burst type REs are identified to have occurred during the observation period. Of these, 3 burst type RE sequences (Sequences 1, 8, and 25) are located off the major fault planes that are inferred to creep and are composed only of two events each (Figure 3.2). Individual events within these 3 RE sequences occurred within 3 days of each other. Sequences 1 and 8 occurred near the northeast segment of the Quien Sabe fault zone and do not appear to be directly associated with the timing of nearby larger events (Figures 3.6 and 3.S1). Sequence 1 occurred in 1986, a few months after the Ml 5.5 Tres Piños earthquake while Sequence 8 occurred in 1990, 4 years after the Tres Piños event and more than 2 years after the nearest event greater than M4.0. Sequence 25 is located between the Calaveras and San Andreas fault and occurred in 1998, several months before the nearby Mw5.1 San Juan Bautista event would occur on the San Andreas fault (Figures 3.5 and 3.S3).

The remaining 21 burst sequences all occurred on the San Andreas fault and had between 2 and 4 individual events within each sequence. The shortest time interval between events within a sequence on the San Andreas fault was less than one minute. Interestingly, burst sequences containing 4 events typically had the first three events occur between minutes to days of one another while the last event often occurred between months to up to 1.5 years apart from the other sequence members. Of the 21 burst type events located here,14 occurred close in time and space to the Mw5.1 San Juan Bautista event and subsequent slow earthquake (Figures 3.S9 and 3.S10). The remaining 7 were located to the south of the San Juan Bautista segment and do not appear to be clustered in either time or space (Figures 3.S9 and 3.S10). All burst-type sequences are seen to be preferentially located along the lower edge of the areas in which RE sequences are identified.

3.4.5 Southern Coast Ranges REs

It has been suggested that one reason for the occurrence of creep on faults lies in the mineralogy of fault zone rocks. Along the San Andreas fault system, particular attention has been paid to the apparent correspondence of outcrops of serpentinite and the ability of the fault to creep (Irwin and Barnes, 1975). To investigate the occurrence of REs on fault planes not associated with the material contrasts across the primary San Andreas fault system, we examine the seismicity west of the creeping segment of the San Andreas fault (Box B in Figure 3.1). The southern Coast Ranges are dominantly made up of Salinian granites and associated sedimentary and metamorphic units. However, this area also includes the fault that produced the Mw6.5

22 December 2003 San Simeon earthquake and associated aftershock sequence, which

appears to have occurred entirely within coastal Franciscan rocks (Hauksson et al.,

2004). Our analysis shows that only 6 burst type REs occurred within this area

between 1 March 1984 and 1 May 2005 (Figure 3.2B) and that no non-burst type

sequences occurred. The burst sequences were only active for 1 – 42 days and seem to

cluster to the north of the main rupture area of the San Simeon earthquake. A small

M4.3 earthquake, which occurred in 1985, also appears to have occurred nearby.

However, it is unclear if it affected the timing of the burst events. Since the last burst

type RE observed in this area occurred in 2000, none were temporally associated with

the aftershock sequence of the San Simeon earthquake, which produced ~5,500 of the

events investigated in this study region, but not a single RE pair.

1	36.8822	-121.3462	6.21	1.39	4.9	0.23	
	1986.287.012625	36.8820		-121.3432		6.58	1.36
	1986.290.150349	36.8825		-121.3493		5.85	1.42
2	36.8508	-121.3144	5.67	1.95	9.2	0.42	
	1987.041.081555	36.8505		-121.3152		5.57	2.08
	1994.043.163835	36.8508		-121.3148		5.71	1.80
	2005.214.165507	36.8512		-121.3132		5.72	1.96
3	36.8401	-121.3019	4.29	2.33	8.6	0.39	
	1986.336.023245	36.8400		-121.3015		4.32	2.34
	1992.351.062630	36.8402		-121.3023		4.25	2.32
4	36.8396	-121.3014	4.32	2.15	15.7	0.72	
	1986.126.234806	36.8382		-121.3017		4.03	1.84
	1988.279.230916	36.8392		-121.3017		4.41	2.33
	2004.322.164418	36.8413		-121.3010		4.51	2.27

Table 3.1A: First line within each row indicates the sequence label number, average
sequence latitude, average sequence longitude, average sequence depth, average
sequence magnitude, total amount of slip (cm), and slip rate (mm/yr) at sequence
location. Following lines indicate earthquake time, earthquake latitude, earthquake
longitude, earthquake depth, and earthquake magnitude for each individual event
within a repeating earthquake sequence.

	Lat	Lon	Depth	Mag	Slip	Slip rate
5	36.8375	-121.3014	4.09	1.69	11.8	0.54
1986.031.024320	36.8378	-121.3013	4.15	1.71		
1986.141.133948	36.8373	-121.3008	4.08	1.73		
1987.312.130323	36.8373	-121.3020	4.03	1.63		
6	36.8336	-121.2963	4.09	1.62	5.7	0.26
1987.175.092323	36.8328	-121.2962	3.98	1.50		
2000.327.023425	36.8343	-121.2963	4.21	1.70		
7	36.8327	-121.2949	3.65	1.38	15.6	0.72
1986.038.053103	36.8323	-121.2948	3.68	1.37		
1986.147.020422	36.8347	-121.2947	3.73	1.45		
1987.033.231814	36.8320	-121.2953	3.44	1.25		
1991.079.123647	36.8318	-121.2942	3.64	1.39		
2005.325.131528	36.8328	-121.2953	3.76	1.46		
8	36.8310	-121.2903	6.03	2.03	7.2	0.33
1990.274.151720	36.8310	-121.2903	5.95	2.13		
1990.276.162009	36.8310	-121.2903	6.11	1.88		
9	36.7770	-121.2855	9.24	1.78	24.8	1.14
1986.268.110034	36.7757	-121.2860	9.11	1.70		
1991.181.225923	36.7772	-121.2860	9.42	1.84		
1994.333.051017	36.7765	-121.2857	9.13	1.74		
1998.352.043752	36.7777	-121.2852	9.33	1.80		
2002.207.114807	36.7780	-121.2848	9.23	1.78		
10	36.7715	-121.2859	8.05	1.39	10.5	0.48
1985.068.092002	36.7710	-121.2865	7.88	1.24		
1991.197.114701	36.7715	-121.2850	8.09	1.37		
1997.269.091506	36.7720	-121.2862	8.17	1.57		
11	36.7598	-121.2732	7.88	1.66	23.1	1.06
1988.303.160739	36.7585	-121.2755	8.11	1.61		
1992.281.065555	36.7582	-121.2740	7.97	1.67		
1997.034.171328	36.7610	-121.2697	7.75	1.62		
2000.331.162358	36.7615	-121.2742	7.70	1.71		
2004.168.060645	36.7598	-121.2728	7.87	1.67		

Table 3.1B: First line within each row indicates the sequence label number, average sequence latitude, average sequence longitude, average sequence depth, average sequence magnitude, total amount of slip (cm), and slip rate (mm/yr) at sequence location. Following lines indicate earthquake time, earthquake latitude, earthquake longitude, earthquake depth, and earthquake magnitude for each individual event within a repeating earthquake sequence.

12	36.7552	-121.2575	9.95	1.64	22.9	1.05
1992.050.161728	36.7538	-121.2560	9.45	1.60		
1998.023.220648	36.7557	-121.2570	9.96	1.59		
2001.137.090320	36.7552	-121.2573	10.18	1.47		
2001.137.091621	36.7562	-121.2587	10.32	1.26		
2003.336.085237	36.7550	-121.2585	9.86	1.87		
13	36.7390	-121.2042	9.57	1.43	10.1	0.46
1988.113.011141	36.7388	-121.2048	9.78	1.32		
1994.035.101918	36.7370	-121.2050	9.22	1.44		
2000.344.024753	36.7412	-121.2028	9.72	1.49		
14	36.9054	-121.4226	3.88	1.68	11.7	0.54
1984.118.024658	36.9075	-121.4223	3.68	1.81		
1993.354.034334	36.9043	-121.4227	3.71	1.60		
2004.108.042349	36.9043	-121.4228	4.26	1.56		
15	36.8848	-121.4156	7.36	1.81	12.8	0.59
1986.335.233040	36.8842	-121.4157	6.75	1.63		
1994.032.023608	36.8847	-121.4155	7.84	1.82		
2004.093.012458	36.8855	-121.4155	7.49	1.97		
16	36.8837	-121.4144	7.71	2.10	7.5	0.34
1989.348.214135	36.8828	-121.4168	7.08	1.95		
2000.329.123504	36.8845	-121.4120	8.35	2.19		
17	36.8777	-121.4142	7.90	1.54	10.8	0.49
1987.307.123255	36.8767	-121.4150	7.44	1.42		
1994.261.114157	36.8777	-121.4135	8.04	1.69		
2002.207.125728	36.8788	-121.4142	8.21	1.42		
18	36.8768	-121.4137	7.11	1.89	13.3	0.61
1986.149.192036	36.8762	-121.4137	7.14	1.83		
1993.106.171630	36.8767	-121.4140	7.24	1.96		
2003.187.104403	36.8777	-121.4135	6.95	1.88		

Table 3.1C: First line within each row indicates the sequence label number, average sequence latitude, average sequence longitude, average sequence depth, average sequence magnitude, total amount of slip (cm), and slip rate (mm/yr) at sequence location. Following lines indicate earthquake time, earthquake latitude, earthquake longitude, earthquake depth, and earthquake magnitude for each individual event within a repeating earthquake sequence.

19	36.8580	-121.4168	4.29	1.52	5.3	0.24	
	1987.011.083259	36.8570		-121.4158		3.96	1.40
	2001.319.100445	36.8590		-121.4178		4.63	1.61
20	36.8372	-121.4093	8.44	2.09	7.4	0.34	
	1992.104.113535	36.8363		-121.4082		8.45	2.12
	1998.015.065327	36.8380		-121.4105		8.43	2.05
21	36.8301	-121.4082	8.23	1.34	4.8	0.22	
	1985.034.151654	36.8302		-121.4088		7.92	1.24
	1992.150.143602	36.8300		-121.4075		8.54	1.43
22	36.8305	-121.4078	8.51	1.57	13.2	0.60	
	1990.002.160818	36.8313		-121.4107		7.73	1.43
	1995.212.230230	36.8287		-121.4052		8.84	1.28
	1997.142.065559	36.8310		-121.4083		8.47	1.91
	2005.284.003258	36.8310		-121.4072		9.01	1.67
23	36.8042	-121.3900	6.14	1.32	14.1	0.65	
	1988.117.162731	36.8043		-121.3900		5.97	1.28
	2002.189.095808	36.8050		-121.3897		6.77	1.41
	2003.080.105655	36.8038		-121.3907		5.85	1.22
	2004.180.075313	36.8038		-121.3895		5.97	1.29
24	36.8010	-121.3882	6.76	2.15	7.7	0.35	
	1991.262.220820	36.8012		-121.3877		6.34	2.22
	2002.176.211023	36.8008		-121.3888		7.18	2.06
25	36.7858	-121.4076	8.67	1.46	5.1	0.24	
	1998.075.010646	36.7900		-121.4143		9.05	1.46
	1998.075.025955	36.7815		-121.4008		8.29	1.46
26	36.6894	-121.2828	4.66	1.57	11.0	0.51	
	1988.148.150832	36.6893		-121.2823		4.43	1.53
	1992.307.032239	36.6890		-121.2847		4.65	1.52
	2003.134.111235	36.6900		-121.2815		4.90	1.67

Table 3.1D: First line within each row indicates the sequence label number, average sequence latitude, average sequence longitude, average sequence depth, average sequence magnitude, total amount of slip (cm), and slip rate (mm/yr) at sequence location. Following lines indicate earthquake time, earthquake latitude, earthquake longitude, earthquake depth, and earthquake magnitude for each individual event within a repeating earthquake sequence.

27	36.6872	-121.2814	4.55	1.69	5.9	0.27	
	1989.307.075612	36.6882		-121.2813		4.78	1.81
	1995.318.195757	36.6863		-121.2815		4.33	1.48
28	36.6863	-121.2803	5.14	1.54	5.4	0.25	
	1989.183.203342	36.6862		-121.2798		5.06	1.61
	2000.299.183005	36.6865		-121.2808		5.23	1.44
29	36.6812	-121.2764	5.17	1.72	6.0	0.27	
	1990.030.100609	36.6807		-121.2760		5.25	1.70
	2002.102.074911	36.6818		-121.2768		5.09	1.73
30	36.6706	-121.2633	4.33	1.67	5.8	0.27	
	1990.180.015856	36.6708		-121.2640		4.42	1.76
	2003.304.112334	36.6703		-121.2627		4.25	1.54
31	36.8248	-121.5437	4.30	1.91	26.8	1.23	
	1990.357.105918	36.8258		-121.5415		4.54	2.01
	1993.222.023809	36.8247		-121.5428		4.58	1.91
	1996.290.082711	36.8247		-121.5438		4.56	1.89
	1999.101.092944	36.8255		-121.5440		4.22	1.86
	2002.055.013356	36.8232		-121.5462		3.58	1.95
32	36.8238	-121.5462	5.88	2.09	37.2	1.70	
	1989.305.145200	36.8233		-121.5463		5.69	2.03
	1992.148.151316	36.8248		-121.5482		6.03	2.08
	1995.335.033532	36.8235		-121.5462		6.17	2.13
	1998.152.122936	36.8243		-121.5458		5.61	1.99
	2000.198.083816	36.8240		-121.5467		6.22	2.11
	2004.037.193757	36.8232		-121.5440		5.54	2.10
33	36.8242	-121.5483	6.30	2.69	42.3	1.94	
	1990.048.184836	36.8237		-121.5463		6.17	2.70
	1992.347.170455	36.8245		-121.5487		6.50	2.69
	1995.336.065633	36.8237		-121.5478		6.15	2.64
	2000.206.183004	36.8232		-121.5455		6.17	2.69
	2004.264.144029	36.8260		-121.5530		6.51	2.72

Table 3.1E: First line within each row indicates the sequence label number, average sequence latitude, average sequence longitude, average sequence depth, average sequence magnitude, total amount of slip (cm), and slip rate (mm/yr) at sequence location. Following lines indicate earthquake time, earthquake latitude, earthquake longitude, earthquake depth, and earthquake magnitude for each individual event within a repeating earthquake sequence.

34	36.8194	-121.5362	5.23	2.65	41.4	1.89	
	1989.349.083832	36.8203	-121.5380	5.66	2.65		
	1993.169.233628	36.8173	-121.5332	4.78	2.56		
	1996.277.135708	36.8178	-121.5335	4.66	2.68		
	1999.190.032220	36.8202	-121.5375	5.74	2.42		
	2003.176.090818	36.8213	-121.5388	5.30	2.72		
35	36.8192	-121.5338	4.48	1.58	27.6	1.26	
	1985.354.225323	36.8192	-121.5310	4.66	1.53		
	1992.325.075643	36.8185	-121.5347	4.47	1.56		
	1995.337.123023	36.8198	-121.5368	5.00	1.65		
	1999.153.182841	36.8190	-121.5315	4.12	1.62		
	2001.238.084333	36.8187	-121.5312	4.37	1.60		
	2004.162.023924	36.8197	-121.5377	4.23	1.31		
36	36.8119	-121.5311	6.59	1.59	27.7	1.27	
	1989.256.024054	36.8122	-121.5307	6.53	1.54		
	1993.116.202008	36.8132	-121.5318	6.71	1.53		
	1995.337.093550	36.8125	-121.5345	7.20	1.67		
	1998.181.153430	36.8117	-121.5302	6.46	1.60		
	2001.060.123957	36.8113	-121.5293	6.51	1.59		
	2003.087.065914	36.8107	-121.5302	6.12	1.61		
37	36.8125	-121.5285	5.15	2.14	15.3	0.70	
	1986.326.112338	36.8118	-121.5295	4.58	2.24		
	1993.289.161909	36.8113	-121.5272	5.05	2.14		
	1999.148.083539	36.8145	-121.5288	5.82	2.09		
38	36.8112	-121.5286	5.57	2.39	26.6	1.22	
	1988.168.203227	36.8115	-121.5275	5.23	2.42		
	1991.265.021843	36.8112	-121.5288	5.83	2.36		
	1995.345.211440	36.8112	-121.5298	5.50	2.56		
	2001.319.185806	36.8108	-121.5285	5.71	2.37		
39	36.8117	-121.5229	4.93	2.55	9.8	0.45	
	1988.046.162841	36.8098	-121.5195	4.21	2.49		
	1994.228.210154	36.8135	-121.5262	5.65	2.59		

Table 3.1F: First line within each row indicates the sequence label number, average sequence latitude, average sequence longitude, average sequence depth, average sequence magnitude, total amount of slip (cm), and slip rate (mm/yr) at sequence location. Following lines indicate earthquake time, earthquake latitude, earthquake longitude, earthquake depth, and earthquake magnitude for each individual event within a repeating earthquake sequence.

40	36.8102	-121.5265	5.31	1.51	26.5	1.21	
	1985.306.072639	36.8118	-121.5262	5.07	1.49		
	1990.041.104339	36.8103	-121.5257	5.24	1.53		
	1991.349.171640	36.8097	-121.5270	5.35	1.51		
	1995.013.220048	36.8102	-121.5267	5.54	1.52		
	1996.352.114632	36.8090	-121.5263	5.27	1.46		
	1999.226.035627	36.8100	-121.5270	5.40	1.56		
41	36.8041	-121.5264	7.35	2.12	37.9	1.73	
	1987.123.161225	36.8033	-121.5277	7.54	2.20		
	1992.316.090153	36.8045	-121.5265	7.51	2.14		
	1996.180.015453	36.8035	-121.5257	6.94	2.10		
	1998.152.142450	36.8033	-121.5260	7.31	2.19		
	1999.087.132726	36.8052	-121.5268	7.46	2.06		
	2001.281.014139	36.8050	-121.5258	7.33	1.97		
42	36.8074	-121.5199	3.89	1.62	11.3	0.52	
	1989.162.112214	36.8040	-121.5197	2.86	1.62		
	1991.060.122450	36.8105	-121.5195	4.06	1.60		
	1995.259.224551	36.8078	-121.5205	4.75	1.76		
43	36.7990	-121.5240	7.34	2.49	18.8	0.86	
	1986.102.115112	36.7997	-121.5267	7.57	2.14		
	1992.306.175815	36.7982	-121.5212	6.82	2.50		
	1998.150.125144	36.7992	-121.5242	7.63	2.49		
44	36.7985	-121.5204	7.05	2.23	32.3	1.48	
	1989.311.071244	36.7983	-121.5220	7.98	2.38		
	1992.307.030916	36.7987	-121.5195	6.98	2.33		
	1995.148.040959	36.7975	-121.5203	6.90	1.97		
	1999.172.034437	36.7990	-121.5197	6.24	2.13		
	2005.038.002158	36.7992	-121.5207	7.15	2.23		

Table 3.1G: First line within each row indicates the sequence label number, average sequence latitude, average sequence longitude, average sequence depth, average sequence magnitude, total amount of slip (cm), and slip rate (mm/yr) at sequence location. Following lines indicate earthquake time, earthquake latitude, earthquake longitude, earthquake depth, and earthquake magnitude for each individual event within a repeating earthquake sequence.

45	36.7983	-121.5094	6.67	1.25	27.3	1.25
	1990.294.214701	36.7985	-121.5102	7.10	1.19	
	1992.344.120245	36.7968	-121.5050	6.80	1.23	
	1995.333.192325	36.7992	-121.5120	6.21	1.43	
	1996.207.233211	36.7985	-121.5090	5.81	1.39	
	1998.234.025259	36.7993	-121.5095	6.54	1.25	
	2001.043.025659	36.7978	-121.5085	6.96	1.25	
	2002.018.024738	36.7980	-121.5113	7.25	1.33	
46	36.7822	-121.4809	4.38	1.74	24.2	1.11
	1990.034.230635	36.7808	-121.4778	2.97	1.77	
	1993.028.160939	36.7815	-121.4778	5.04	1.74	
	1995.333.173115	36.7837	-121.4825	4.58	1.61	
	1999.330.111921	36.7832	-121.4830	5.50	1.62	
	2002.054.105024	36.7818	-121.4833	3.82	1.78	
47	36.7748	-121.4719	4.73	2.85	46.5	2.13
	1985.305.104857	36.7750	-121.4700	4.53	2.88	
	1991.322.191637	36.7753	-121.4712	4.95	2.87	
	1997.072.032429	36.7740	-121.4733	5.01	2.84	
	2000.217.073214	36.7743	-121.4723	4.73	2.85	
	2004.121.080214	36.7755	-121.4727	4.42	2.84	
48	36.7738	-121.4744	6.46	1.58	5.5	0.25
	1989.325.133541	36.7742	-121.4717	6.38	1.54	
	1998.225.082335	36.7735	-121.4772	6.55	1.62	
49	36.7689	-121.4740	6.49	2.27	8.3	0.38
	1984.251.040304	36.7692	-121.4727	6.47	2.42	
	1993.270.182605	36.7685	-121.4752	6.51	1.96	
50	36.7702	-121.4741	6.89	2.02	14.3	0.65
	1987.127.161215	36.7697	-121.4740	6.86	2.10	
	1999.002.054002	36.7703	-121.4742	6.89	2.02	
	2000.167.020225	36.7707	-121.4740	6.93	2.00	

Table 3.1H: First line within each row indicates the sequence label number, average sequence latitude, average sequence longitude, average sequence depth, average sequence magnitude, total amount of slip (cm), and slip rate (mm/yr) at sequence location. Following lines indicate earthquake time, earthquake latitude, earthquake longitude, earthquake depth, and earthquake magnitude for each individual event within a repeating earthquake sequence.

51	36.7711	-121.4742	7.22	1.63	17.0	0.78	
	1987.211.121238	36.7732	-121.4722	7.21	1.59		
	1997.327.175442	36.7687	-121.4755	7.31	1.68		
	1998.227.081101	36.7710	-121.4757	7.09	1.56		
	1999.318.021134	36.7715	-121.4732	7.29	1.66		
52	36.7731	-121.4699	7.06	1.22	17.9	0.82	
	1991.007.075803	36.7738	-121.4723	7.39	1.19		
	1992.059.214445	36.7767	-121.4722	7.86	1.22		
	1998.225.071559	36.7747	-121.4717	7.02	1.35		
	1998.343.154558	36.7710	-121.4720	6.99	1.20		
	2000.209.004651	36.7695	-121.4615	6.02	1.22		
53	36.7680	-121.4666	7.04	1.65	17.2	0.79	
	1992.185.004039	36.7728	-121.4688	7.72	1.74		
	1998.216.111435	36.7663	-121.4693	6.72	1.62		
	1999.343.232200	36.7667	-121.4657	7.15	1.55		
	2002.199.151747	36.7662	-121.4625	6.55	1.67		
54	36.7627	-121.4642	6.94	2.98	12.6	0.57	
	1986.112.174750	36.7633	-121.4618	6.80	3.02		
	1998.340.141448	36.7620	-121.4667	7.08	2.94		
55	36.7662	-121.4578	4.92	2.27	24.8	1.14	
	1988.146.060417	36.7660	-121.4572	4.87	2.24		
	1994.162.040419	36.7668	-121.4568	5.15	2.29		
	2000.062.204842	36.7665	-121.4578	4.88	2.26		
	2005.029.130812	36.7655	-121.4592	4.77	2.28		
56	36.7609	-121.4567	6.50	2.20	15.9	0.73	
	1989.072.002258	36.7612	-121.4535	6.66	2.20		
	1998.225.011917	36.7608	-121.4575	6.53	2.29		
	1998.353.200952	36.7607	-121.4592	6.31	2.14		

Table 3.1I: First line within each row indicates the sequence label number, average sequence latitude, average sequence longitude, average sequence depth, average sequence magnitude, total amount of slip (cm), and slip rate (mm/yr) at sequence location. Following lines indicate earthquake time, earthquake latitude, earthquake longitude, earthquake depth, and earthquake magnitude for each individual event within a repeating earthquake sequence.

57	36.7498	-121.4537	8.82	1.65	28.7	1.32	
	1985.095.064200	36.7508	-121.4525	8.51	1.62		
	1988.263.021511	36.7492	-121.4552	8.46	1.62		
	1991.209.205109	36.7523	-121.4557	9.08	1.68		
	1999.095.102853	36.7483	-121.4548	8.77	1.67		
	2000.116.011028	36.7493	-121.4507	8.83	1.71		
	2001.262.150343	36.7488	-121.4535	9.26	1.61		
58	36.7487	-121.4602	9.44	2.58	19.9	0.91	
	1985.327.071004	36.7483	-121.4582	9.27	2.59		
	1994.194.172839	36.7498	-121.4615	9.53	2.53		
	2001.006.050451	36.7480	-121.4610	9.52	2.58		
59	36.7533	-121.4444	6.10	2.09	29.8	1.36	
	1984.289.215729	36.7557	-121.4457	6.67	2.09		
	1989.321.234406	36.7498	-121.4405	6.28	2.11		
	1993.101.194113	36.7565	-121.4457	6.82	2.03		
	1999.296.183454	36.7547	-121.4440	6.93	2.01		
	2002.055.120708	36.7498	-121.4463	3.78	2.10		
60	36.7538	-121.4394	6.71	1.87	19.6	0.90	
	1985.159.231028	36.7533	-121.4392	6.71	1.90		
	1998.244.220656	36.7520	-121.4402	6.41	1.92		
	2000.067.154112	36.7580	-121.4390	7.25	1.79		
	2003.028.000004	36.7518	-121.4393	6.49	1.85		
61	36.7488	-121.4469	8.03	2.48	18.7	0.86	
	1987.185.042914	36.7488	-121.4453	7.74	2.40		
	1993.088.045244	36.7493	-121.4463	8.09	2.53		
	1999.173.205648	36.7482	-121.4490	8.26	2.48		
62	36.7449	-121.4317	6.34	2.21	31.9	1.46	
	1988.220.121341	36.7447	-121.4310	6.32	2.25		
	1991.153.184838	36.7447	-121.4313	6.60	2.21		
	1996.138.173617	36.7458	-121.4342	5.92	2.29		
	2002.103.012118	36.7440	-121.4300	6.34	1.97		
	2002.103.021916	36.7453	-121.4318	6.52	2.07		

Table 3.1J: First line within each row indicates the sequence label number, average sequence latitude, average sequence longitude, average sequence depth, average sequence magnitude, total amount of slip (cm), and slip rate (mm/yr) at sequence location. Following lines indicate earthquake time, earthquake latitude, earthquake longitude, earthquake depth, and earthquake magnitude for each individual event within a repeating earthquake sequence.

63	36.7400	-121.4166	6.85	1.58	22.1	1.01
1989.006.030820	36.7417	-121.4178	7.18	1.58		
1995.315.173538	36.7333	-121.4155	6.02	1.67		
1998.256.115341	36.7375	-121.4178	6.49	1.71		
1999.315.091119	36.7435	-121.4157	7.14	1.57		
2001.299.234030	36.7440	-121.4162	7.42	1.55		
64	36.7401	-121.4106	6.77	1.79	12.5	0.57
1990.249.172655	36.7402	-121.4098	6.88	1.79		
1998.255.060027	36.7412	-121.4103	6.59	1.79		
2005.053.120810	36.7390	-121.4118	6.83	1.84		
65	36.7360	-121.4051	6.95	1.96	20.7	0.95
1987.174.202249	36.7370	-121.4055	6.83	1.95		
1993.126.105054	36.7343	-121.4060	7.19	1.97		
1999.239.181509	36.7353	-121.4028	6.80	1.99		
2003.208.042843	36.7372	-121.4060	6.97	1.82		
66	36.7350	-121.4026	6.33	2.38	26.5	1.21
1985.353.195842	36.7352	-121.4018	6.37	2.33		
1990.197.195820	36.7352	-121.4040	6.42	2.36		
1999.079.122740	36.7350	-121.4027	6.32	2.40		
2002.294.021906	36.7347	-121.4018	6.19	2.40		
67	36.7356	-121.4030	6.89	1.78	31.0	1.42
1985.106.121635	36.7355	-121.4032	6.81	1.77		
1987.173.031808	36.7378	-121.4028	7.24	1.71		
1990.082.205956	36.7352	-121.4043	7.06	1.76		
1997.036.194807	36.7365	-121.4028	6.55	1.79		
2001.040.011508	36.7343	-121.4012	6.63	1.89		
2003.144.085124	36.7342	-121.4037	7.03	1.90		
68	36.7329	-121.3867	2.91	1.85	19.4	0.89
1985.328.100232	36.7327	-121.3868	2.97	1.82		
1989.358.061213	36.7320	-121.3862	2.77	1.85		
1995.238.132825	36.7337	-121.3865	3.07	1.88		
2001.095.120433	36.7332	-121.3873	2.81	1.86		

Table 3.1K: First line within each row indicates the sequence label number, average sequence latitude, average sequence longitude, average sequence depth, average sequence magnitude, total amount of slip (cm), and slip rate (mm/yr) at sequence location. Following lines indicate earthquake time, earthquake latitude, earthquake longitude, earthquake depth, and earthquake magnitude for each individual event within a repeating earthquake sequence.

69	36.7234	-121.3680	2.80	2.08	37.0	1.69	
	1986.112.050420	36.7238	-121.3678	2.91	1.97		
	1991.112.234049	36.7232	-121.3682	2.71	2.11		
	1995.011.172006	36.7232	-121.3698	2.59	2.16		
	1999.074.185312	36.7238	-121.3673	2.88	2.13		
	2000.211.152009	36.7232	-121.3677	2.93	1.98		
	2003.317.000629	36.7230	-121.3673	2.81	2.04		
70	36.7226	-121.3674	2.98	1.84	51.4	2.36	
	1986.161.183027	36.7228	-121.3678	3.04	1.84		
	1989.061.014251	36.7225	-121.3672	3.17	1.79		
	1991.130.024009	36.7223	-121.3668	2.96	1.94		
	1994.214.054226	36.7230	-121.3682	2.97	1.83		
	1996.105.182755	36.7228	-121.3682	2.95	1.57		
	1997.262.012045	36.7227	-121.3682	2.94	1.56		
	2000.166.182318	36.7222	-121.3670	2.88	1.85		
	2001.275.130200	36.7222	-121.3675	2.98	1.92		
	2004.235.131809	36.7230	-121.3660	2.96	1.97		
71	36.7207	-121.3638	2.97	2.14	30.7	1.40	
	1988.206.144307	36.7177	-121.3645	2.66	2.30		
	1990.203.233821	36.7218	-121.3623	3.21	2.02		
	1994.211.150946	36.7210	-121.3653	2.83	2.14		
	1998.014.211000	36.7223	-121.3638	3.13	2.08		
	2001.284.133104	36.7208	-121.3632	3.02	2.14		
72	36.7145	-121.3560	2.96	2.21	47.9	2.19	
	1984.173.071357	36.7148	-121.3540	3.14	2.45		
	1989.279.091415	36.7147	-121.3522	2.42	2.21		
	1991.334.013427	36.7143	-121.3573	3.18	2.27		
	1994.353.112838	36.7143	-121.3577	2.97	2.21		
	1999.001.205139	36.7155	-121.3565	3.06	2.28		
	2001.221.202011	36.7145	-121.3577	3.16	2.21		
	2003.181.023150	36.7133	-121.3567	2.80	2.09		

Table 3.1L: First line within each row indicates the sequence label number, average sequence latitude, average sequence longitude, average sequence depth, average sequence magnitude, total amount of slip (cm), and slip rate (mm/yr) at sequence location. Following lines indicate earthquake time, earthquake latitude, earthquake longitude, earthquake depth, and earthquake magnitude for each individual event within a repeating earthquake sequence.

73	36.7139	-121.3577	2.67	1.91	46.9	2.15	
	1984.279.061109	36.7140	-121.3553	2.88	1.68		
	1988.253.114707	36.7135	-121.3588	2.69	1.89		
	1990.307.022934	36.7135	-121.3577	2.50	1.94		
	1992.196.005405	36.7145	-121.3595	2.50	1.92		
	1995.348.212833	36.7135	-121.3575	2.64	2.10		
	1998.243.125717	36.7143	-121.3570	2.70	1.97		
	2000.199.005258	36.7138	-121.3590	2.70	1.89		
	2004.314.150629	36.7137	-121.3567	2.73	1.91		
74	36.7142	-121.3558	3.08	1.90	39.9	1.83	
	1987.098.022828	36.7132	-121.3570	3.12	1.84		
	1990.081.213256	36.7142	-121.3543	3.12	2.09		
	1993.033.063257	36.7148	-121.3575	3.04	2.01		
	1996.142.235807	36.7142	-121.3555	2.84	1.83		
	1999.279.012625	36.7142	-121.3570	3.15	1.82		
	2001.326.220435	36.7140	-121.3568	3.14	1.90		
	2004.089.053853	36.7147	-121.3522	3.16	2.07		
75	36.7127	-121.3457	1.51	2.27	41.4	1.89	
	1986.167.212217	36.7122	-121.3428	1.38	2.27		
	1990.335.095610	36.7128	-121.3455	1.44	2.46		
	1994.061.193902	36.7130	-121.3467	1.61	2.24		
	1996.170.075924	36.7128	-121.3470	1.45	2.09		
	2000.217.032941	36.7130	-121.3468	1.54	2.27		
	2003.108.121919	36.7123	-121.3452	1.65	2.30		
76	36.7120	-121.3477	1.33	2.11	7.5	0.34	
	1989.086.154047	36.7117	-121.3468	1.32	2.11		
	1994.070.013245	36.7122	-121.3485	1.33	2.10		

Table 3.1M: First line within each row indicates the sequence label number, average sequence latitude, average sequence longitude, average sequence depth, average sequence magnitude, total amount of slip (cm), and slip rate (mm/yr) at sequence location. Following lines indicate earthquake time, earthquake latitude, earthquake longitude, earthquake depth, and earthquake magnitude for each individual event within a repeating earthquake sequence.

77	36.7082	-121.3458	2.95	1.73	42.2	1.93
	1989.289.195623	36.7063	-121.3453	2.71	1.88	
	1990.246.140820	36.7078	-121.3478	2.83	1.55	
	1991.316.183808	36.7090	-121.3457	2.95	1.64	
	1995.085.053821	36.7082	-121.3463	2.85	1.84	
	1997.290.081219	36.7083	-121.3453	3.04	1.79	
	2000.294.081240	36.7092	-121.3442	3.21	1.76	
	2002.178.232517	36.7095	-121.3460	3.09	1.71	
	2004.122.132326	36.7077	-121.3460	2.92	1.70	
78	36.7031	-121.3383	4.73	2.17	39.0	1.79
	1984.210.101151	36.7025	-121.3393	4.57	2.17	
	1989.280.025207	36.7030	-121.3383	4.99	2.14	
	1993.272.164939	36.7033	-121.3375	4.56	2.18	
	1998.176.161229	36.7033	-121.3392	4.61	2.15	
	2001.213.173228	36.7042	-121.3385	4.71	2.21	
	2004.225.064948	36.7022	-121.3368	4.94	2.17	
79	36.7045	-121.3354	2.96	2.35	8.7	0.40
	1990.237.192644	36.7048	-121.3340	3.09	2.36	
	1995.004.150157	36.7043	-121.3368	2.83	2.33	
80	36.6994	-121.3314	2.97	2.06	29.2	1.34
	1984.309.180200	36.6998	-121.3322	2.82	2.09	
	1992.149.231117	36.6983	-121.3315	2.82	2.06	
	1996.090.162312	36.7008	-121.3292	3.27	2.09	
	2000.044.152259	36.6992	-121.3325	2.84	1.94	
	2001.318.123934	36.6988	-121.3318	3.12	1.92	
81	36.6992	-121.3326	4.07	2.27	16.5	0.76
	1989.352.174944	36.6995	-121.3332	4.06	2.27	
	1995.316.215126	36.6988	-121.3335	4.08	2.27	
	2003.246.121537	36.6992	-121.3310	4.06	2.15	
82	36.6942	-121.3248	4.78	2.47	9.3	0.43
	1988.171.105206	36.6947	-121.3248	4.71	2.43	
	1995.344.083813	36.6937	-121.3248	4.85	2.51	

Table 3.1N: First line within each row indicates the sequence label number, average sequence latitude, average sequence longitude, average sequence depth, average sequence magnitude, total amount of slip (cm), and slip rate (mm/yr) at sequence location. Following lines indicate earthquake time, earthquake latitude, earthquake longitude, earthquake depth, and earthquake magnitude for each individual event within a repeating earthquake sequence.

83	36.6930	-121.3244	4.67	1.95	34.3	1.57	
	1984.263.113325	36.6927	-121.3257	4.76	1.92		
	1989.041.112609	36.6938	-121.3243	4.51	1.96		
	1989.346.171312	36.6928	-121.3220	4.20	2.03		
	1990.276.134057	36.6928	-121.3245	4.76	1.94		
	2001.185.075855	36.6930	-121.3248	4.96	2.19		
	2003.299.055436	36.6930	-121.3252	4.83	1.84		
84	36.6932	-121.3240	3.85	1.84	45.0	2.06	
	1985.111.045120	36.6933	-121.3248	3.84	1.82		
	1986.135.032532	36.6927	-121.3243	3.71	1.85		
	1990.028.180726	36.6940	-121.3232	3.96	2.30		
	1990.346.094147	36.6932	-121.3228	3.92	1.83		
	1994.355.204615	36.6932	-121.3255	3.72	1.78		
	2001.031.100529	36.6927	-121.3238	3.84	1.94		
	2001.285.234151	36.6932	-121.3248	3.73	1.91		
	2004.032.035957	36.6930	-121.3227	4.07	1.74		
85	36.6890	-121.3171	4.23	2.23	24.2	1.11	
	1986.105.130251	36.6883	-121.3167	4.30	2.29		
	1990.247.135110	36.6888	-121.3172	4.32	2.18		
	1996.081.232952	36.6890	-121.3172	3.93	2.19		
	2001.185.103913	36.6897	-121.3175	4.38	2.27		
86	36.6882	-121.3171	4.40	1.85	58.2	2.67	
	1984.061.093357	36.6882	-121.3177	4.54	1.83		
	1987.164.095910	36.6882	-121.3163	4.28	1.63		
	1990.025.134829	36.6880	-121.3163	4.27	1.95		
	1990.044.035222	36.6882	-121.3170	4.44	1.85		
	1991.256.141444	36.6880	-121.3165	4.53	1.87		
	1996.015.125014	36.6880	-121.3167	4.28	1.85		
	1997.324.185928	36.6888	-121.3175	4.49	2.03		
	2001.184.220417	36.6883	-121.3180	4.32	1.65		
	2001.249.102634	36.6878	-121.3173	4.40	1.95		
	2003.302.220109	36.6885	-121.3180	4.45	1.80		

Table 3.1O: First line within each row indicates the sequence label number, average sequence latitude, average sequence longitude, average sequence depth, average sequence magnitude, total amount of slip (cm), and slip rate (mm/yr) at sequence location. Following lines indicate earthquake time, earthquake latitude, earthquake longitude, earthquake depth, and earthquake magnitude for each individual event within a repeating earthquake sequence.

87	36.6859	-121.3172	5.97	1.68	17.6	0.80
	1989.353.200532	36.6857	-121.3177	5.85	1.71	
	1990.252.071717	36.6860	-121.3165	6.07	1.74	
	1999.090.011908	36.6862	-121.3172	5.76	1.61	
	2001.258.075954	36.6855	-121.3175	6.20	1.65	
88	36.6852	-121.3143	5.52	1.84	25.7	1.18
	1986.364.175730	36.6845	-121.3130	5.56	1.94	
	1990.253.174412	36.6855	-121.3152	5.57	1.84	
	1995.242.141910	36.6852	-121.3160	5.43	1.74	
	2000.208.181914	36.6850	-121.3128	5.24	1.71	
	2004.323.040749	36.6860	-121.3147	5.79	1.94	
89	36.6857	-121.3137	4.28	1.85	45.2	2.07
	1984.306.193748	36.6852	-121.3153	4.05	1.75	
	1990.014.062004	36.6868	-121.3140	4.03	1.88	
	1990.362.133316	36.6860	-121.3130	4.34	1.83	
	1993.242.081357	36.6850	-121.3135	4.33	1.76	
	1996.086.055845	36.6850	-121.3145	4.25	1.79	
	1998.127.124117	36.6860	-121.3128	4.45	1.86	
	2001.185.014052	36.6857	-121.3137	4.38	1.90	
	2003.137.041722	36.6862	-121.3128	4.40	1.91	
90	36.6837	-121.3083	4.01	2.05	14.5	0.67
	1984.246.034042	36.6837	-121.3082	3.80	1.97	
	1990.354.162410	36.6833	-121.3083	4.07	2.05	
	1996.215.095348	36.6842	-121.3083	4.17	2.20	
91	36.6827	-121.3075	3.89	2.05	29.1	1.33
	1986.156.004300	36.6818	-121.3073	4.16	2.09	
	1990.053.230943	36.6833	-121.3070	3.52	2.11	
	1991.200.161019	36.6827	-121.3080	4.06	2.05	
	1994.032.162954	36.6830	-121.3075	3.93	1.91	
	2001.353.005000	36.6825	-121.3077	3.78	2.02	

Table 3.1P: First line within each row indicates the sequence label number, average sequence latitude, average sequence longitude, average sequence depth, average sequence magnitude, total amount of slip (cm), and slip rate (mm/yr) at sequence location. Following lines indicate earthquake time, earthquake latitude, earthquake longitude, earthquake depth, and earthquake magnitude for each individual event within a repeating earthquake sequence.

92	36.6802	-121.3065	2.78	2.04	14.4	0.66
1984.063.031604	36.6802	-121.3065	2.54	1.95		
1994.104.043353	36.6805	-121.3062	2.86	2.09		
2002.340.012241	36.6798	-121.3067	2.94	2.04		
93	36.6788	-121.3039	5.38	2.47	9.3	0.43
1990.243.190518	36.6788	-121.3032	5.26	2.47		
1998.233.173333	36.6787	-121.3045	5.51	2.46		
94	36.6769	-121.2996	3.00	2.19	23.7	1.08
1988.089.012614	36.6773	-121.2982	3.01	2.21		
1993.068.215401	36.6775	-121.2990	3.07	2.18		
1998.191.102738	36.6757	-121.3008	2.94	2.16		
2003.126.193620	36.6770	-121.3003	2.96	2.19		
95	36.6746	-121.2967	3.85	1.81	31.6	1.45
1987.238.215037	36.6755	-121.2948	3.61	1.83		
1990.245.101402	36.6745	-121.2963	3.93	1.78		
1993.137.181546	36.6745	-121.2968	3.91	1.86		
1996.050.083959	36.6750	-121.2980	3.76	1.80		
1999.079.053238	36.6740	-121.2970	3.94	1.73		
2001.223.124508	36.6742	-121.2975	3.92	1.88		
96	36.6745	-121.2966	4.34	2.34	8.6	0.39
1985.117.060617	36.6740	-121.2968	4.28	2.28		
1990.106.131341	36.6750	-121.2965	4.40	2.39		
97	36.6741	-121.2959	3.93	2.28	33.3	1.52
1984.221.075349	36.6742	-121.2967	3.81	2.30		
1989.357.070129	36.6737	-121.2958	3.68	2.22		
1995.206.140915	36.6740	-121.2952	4.07	2.31		
2000.179.223842	36.6747	-121.2960	4.08	2.28		
2003.061.032209	36.6738	-121.2958	3.99	2.15		

Table 3.1Q: First line within each row indicates the sequence label number, average sequence latitude, average sequence longitude, average sequence depth, average sequence magnitude, total amount of slip (cm), and slip rate (mm/yr) at sequence location. Following lines indicate earthquake time, earthquake latitude, earthquake longitude, earthquake depth, and earthquake magnitude for each individual event within a repeating earthquake sequence.

98	36.6687	-121.2870	3.04	2.69	21.2	0.97	
	1986.200.110036	36.6692	-121.2870	3.03	2.69		
	1991.295.042930	36.6680	-121.2865	3.14	2.72		
	1998.239.173607	36.6688	-121.2875	2.94	2.66		
99	36.6683	-121.2860	3.25	3.07	39.7	1.82	
	1988.107.184738	36.6685	-121.2858	3.36	3.06		
	1993.088.201502	36.6685	-121.2865	3.36	3.03		
	1999.187.135516	36.6682	-121.2860	3.22	3.08		
	2004.287.232620	36.6678	-121.2858	3.07	3.10		
100	36.6663	-121.2869	2.92	2.32	17.0	0.78	
	1992.274.064600	36.6657	-121.2867	2.74	2.32		
	1998.197.225805	36.6663	-121.2878	3.06	2.31		
	2003.157.115207	36.6670	-121.2863	2.96	2.35		
101	36.6655	-121.2869	5.85	2.15	15.4	0.71	
	1990.245.194507	36.6650	-121.2865	5.73	2.23		
	1996.260.093456	36.6662	-121.2870	5.82	2.15		
	2002.264.010328	36.6653	-121.2872	6.00	2.15		
102	36.6616	-121.2846	6.53	2.96	12.4	0.57	
	1990.136.042803	36.6610	-121.2842	6.50	2.99		
	1999.094.072725	36.6622	-121.2850	6.56	2.92		
103	36.6594	-121.2858	7.66	2.79	11.2	0.51	
	1990.138.030239	36.6588	-121.2858	7.75	2.88		
	1995.055.190220	36.6600	-121.2858	7.56	2.66		
104	36.6604	-121.2771	3.41	3.17	42.1	1.93	
	1985.316.221108	36.6603	-121.2767	3.33	3.23		
	1989.355.091807	36.6603	-121.2773	3.38	3.04		
	1994.220.003752	36.6605	-121.2768	3.45	3.24		
	1998.342.233233	36.6607	-121.2775	3.47	3.08		

Table 3.1R: First line within each row indicates the sequence label number, average sequence latitude, average sequence longitude, average sequence depth, average sequence magnitude, total amount of slip (cm), and slip rate (mm/yr) at sequence location. Following lines indicate earthquake time, earthquake latitude, earthquake longitude, earthquake depth, and earthquake magnitude for each individual event within a repeating earthquake sequence.

105	36.6578	-121.2752	3.34	2.38	26.5	1.21
1989.355.094516	36.6573	-121.2752	3.22	2.57		
1998.198.052712	36.6580	-121.2753	3.11	2.38		
2001.121.135745	36.6585	-121.2758	3.87	2.32		
2004.297.134459	36.6575	-121.2747	3.15	2.38		
106	36.6563	-121.2749	5.57	2.64	30.8	1.41
1985.121.030527	36.6560	-121.2758	5.54	2.71		
1991.021.064045	36.6562	-121.2748	5.38	2.67		
1996.331.092305	36.6563	-121.2745	5.66	2.61		
2001.081.110253	36.6568	-121.2743	5.71	2.56		
107	36.6570	-121.2716	3.47	2.73	10.8	0.50
1986.350.184542	36.6567	-121.2703	3.48	2.72		
1994.363.035619	36.6572	-121.2728	3.47	2.74		
108	36.6564	-121.2818	8.36	2.91	24.1	1.10
1986.023.211109	36.6557	-121.2818	8.14	2.95		
1994.227.051346	36.6560	-121.2818	8.46	2.91		
2002.259.122218	36.6575	-121.2818	8.49	2.88		
109	36.6550	-121.2807	7.52	2.50	18.9	0.87
1986.218.024949	36.6547	-121.2812	7.21	2.49		
1995.004.233509	36.6552	-121.2812	7.63	2.55		
2003.271.005919	36.6552	-121.2797	7.71	2.50		
110	36.6543	-121.2801	7.74	2.56	9.8	0.45
1986.216.091150	36.6540	-121.2807	7.54	2.46		
1994.365.205933	36.6545	-121.2795	7.94	2.63		
111	36.6535	-121.2781	7.53	2.20	15.9	0.73
1986.216.091358	36.6535	-121.2795	7.28	2.23		
1994.365.210235	36.6532	-121.2785	7.77	2.20		
2000.050.140809	36.6538	-121.2762	7.53	2.13		

Table 3.1S: First line within each row indicates the sequence label number, average sequence latitude, average sequence longitude, average sequence depth, average sequence magnitude, total amount of slip (cm), and slip rate (mm/yr) at sequence location. Following lines indicate earthquake time, earthquake latitude, earthquake longitude, earthquake depth, and earthquake magnitude for each individual event within a repeating earthquake sequence.

112	36.6529	-121.2770	7.47	2.27	24.8	1.14
1986.155.113658	36.6517	-121.2768	7.25	1.79		
1993.098.155923	36.6533	-121.2773	7.62	2.27		
1996.156.064609	36.6532	-121.2772	7.36	2.26		
2000.329.151741	36.6532	-121.2768	7.67	2.34		
113	36.6527	-121.2742	6.58	2.43	36.4	1.67
1985.326.221651	36.6525	-121.2742	6.17	2.40		
1990.139.021414	36.6523	-121.2743	6.42	2.45		
1994.118.030948	36.6527	-121.2740	6.86	2.43		
1999.108.074753	36.6528	-121.2745	6.69	2.43		
2002.103.182125	36.6533	-121.2742	6.74	2.33		
114	36.6521	-121.2733	6.80	2.16	15.5	0.71
1991.304.153545	36.6517	-121.2728	6.64	2.22		
1999.109.021106	36.6522	-121.2738	6.70	2.16		
2002.103.214532	36.6523	-121.2732	7.06	2.04		
115	36.6507	-121.2721	6.61	2.23	32.3	1.48
1985.327.202854	36.6503	-121.2722	6.75	2.23		
1994.244.153928	36.6505	-121.2728	6.56	2.25		
1999.108.071235	36.6508	-121.2717	6.63	2.35		
2000.305.181651	36.6502	-121.2720	6.60	1.78		
2002.107.124347	36.6515	-121.2720	6.53	2.17		
116	36.6506	-121.2710	6.73	2.55	39.0	1.79
1985.327.202946	36.6500	-121.2717	6.55	2.79		
1994.244.153553	36.6498	-121.2708	6.72	2.84		
1998.336.171850	36.6513	-121.2707	6.73	2.55		
2000.305.181714	36.6508	-121.2712	6.80	2.53		
2002.107.113128	36.6512	-121.2708	6.83	2.35		
117	36.6530	-121.2700	3.34	2.04	14.4	0.66
1986.154.124846	36.6525	-121.2720	3.31	1.86		
1988.139.230744	36.6535	-121.2698	3.39	2.10		
1998.094.174334	36.6530	-121.2682	3.31	2.04		

Table 3.1T: First line within each row indicates the sequence label number, average sequence latitude, average sequence longitude, average sequence depth, average sequence magnitude, total amount of slip (cm), and slip rate (mm/yr) at sequence location. Following lines indicate earthquake time, earthquake latitude, earthquake longitude, earthquake depth, and earthquake magnitude for each individual event within a repeating earthquake sequence.

118	36.6514	-121.2683	5.13	2.55	39.0	1.79	
	1987.335.172032	36.6520		-121.2685	5.06	2.69	
	1992.043.030827	36.6515		-121.2685	5.31	2.69	
	1996.035.100917	36.6502		-121.2677	5.05	2.53	
	1999.298.025613	36.6517		-121.2683	5.30	2.55	
	2002.118.141720	36.6515		-121.2687	4.92	2.37	
119	36.6515	-121.2649	3.72	3.07	26.5	1.21	
	1986.266.061550	36.6520		-121.2640	3.57	3.12	
	1992.170.095105	36.6512		-121.2655	3.78	3.07	
	1998.244.105644	36.6512		-121.2653	3.80	3.05	
120	36.6492	-121.2664	5.50	2.06	29.2	1.34	
	1987.163.184203	36.6492		-121.2657	5.45	2.02	
	1991.251.155325	36.6488		-121.2670	5.38	1.99	
	1996.054.122659	36.6498		-121.2667	5.58	2.16	
	2000.060.205813	36.6490		-121.2663	5.49	2.06	
	2003.162.082128	36.6490		-121.2662	5.58	2.15	
121	36.6458	-121.2677	7.29	2.54	19.4	0.89	
	1986.117.030200	36.6457		-121.2680	7.36	2.61	
	1991.225.233122	36.6453		-121.2675	6.93	2.47	
	1999.235.022044	36.6463		-121.2677	7.59	2.54	
122	36.6431	-121.2647	8.56	2.49	9.4	0.43	
	1987.320.081102	36.6428		-121.2645	8.41	2.57	
	1992.156.125436	36.6433		-121.2650	8.71	2.38	
123	36.6452	-121.2585	4.61	2.23	40.4	1.85	
	1986.200.045631	36.6442		-121.2582	4.14	2.11	
	1988.354.191400	36.6450		-121.2578	4.69	2.31	
	1993.156.021101	36.6452		-121.2590	4.69	1.96	
	1997.021.141616	36.6455		-121.2578	4.78	2.31	
	2000.185.030226	36.6457		-121.2587	4.70	2.38	
	2004.066.154827	36.6455		-121.2595	4.64	2.13	

Table 3.1U: First line within each row indicates the sequence label number, average sequence latitude, average sequence longitude, average sequence depth, average sequence magnitude, total amount of slip (cm), and slip rate (mm/yr) at sequence location. Following lines indicate earthquake time, earthquake latitude, earthquake longitude, earthquake depth, and earthquake magnitude for each individual event within a repeating earthquake sequence.

124	36.6440	-121.2595	5.74	2.01	21.3	0.98	
	1986.152.014213	36.6435		-121.2595	5.63	2.04	
	1988.058.091109	36.6440		-121.2600	5.80	1.87	
	1996.259.234237	36.6447		-121.2590	5.62	1.98	
	2002.011.053501	36.6438		-121.2593	5.89	2.15	
125	36.6422	-121.2609	7.12	2.52	9.6	0.44	
	1994.344.065847	36.6420		-121.2610	7.00	2.54	
	1999.232.005458	36.6423		-121.2608	7.24	2.50	
126	36.6425	-121.2569	5.69	2.57	29.6	1.36	
	1986.151.225525	36.6425		-121.2573	5.38	2.40	
	1991.332.210241	36.6427		-121.2562	5.82	2.56	
	2000.004.134809	36.6422		-121.2568	5.66	2.60	
	2003.321.022746	36.6427		-121.2573	5.89	2.57	
127	36.6432	-121.2548	3.95	2.48	18.7	0.86	
	1990.039.171610	36.6430		-121.2558	4.00	2.49	
	1995.212.050051	36.6432		-121.2537	3.64	2.48	
	2002.327.110618	36.6433		-121.2548	4.20	2.45	
128	36.6422	-121.2554	4.50	2.19	39.5	1.81	
	1986.163.192731	36.6415		-121.2568	4.09	1.90	
	1990.013.095508	36.6420		-121.2548	4.47	2.21	
	1993.111.154535	36.6427		-121.2555	4.65	2.24	
	1999.081.195114	36.6420		-121.2548	4.53	2.28	
	2002.009.232435	36.6425		-121.2552	4.56	2.07	
	2004.074.223232	36.6423		-121.2553	4.68	2.18	
129	36.6411	-121.2542	5.58	2.77	11.1	0.51	
	1986.152.193445	36.6403		-121.2548	5.32	2.85	
	1994.086.153447	36.6418		-121.2535	5.84	2.67	
130	36.8036	-121.5311	8.30	1.49	5.2	0.24	
	1998.148.203544	36.8045		-121.5302	7.86	1.56	
	1998.155.061233	36.8027		-121.5320	8.74	1.39	

Table 3.1V: First line within each row indicates the sequence label number, average sequence latitude, average sequence longitude, average sequence depth, average sequence magnitude, total amount of slip (cm), and slip rate (mm/yr) at sequence location. Following lines indicate earthquake time, earthquake latitude, earthquake longitude, earthquake depth, and earthquake magnitude for each individual event within a repeating earthquake sequence.

131	36.7896	-121.5145	8.72	1.75	6.1	0.28
	1998.225.142100	36.7895	-121.5122	8.42	1.73	
	1998.255.195423	36.7897	-121.5168	9.03	1.77	
132	36.7911	-121.5034	6.92	1.47	5.2	0.24
	1998.225.004407	36.7902	-121.5043	7.01	1.46	
	1998.230.073240	36.7920	-121.5025	6.83	1.47	
133	36.7912	-121.5010	6.05	1.33	4.8	0.22
	1998.225.231814	36.7897	-121.5025	6.04	1.39	
	1998.233.021010	36.7927	-121.4995	6.07	1.24	
134	36.7867	-121.5000	6.51	1.88	6.6	0.30
	1998.224.170938	36.7858	-121.5007	6.41	1.92	
	1998.232.053858	36.7875	-121.4993	6.61	1.84	
135	36.7883	-121.4983	6.34	1.44	15.2	0.70
	1998.224.141621	36.7885	-121.5002	6.42	1.28	
	1998.225.121633	36.7875	-121.4987	6.53	1.60	
	1998.237.184653	36.7883	-121.4952	6.37	1.46	
	1999.274.012327	36.7888	-121.4993	6.04	1.26	
136	36.7832	-121.4975	6.69	1.77	6.2	0.28
	1998.224.205242	36.7837	-121.4987	6.84	1.78	
	1998.264.221727	36.7828	-121.4963	6.53	1.75	
137	36.7683	-121.4805	7.65	1.48	5.2	0.24
	1998.224.150639	36.7687	-121.4820	7.97	1.55	
	1998.229.083158	36.7680	-121.4790	7.33	1.38	
138	36.7658	-121.4783	8.31	1.70	17.8	0.81
	1998.224.145508	36.7672	-121.4792	8.41	1.73	
	1998.225.145957	36.7657	-121.4760	8.44	1.68	
	1998.229.100413	36.7657	-121.4790	8.20	1.72	
	1999.357.072207	36.7645	-121.4788	8.19	1.67	

Table 3.1W: First line within each row indicates the sequence label number, average sequence latitude, average sequence longitude, average sequence depth, average sequence magnitude, total amount of slip (cm), and slip rate (mm/yr) at sequence location. Following lines indicate earthquake time, earthquake latitude, earthquake longitude, earthquake depth, and earthquake magnitude for each individual event within a repeating earthquake sequence.

139	36.7613	-121.4714	8.34	1.46	15.4	0.71	
	1998.224.152428	36.7620	-121.4687	8.31	1.47		
	1998.227.082805	36.7593	-121.4777	7.16	0.93		
	1998.234.063121	36.7632	-121.4700	9.02	1.56		
	1999.007.231840	36.7608	-121.4693	8.85	1.56		
144	36.7391	-121.4641	15.17	1.60	5.6	0.26	
	1989.304.182116	36.7407	-121.4667	15.47	1.69		
	1989.313.021931	36.7375	-121.4615	14.87	1.48		
145	36.7195	-121.3571	5.92	1.39	4.9	0.23	
	1992.295.005810	36.7193	-121.3568	5.96	1.38		
	1992.295.015836	36.7197	-121.3573	5.89	1.40		
146	36.6994	-121.3368	4.61	1.72	6.0	0.27	
	1995.323.230644	36.6993	-121.3368	4.61	1.72		
	1995.323.230720	36.6995	-121.3368	4.60	1.72		
147	36.6789	-121.3097	5.81	1.47	5.2	0.24	
	1986.095.025601	36.6788	-121.3098	5.80	1.54		
	1986.096.220451	36.6790	-121.3095	5.83	1.37		
148	36.6767	-121.3052	5.89	1.67	5.8	0.27	
	1990.251.130136	36.6765	-121.3045	5.97	1.73		
	1990.252.022728	36.6768	-121.3058	5.82	1.60		
149	36.6774	-121.3048	6.40	2.77	11.1	0.51	
	1999.082.233354	36.6782	-121.3047	6.41	2.86		
	1999.101.024209	36.6767	-121.3050	6.39	2.62		
150	36.6766	-121.3045	5.35	1.69	5.9	0.27	
	1990.244.030248	36.6767	-121.3047	5.40	1.64		
	1990.253.084913	36.6765	-121.3043	5.29	1.73		
151	36.0401	-120.8766	10.28	2.10	7.5	0.34	
	1985.329.053319	36.0403	-120.8767	10.41	2.20		
	1985.329.053833	36.0398	-120.8765	10.15	1.94		

Table 3.1X: First line within each row indicates the sequence label number, average sequence latitude, average sequence longitude, average sequence depth, average sequence magnitude, total amount of slip (cm), and slip rate (mm/yr) at sequence location. Following lines indicate earthquake time, earthquake latitude, earthquake longitude, earthquake depth, and earthquake magnitude for each individual event within a repeating earthquake sequence.

152	36.0008	-120.9794	11.67	1.70	5.9	0.27	
	1996.236.110248	36.0012	-120.9792		11.87	1.51	
	1996.237.093136	36.0005	-120.9797		11.47	1.81	
153	36.0194	-120.9681	7.58	1.83	6.4	0.29	
	1999.183.222527	36.0213	-120.9670		8.81	1.90	
	1999.225.023202	36.0175	-120.9692		6.34	1.74	
154	36.0182	-120.8778	11.14	1.90	6.7	0.30	
	1999.208.013103	36.0185	-120.8770		11.52	1.57	
	1999.213.165653	36.0178	-120.8787		10.76	2.04	
155	36.0997	-121.0300	11.00	1.22	17.9	0.82	
	2000.344.134929	36.0995	-121.0300		11.29	1.45	
	2000.352.163917	36.1005	-121.0300		10.62	1.48	
	2000.366.150039	36.0983	-121.0300		11.18	1.68	
	2000.344.202751	36.0995	-121.0300		11.29	1.68	
	2000.355.084002	36.1005	-121.0300		10.62	1.70	
156	35.9907	-120.9631	6.35	1.73	6.0	0.28	
	2003.188.191626	35.9900	-120.9642		6.27	1.52	
	2003.189.074547	35.9913	-120.9620		6.43	1.85	

Table 3.1Y: First line within each row indicates the sequence label number, average sequence latitude, average sequence longitude, average sequence depth, average sequence magnitude, total amount of slip (cm), and slip rate (mm/yr) at sequence location. Following lines indicate earthquake time, earthquake latitude, earthquake longitude, earthquake depth, and earthquake magnitude for each individual event within a repeating earthquake sequence.
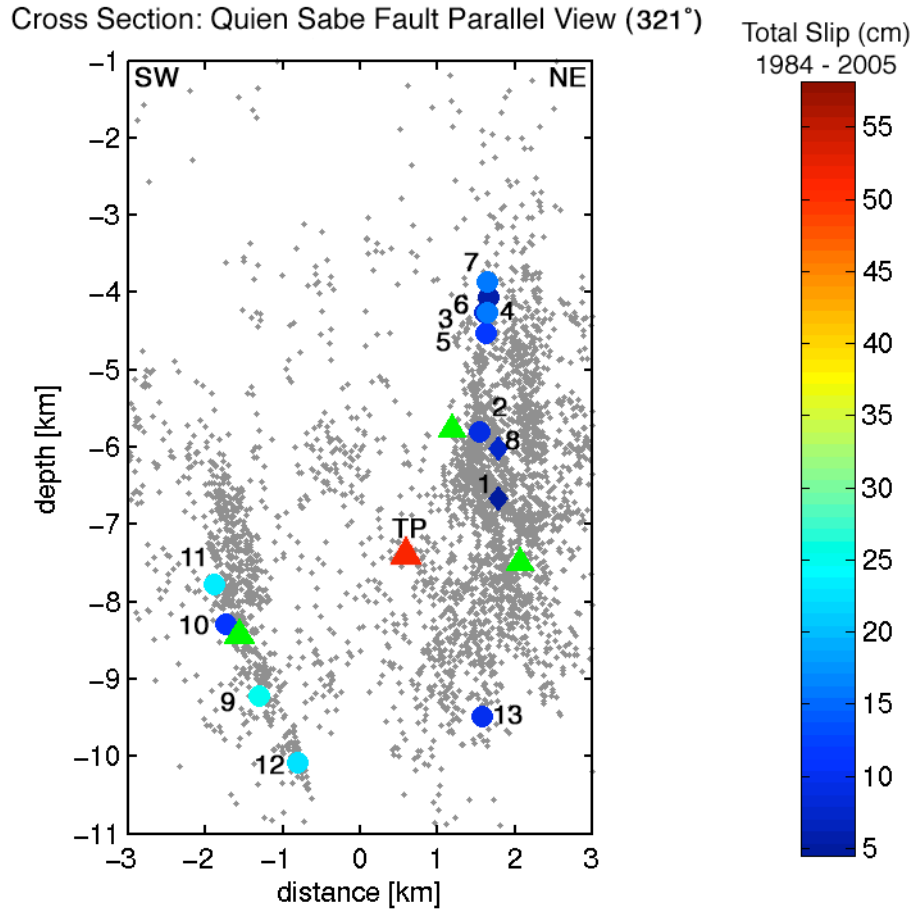
Figure 3.S1: Cross section fault parallel view of Quien Sabe fault.. REs as colored circles and labels are individual sequence names for reference. Color of circles indicates the cumulative amount of slip at each sequence location over the observation period. Burst type REs are colored triangles and labels are individual sequence names for reference. Small dots are background seismicity from the hypoDD-relocated catalog of Ellsworth et al. (2000). Triangles indicate earthquakes larger than M4.0 and green triangles with grey outline indicate catalog locations of earthquakes greater than M4.0 that were not included in the relocated catalog. Red triangle labeled TP is the 1986 Tres Piños earthquake.
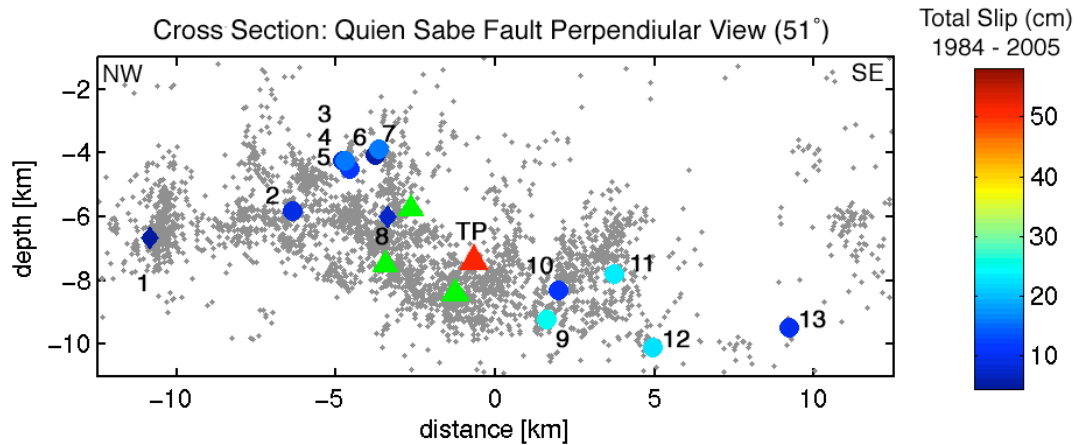
Figure 3.S2: Cross section fault perpendicular view of Quien Sabe fault. REs as colored circles and labels are individual sequence names for reference. Sequence label numbers increase from northwest to southeast. Burst type REs are colored triangles and labels are individual sequence names for reference. Burst type RE sequence label numbers increase from northwest to southeast. Color of circles indicates the cumulative amount of slip at each sequence location over the observation period. Small dots are background seismicity from the hypoDD-relocated catalog of Ellsworth et al. (2000). Triangles indicate earthquakes larger than M4.0 and green triangles with grey outline indicate catalog locations of earthquakes greater than M4.0 that were not included in the relocated catalog. Red triangle labeled TP is the 1986 Tres Piños earthquake.
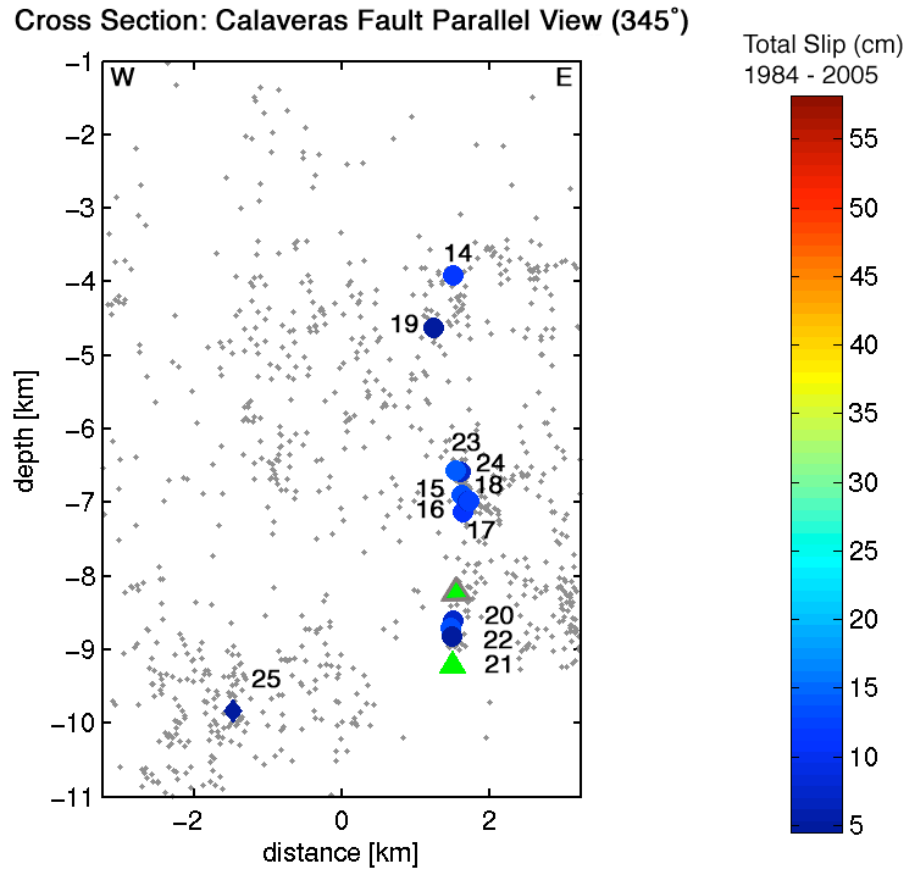
Figure 3.S3: Cross section fault parallel view of Calaveras fault. REs as colored circles and labels are individual sequence names for reference. Burst type REs are colored triangles and labels are individual sequence names for reference. Color of circles indicates the cumulative amount of slip at each sequence location over the observation period. Small dots are background seismicity from the hypoDD-relocated catalog of Ellsworth et al. (2000). Triangles indicate earthquakes larger than M4.0 and green triangles with grey outline indicate catalog locations of earthquakes greater than M4.0 that were not included in the relocated catalog.
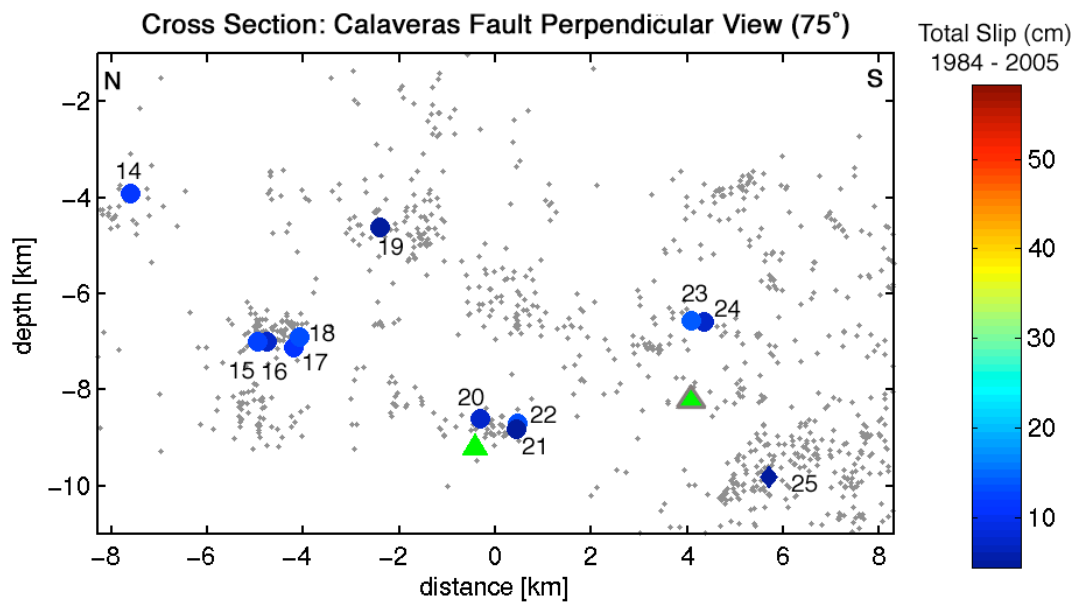
Figure 3.S4: Cross section fault perpendicular view of Calaveras fault. REs as colored circles and labels are individual sequence names for reference. Sequence label numbers increase from northwest to southeast. Burst type REs are colored triangles and labels are individual sequence names for reference. Burst type RE sequence label numbers increase from northwest to southeast. Color of circles indicates the cumulative amount of slip at each sequence location over the observation period. Small dots are background seismicity from the hypoDD-relocated catalog of Ellsworth et al. (2000). Triangles indicate earthquakes larger than M4.0 and green triangles with grey outline indicate catalog locations of earthquakes greater than M4.0 that were not included in the relocated catalog.

Cross Section: Paicines Fault Perpendicular View (45°)

Figure 3.S5: Cross section fault perpendicular view of Paicines fault. REs as colored circles and labels are individual sequence names for reference. Sequence label numbers increase from northwest to southeast. Color of circles indicates the cumulative amount of slip at each sequence location over the observation period. Small dots are background seismicity from the hypoDD-relocated catalog of Ellsworth et al. (2000).

Figure 3.S6: Cross section fault parallel view of southern portion of San Andreas fault and Paicines fault. REs as colored circles and labels are individual sequence names for reference. Burst type REs are colored triangles and labels are individual sequence names for reference. Color of circles indicates the cumulative amount of slip at each sequence location over the observation period. Small dots are background seismicity from the hypoDD-relocated catalog of Ellsworth et al. (2000). Triangles indicate earthquakes larger than M4.0 and green triangles with grey outline indicate catalog locations of earthquakes greater than M4.0 that were not included in the relocated catalog.
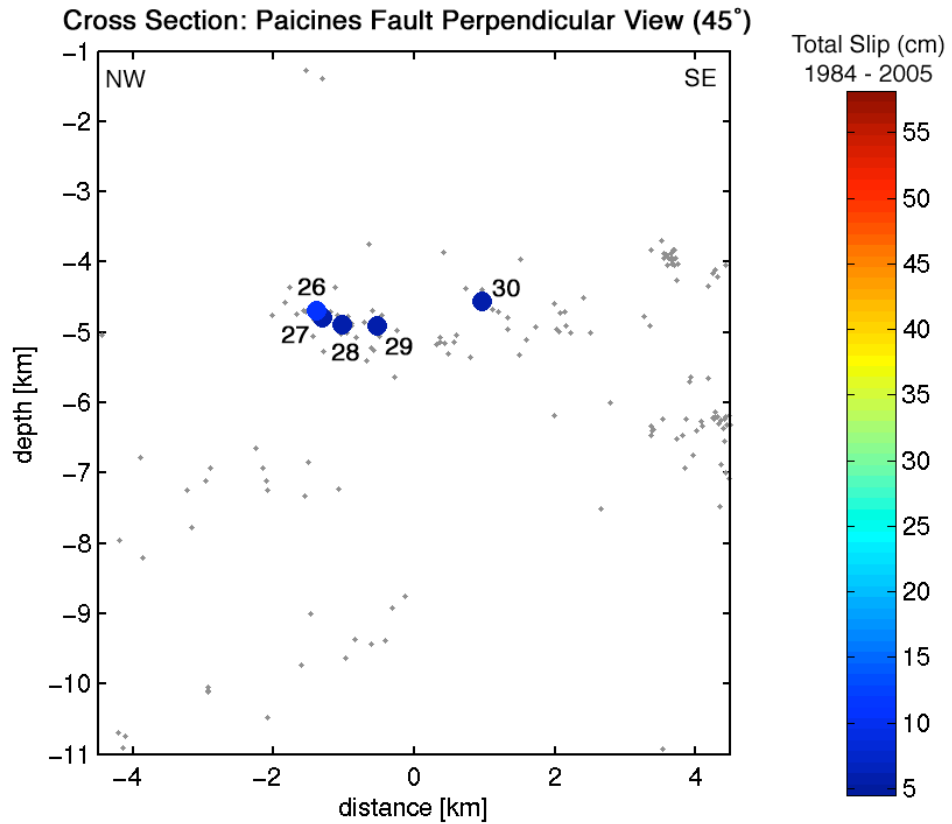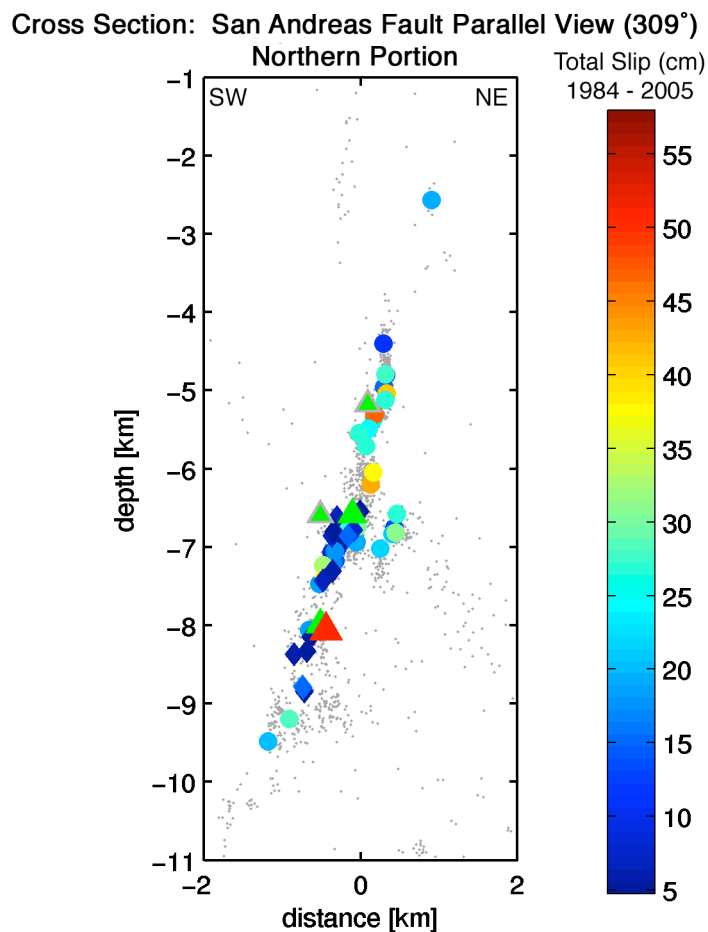
Figure 3.S7: Cross section fault parallel view of northern portion of San Andreas fault. REs as colored circles and labels are individual sequence names for reference. Burst type REs are colored triangles and labels are individual sequence names for reference. Color of circles indicates the cumulative amount of slip at each sequence location over the observation period. Small dots are background seismicity from the hypoDD-relocated catalog of Ellsworth et al. (2000). Triangles indicate earthquakes larger than M4.0 and green triangles with grey outline indicate catalog locations of earthquakes greater than M4.0 that were not included in the relocated catalog.
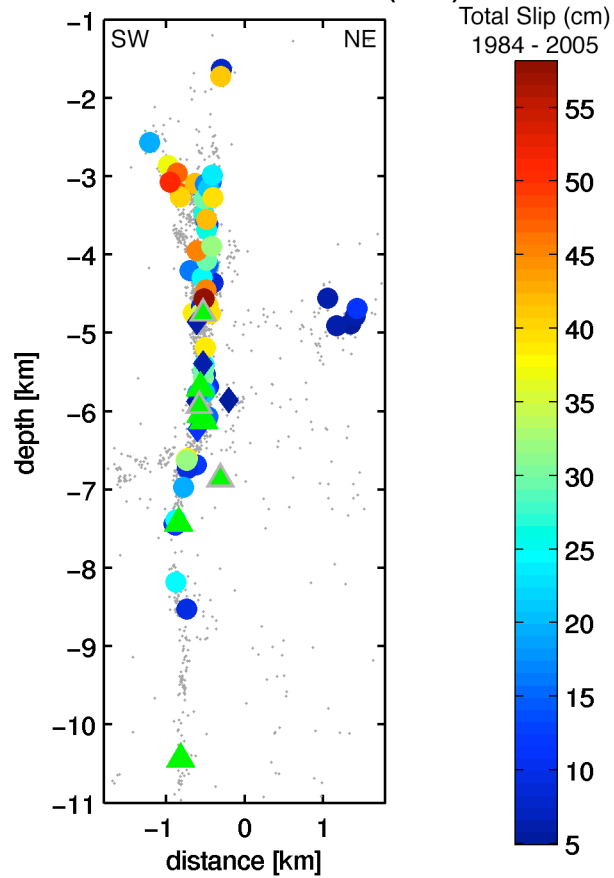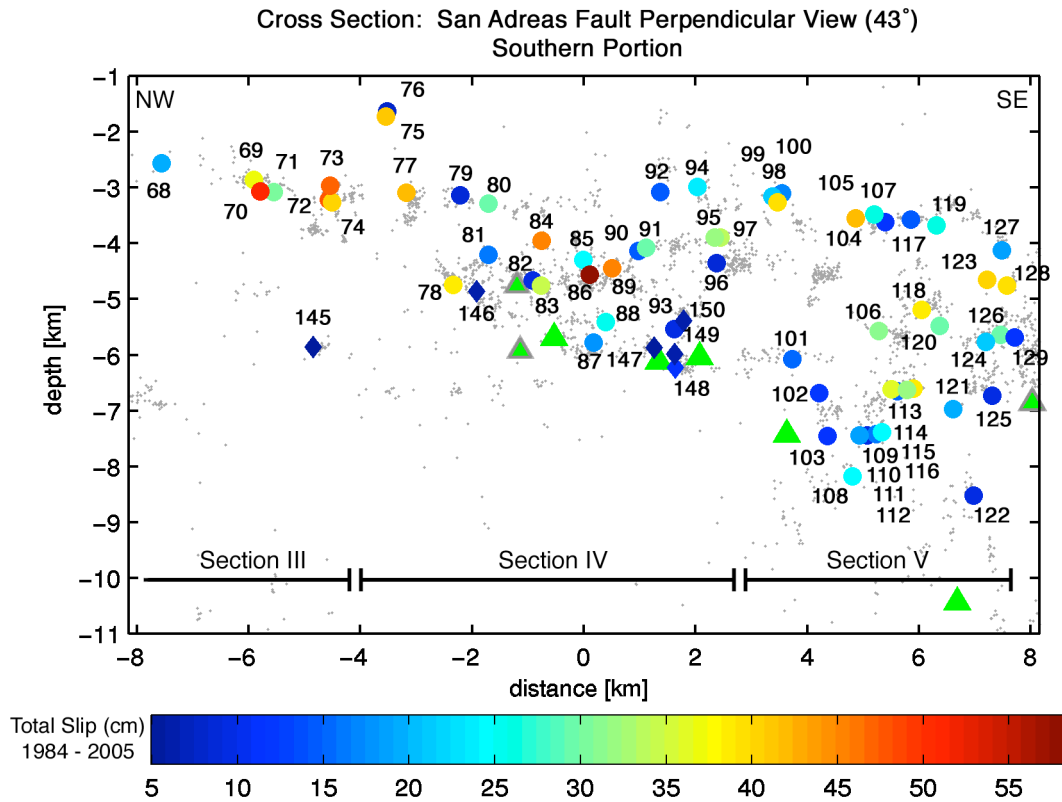
Figure 3.S8: Cross section fault perpendicular view of southern portion of San Andreas fault. REs as colored circles and labels are individual sequence names for reference. Sequence label numbers increase from northwest to southeast. Burst type REs are colored triangles and labels are individual sequence names for reference. Burst type RE sequence label numbers increase from northwest to southeast. Color of circles indicates the cumulative amount of slip at each sequence location over the observation period. Small dots are background seismicity from the hypoDD-relocated catalog of Ellsworth et al. (2000). Triangles indicate earthquakes larger than M4.0 and green triangles with grey outline indicate catalog locations of earthquakes greater than M4.0 that were not included in the relocated catalog.

Figure 3.S9: Cross section fault perpendicular view of burst type REs on San Andreas fault.
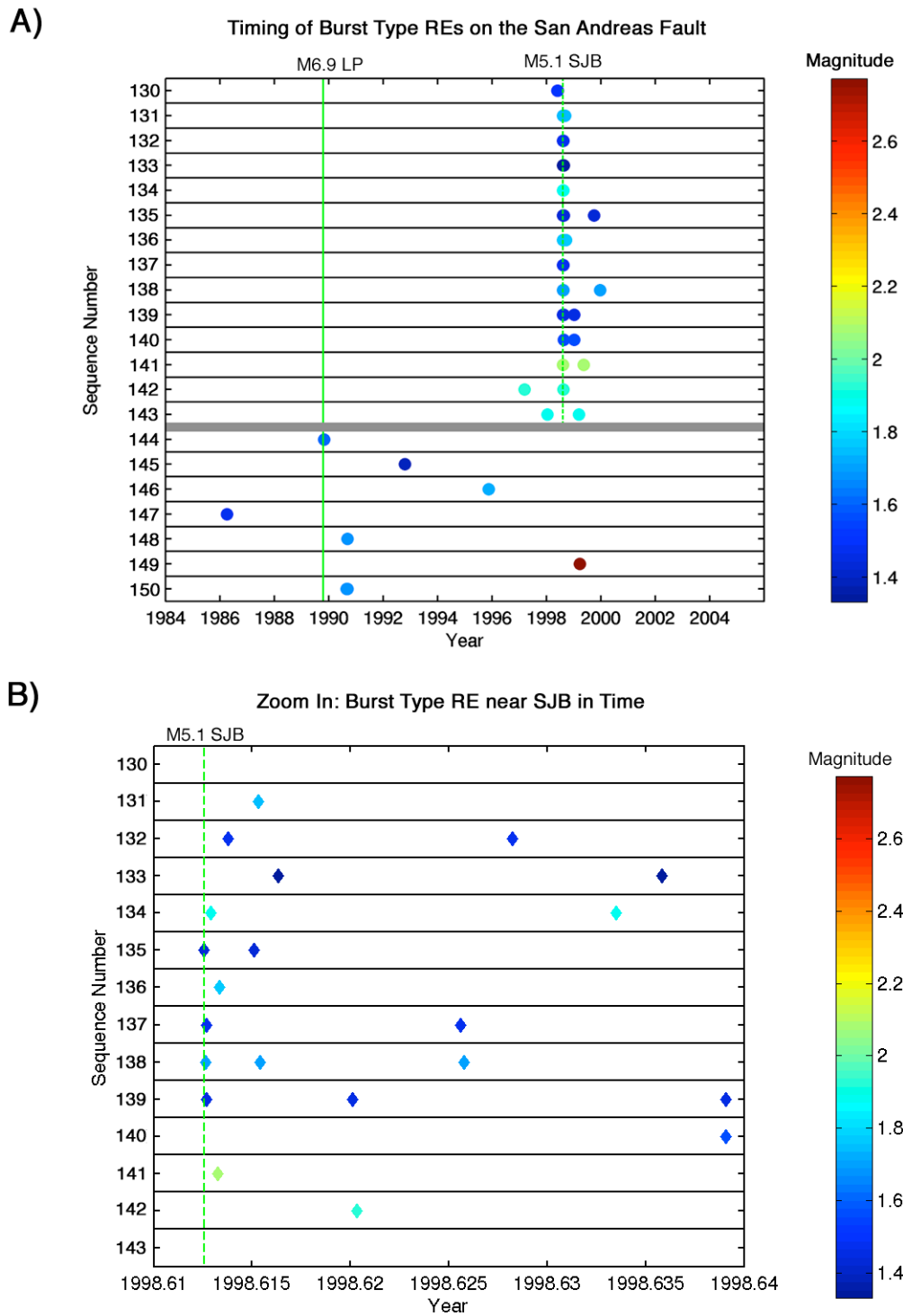
Figure 3.S10: Timing of burst type REs on the San Andreas fault. Color indicates average magnitude of events within burst sequence. LP indicates time of 1989 Loma Prieta earthquake and SJB indicates time of 1998 San Juan Bautista earthquake.
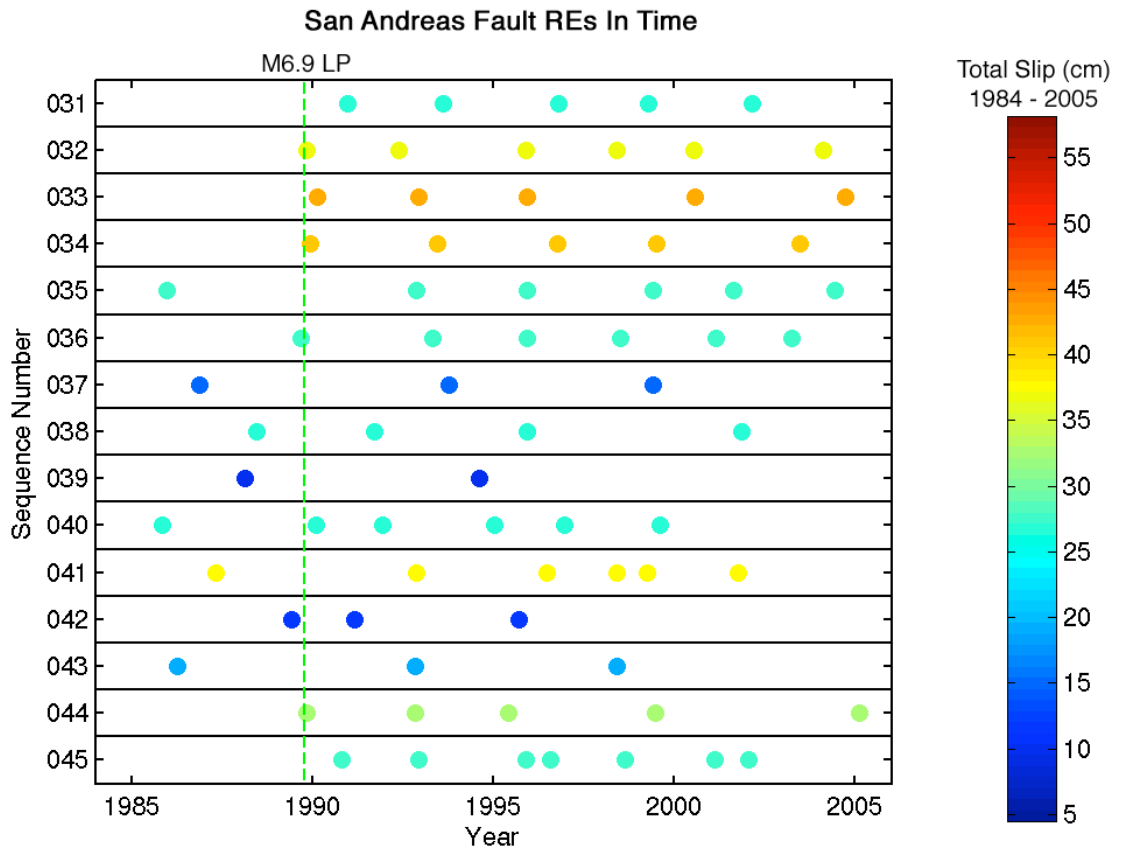
Figure 3.S11: Timing of non-burst type REs on the San Andreas fault. Color indicates total amount of slip at sequence location over observation period. LP indicates time of 1989 Loma Prieta earthquake.
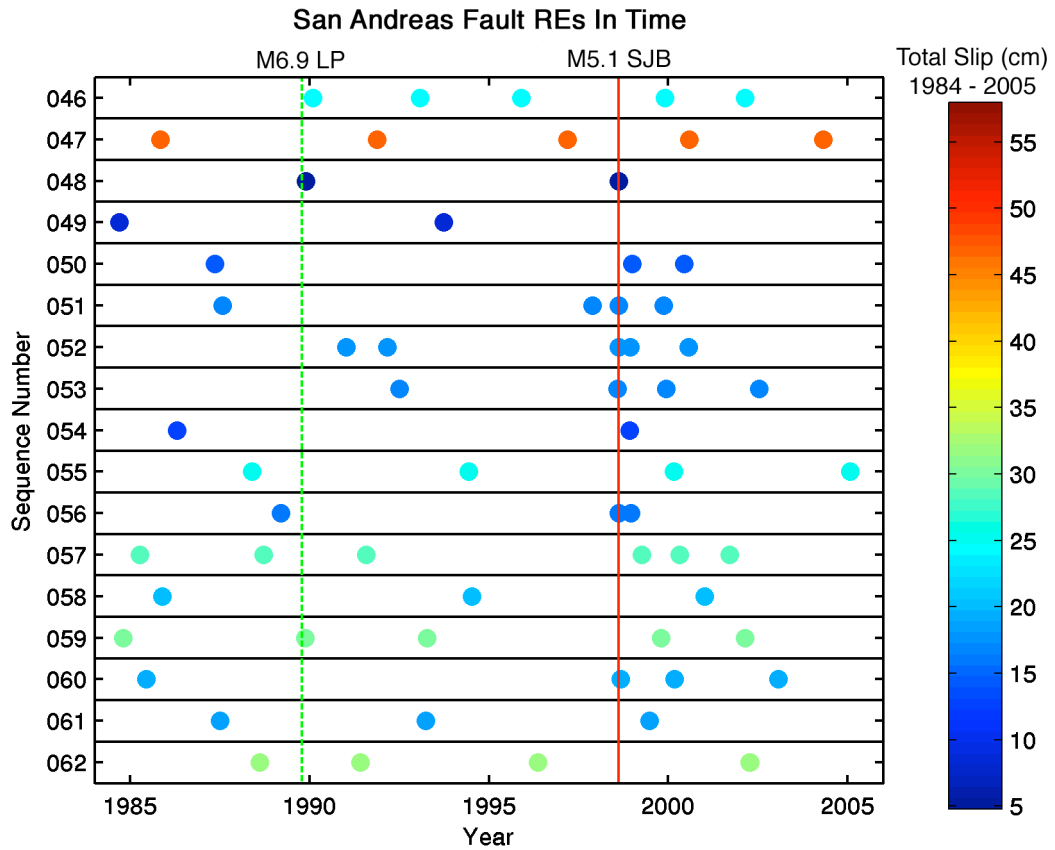
Figure 3.S12: Timing of non-burst type REs on San Andreas fault. Color indicates total amount of slip at sequence location over observation window. LP indicates time of 1989 Loma Prieta earthquake and SJB indicates time of 1998 San Juan Bautista earthquake.
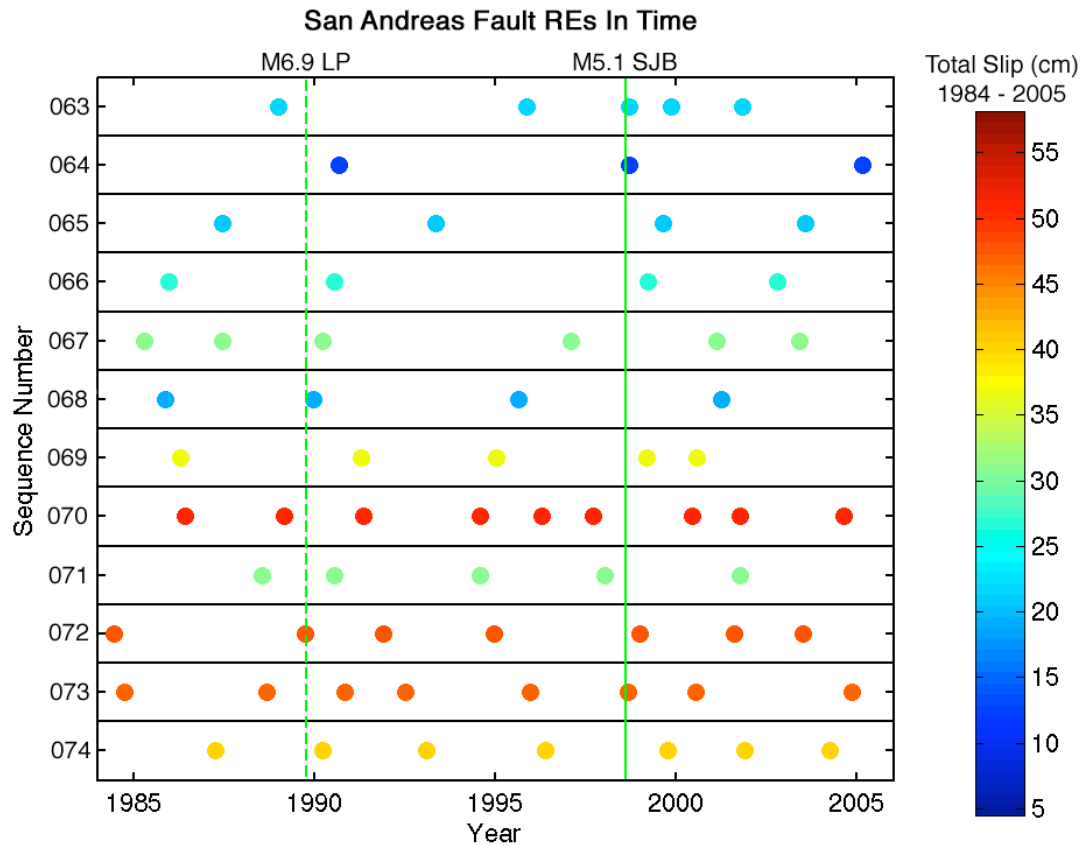
Figure 3.S13: Timing of non-burst type REs on San Andreas fault. Color indicates total amount of slip at sequence location over observation window. LP indicates time of 1989 Loma Prieta earthquake and SJB indicates time of 1998 San Juan Bautista earthquake.
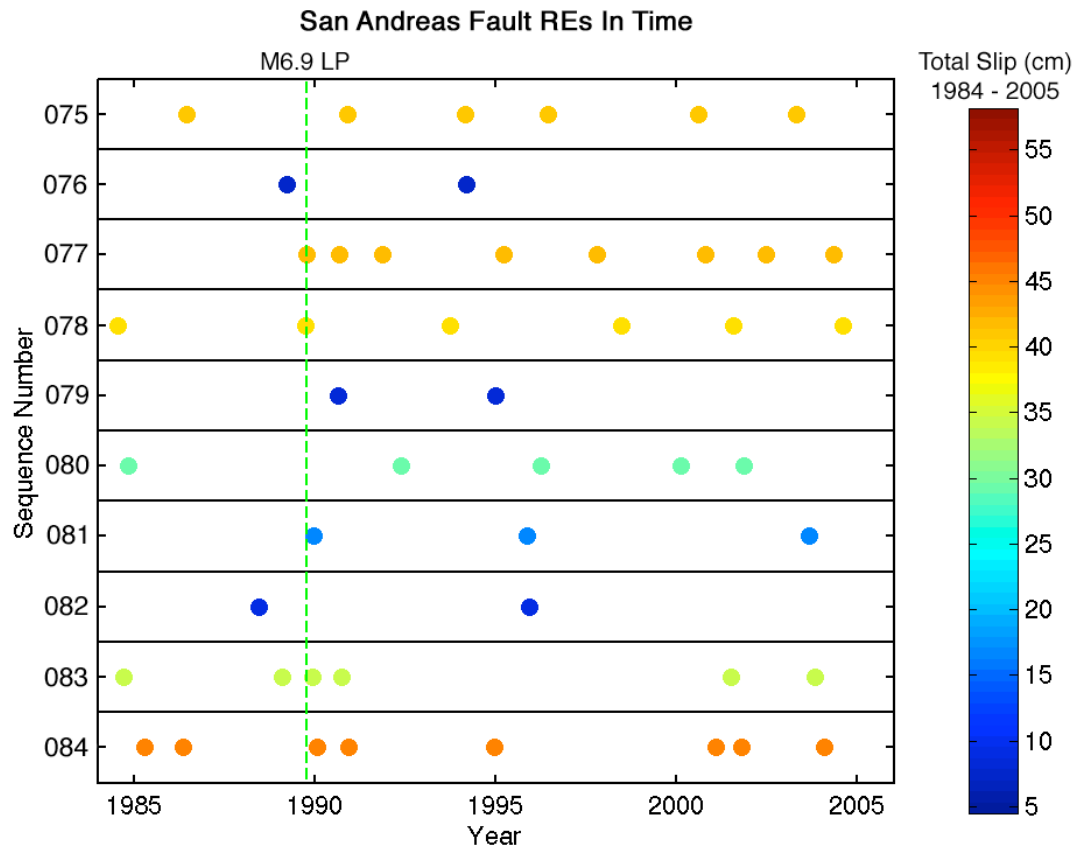
Figure 3.S14: Timing of non-burst type REs on San Andreas fault. Color indicates total amount of slip at sequence location over observation window. LP indicates time of 1989 Loma Prieta earthquake.
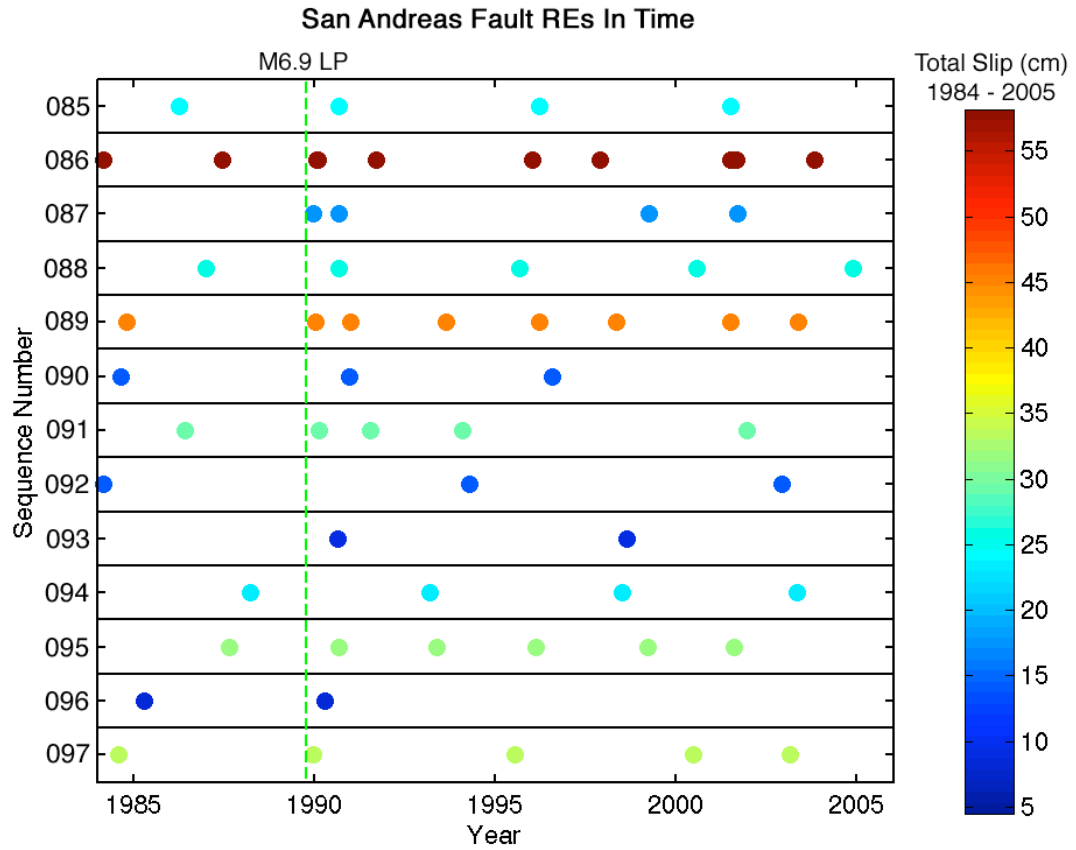
Figure 3.S15: Timing of non-burst type REs on San Andreas fault. Color indicates total amount of slip at sequence location over observation window. LP indicates time of 1989 Loma Prieta earthquake.
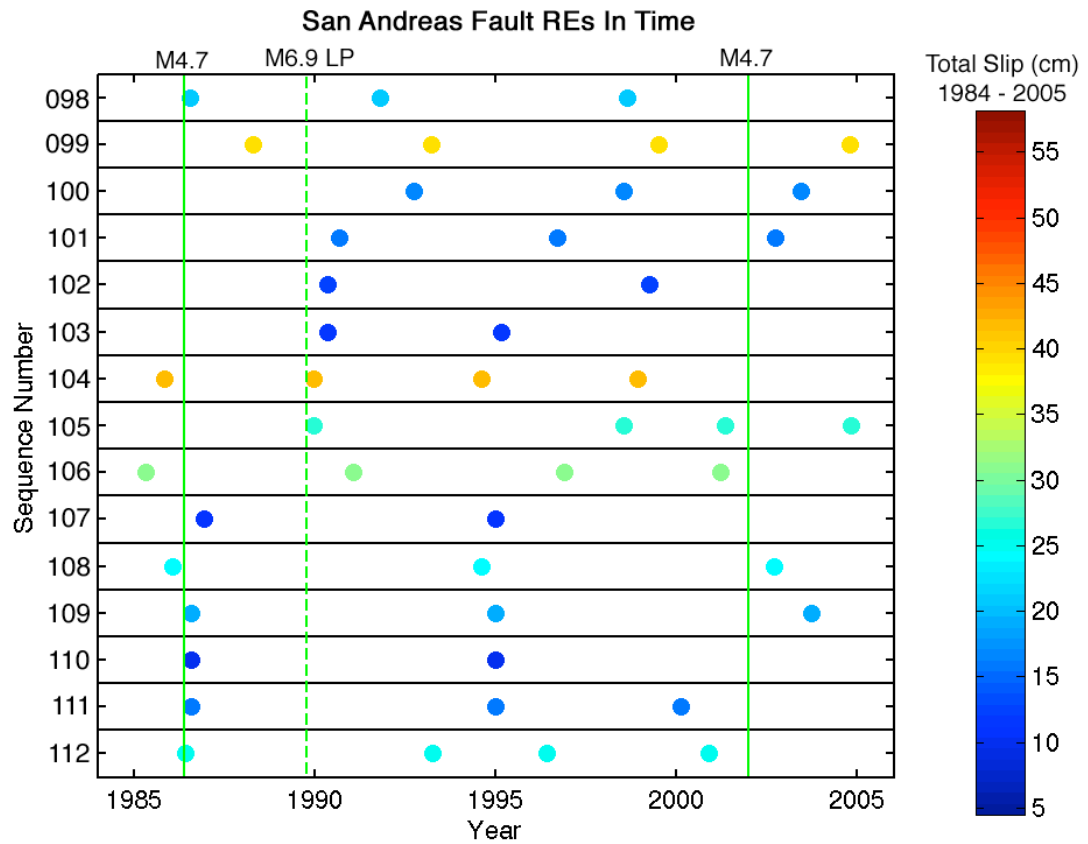
Figure 3.S16: Timing of non-burst type REs on San Andreas fault. Color indicates total amount of slip at sequence location over observation window. LP indicates time of 1989 Loma Preita earthquake. Two vertical lines indicate times of nearby M4.7 earthquakes.
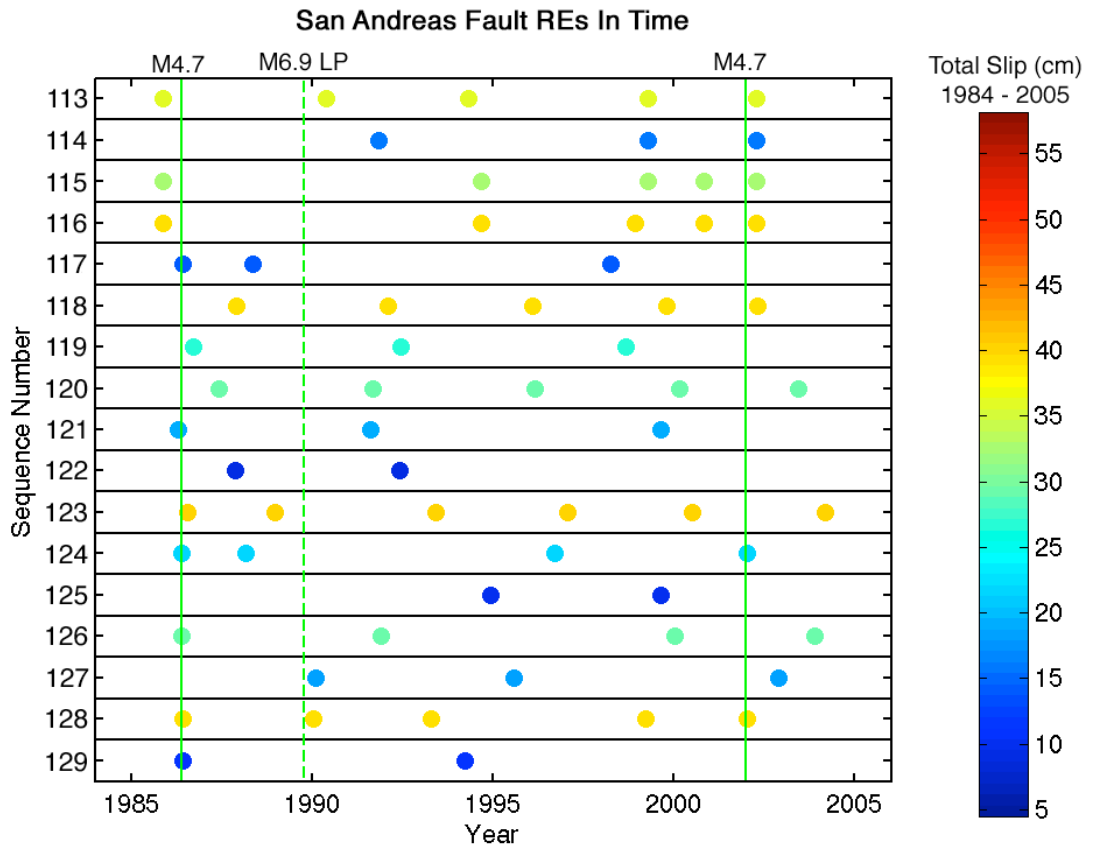
Figure 3.S17: Timing of non-burst type REs on San Andreas fault. Color indicates total amount of slip at sequence location over observation window. LP indicates time of 1989 Loma Preita earthquake. Two vertical lines indicate times of nearby M4.7 earthquakes.
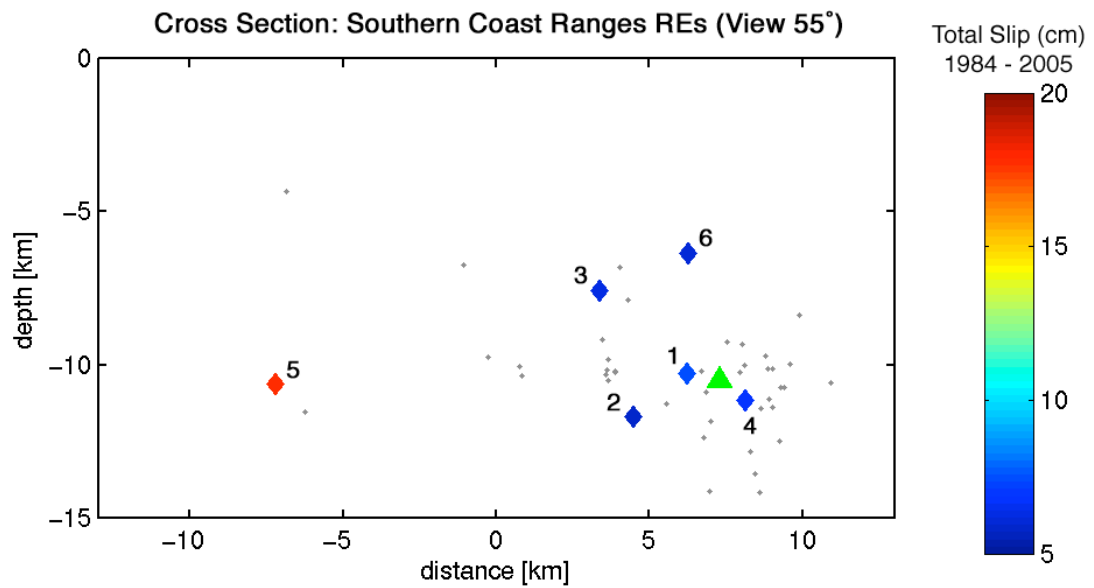
Figure 3.S18: Cross section view of southern Coast Ranges REs. Burst type REs are colored triangles and labels are individual sequence names for reference. Color indicates the cumulative amount of slip at each sequence location over the observation period. Small dots are background seismicity. Triangle indicates earthquake larger than M4.0.
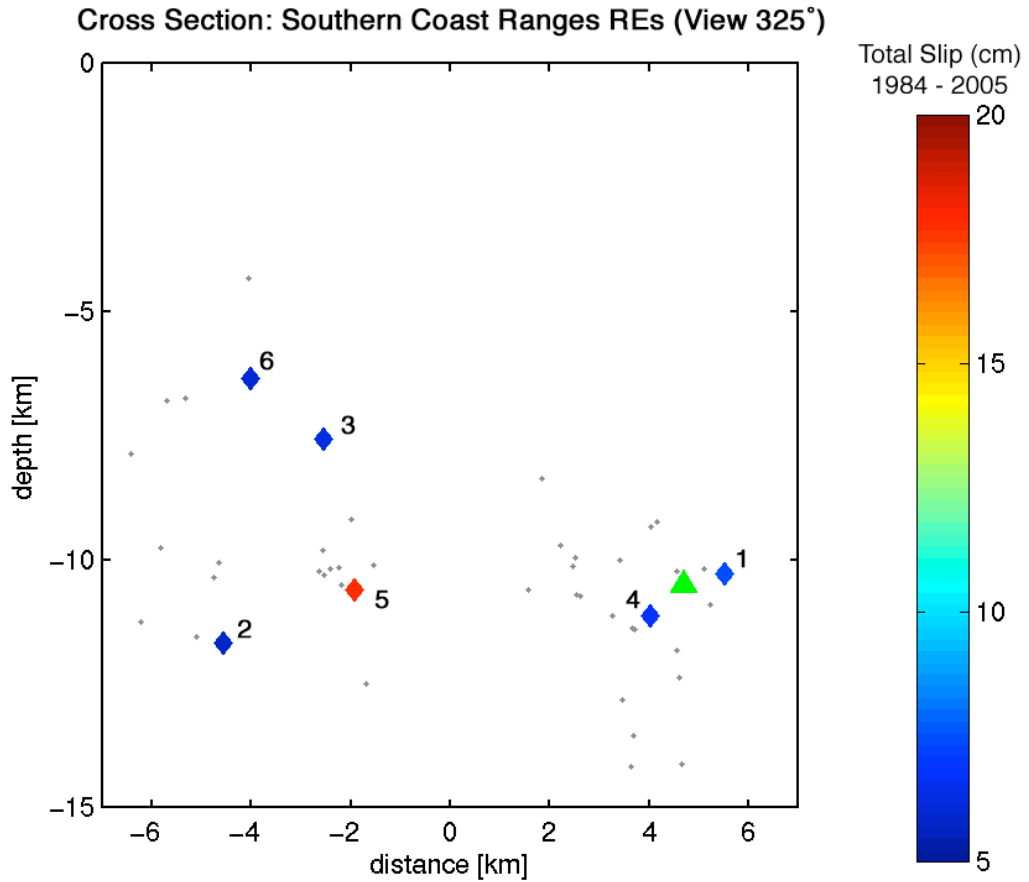
Figure 3.S19: Cross section view of southern Coast Ranges REs. Burst type REs are colored triangles and labels are individual sequence names for reference. Color indicates the cumulative amount of slip at each sequence location over the observation period. Small dots are background seismicity. Triangle indicates earthquake larger than M4.0.
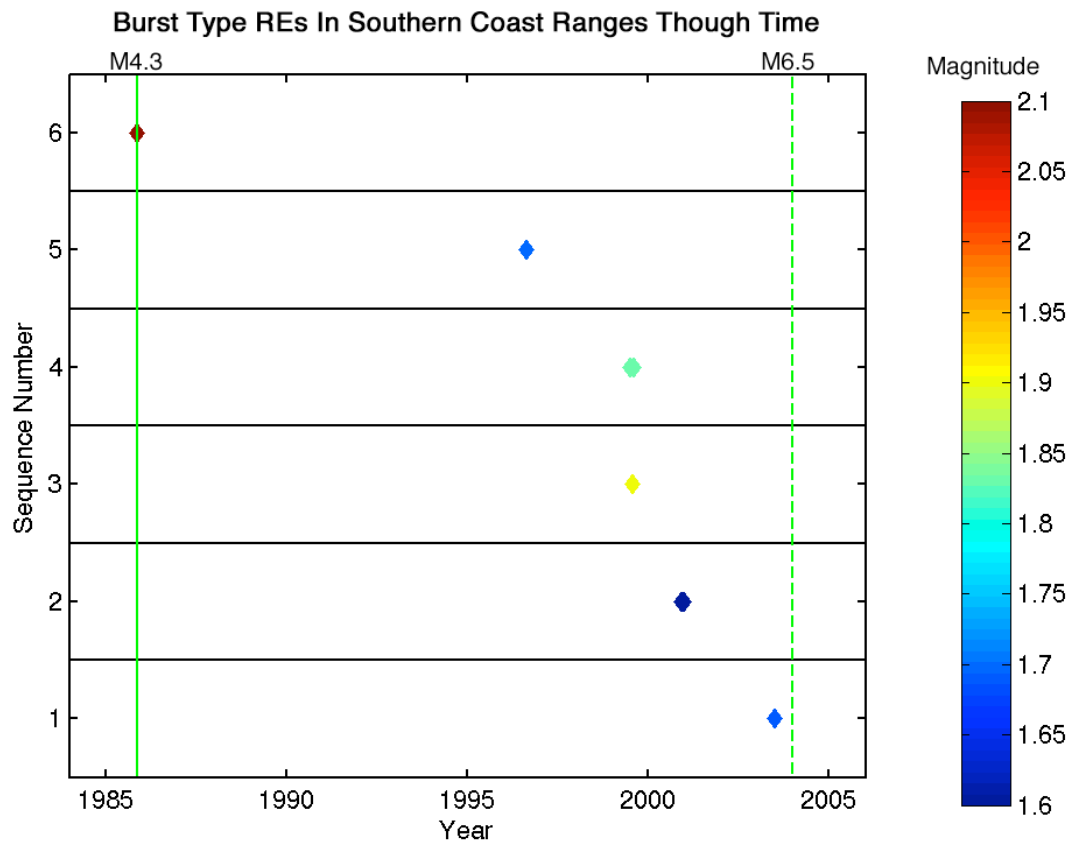
Figure 3.S20: Timing of burst type REs on southern Coast Ranges. Color indicates average magnitude of events within sequence. Two vertical lines indicate times of nearby larger earthquakes.

3.5 Discussion

3.5.1 Comparison With Geologic and Geodetic Data

Within the juncture study area, the San Andreas and southern Calaveras-Paicines faults are known to creep aseismically from surface data (Galehouse and Lienkaemper, 2003 ; Lisowski and Prescott, 1981). The identification of RE sequences along these faults identifies portions of the fault that are actively slipping at depth as well. No surface creep measurements have been taken across the Quien Sabe fault zone and space geodetic measurements have been inconclusive as well, possibly hampered by non-tectonic vertical deformation due to groundwater movement in this area (Johanson and Bürgmann, 2005). However, the RE seismological data clearly identify two major segments of this fault that actively creeped, at least at depth, over the observation period.

A comparison between the 22+/- 6 mm/yr overall long-term slip rate determined for the San Andreas fault segment north of the branch-off with the southern Calaveras-Paicines fault (Kelson et al., 1992) and slip rates determined in this study by non-burst type RE data at individual sequence locations shows that the majority of the RE slip patches are slipping at rates lower than the long-term slip. The average slip rate for the 99 San Andreas fault RE sequence identified is 11.6 mm/yr, with a maximum slip rate observed at a RE location of 26.7 mm/yr. However, although the RE data are not consistent with the long-term rate, they are consistent with the geodetically determined value of creep of 11 +/- 3 mm/yr (Kelson et al., 1992).

Although slip on the southern Calaveras-Paicines and Quien Sabe fault zones can be highly variable in time, a similar comparison between long-term slip rates and ~22 year RE derived slip rates can be made as well. On the southern Calaveras fault, the 1999 Working Group on California Earthquake Probabilities (WG99) inferred a long-term slip rate of 15 +/- 3 mm/yr (WG99, 1999) while the creep rate is thought to be approximately 12 +/- 6 mm/yr (Kelson et al., 1992). The average slip rates from non-burst type REs is 4.1 mm/yr with a range of 2.2 – 6.5 mm/yr. Thus, the calculated average RE slip rate is lower than either the long-term rate or the geodetic creep rate indicating that the portions of the fault which nucleate REs may have been accumulating strain over the past ~22 years. This could suggest that larger asperities on the fault plane retard creep and then fail in moderate earthquakes (Oppenheimer et al., 1990 ; Manaker et al., 2003).

The Quien Sabe fault zone on the other hand has a geologically determined slip rate of only 1 +/- 1 mm/yr (Bryant, 1985). The average slip rate from non-burst type REs however, is 5.0 mm/yr on the northeast segment, with a range of 2.6 – 7.2 mm/yr, and 9.3 mm/yr on the southeast segment, with a range of 4.8 – 11.4 mm/yr. Our ~22 year averaged values are significantly higher than the geological rates. On the northeast segment this is likely due to a transient creep pulse induced by the Ml 5.5 Tres Piños earthquake. On the southwest segment, it is unclear if the higher calculated slip rates were induced by this larger event since the amount of pre-mainshock data is shorter than some of the recurrence intervals between REs, an immediate temporal triggering is not observed, and the quasi-periodic recurrence intervals indicate that creep on this segment is occurring steadily over the observation period (Figure 3.4).

3.5.2 Effects of Larger Earthquakes

The influence of larger nearby earthquakes can be clearly seen in the timing of events on the San Andreas fault. For example, a clear relationship is seen between the increase in the frequency of RE occurrences within sequences along the San Andreas fault and the timing of the Loma Prieta earthquake (Section I in Figure 3.6). The same also holds true for the 1998 Mw5.1 San Juan Bautista earthquake (Section II in Figure 3.6). In contrast, the largest event to occur in our study area, the Ml 5.5 Tres Piños earthquake on the Quien Sabe fault zone, did not produce a clear effect on the timing of RE sequences on the San Andreas fault although it is known to have caused a small change in its surface creep (Simpson et al., 1988) and to have stimulated RE activity on the Quien Sabe fault. Additionally, although a 1986 M4.7 event just south of our study area on the San Andreas fault affected the timing of REs up to 1.5 km away (Section V in Figure 3.6), a 2001 M4.7 event near the same location did not produce a clear response from nearby sequences.

While some sequences could be immediately triggered by nearby larger earthquakes, other REs even closer to the hypocenter did not immediately recur. This indicates that the timing of rupture of a RE is not only influenced by the magnitude of the additional sudden stress increase induced by nearby larger earthquakes, but also by the state of stress at the sequence location and the temporally varying load increase due to the response of the creeping fault surrounding each RE location to the additional stress. Given all the different factors that could promote a RE recurrence, it is difficult to separate out these influences given the current dataset.

On the southern Calaveras-Paicines fault, it is unclear if larger nearby earthquakes affected RE sequence repeat intervals. On the surface, however, rapid slip pulses on the order of 12 – 14 mm, followed by a temporary but large decrease in creep rate along the southern Calaveras fault until mid-1993, were clearly observed after the 1989 Loma Prieta earthquake at creepmeters in Hollister (Galehouse and Lienkaemper, 2003). If present, a small change in creep at depth could have been masked by the lower background creep rate on this fault combined with the somewhat short pre-Loma Prieta time window. This could also explain why the timing of RE sequences did not appear to be effected by any nearby earthquakes larger than M4.0.

Larger earthquakes on the San Andreas fault did not influence the timing of RE sequences on the Quien Sabe fault. Additionally, although the Ml 5.5 1986 Tres Piños earthquake produced a clear effect on sequences on the northeastern Quien Sabe segment, a M5.1 1988 event also on the Quien Sabe fault zone did not appear to trigger any REs. However, a small effect could have been hidden by the stronger influence that the nearby Ml 5.5 Tres Piños earthquake previously exerted on these sequences.

3.5.3 Burst Type REs

We identify 24 burst type REs on or near all three active faults in the San Andreas fault juncture area. Three burst type REs, located near the creeping southern Calaveras and Quien Sabe faults (Figure 3.2A), do not appear to be associated with nearby larger earthquakes.

Most of the remaining burst type REs occurred on the San Andreas fault after the Mw5.1 San Juan Bautista event and subsequent slow earthquake (Figure 3.7). It is unclear if these burst type REs result from the static stress changes associated with the San Juan Bautista mainshock, from the immediate triggered aseismic slip due to the subsequent 1998 slow slip event, or from a different mechanism entirely.

These San Juan Bautista RE bursts appear to be unique in that neither the Mw6.9 Loma Prieta nor the Ml5.5 Tres Piños earthquakes triggered any bursts. However, it is important to note that the Loma Prieta earthquake occurred 30km to the north of our study area, perhaps too far away for bursts to be triggered within our study area, and that the Tres Piños earthquake occurred on a fault structure separate from those which nucleated the REs on the Quien Sabe fault zone. Moreover, a previous 1996 slow earthquake, which also occurred within our study area on the San Andreas fault and was of comparable moment with the 1998 slow earthquake, did not appear to trigger any bursts. However, at the time of the 1996 slow slip event the San Juan Bautista asperity still had not ruptured and was known to be partially shielding this area from creep (Nadeau and McEvilly, 2004). Therefore, perhaps not enough creep was occurring in this area to nucleate a burst type RE. Slow slip events have also been observed along other portions of the San Andreas fault (Linde et al., 1996), however, studies specifically looking for burst type REs have not yet been conducted near these events.

It is unclear as to why burst type REs south of the San Juan Bautista mainshock do not appear to be temporally correlated with larger events, or in fact with each other. The only common attribute between bursts in the northern and southern

ends of the San Andreas fault studied are that most of these bursts occur on the lowermost boundary of the area where REs are seen to nucleate, (Figure 3.S9), suggesting perhaps a change in fault zone lithology, rheology, physical conditions, and/or a change between locked and creeping behavior on the fault as influences on the occurrence of burst type REs seen on the San Andreas fault.

3.5.4 Southern Coast Ranges REs

In the southern Coast Ranges fault system west of the San Andreas fault, only burst type REs occurred (Figure 3.2B). The Mw6.5 San Simeon event and associated aftershock sequence also occurred within this region within the coastal Franciscan complex. Considering the theory that fault zone lithology may influence fault creep, if one type of rock possibly found within the Franciscan mélange is promoting fault creep, the lack of REs within this complex does not rule out fault zone lithology as an important factor in the ability of faults to nucleate REs. The Franciscan complex is composed of many different types of rocks of different origins, thus the exact composition of the mélange present within the Franciscan complex in the juncture region may be different from that found within the coast Franciscan complex. Within the granitic and metamorphic Salinian block, only burst type REs are seen to occur, suggesting that granitic rocks may not promote active fault creep and cyclic loading of asperities associated with REs. However, the number of earthquakes outside of the San Simeon aftershock zone is rather small (~1,500 events) and we cannot rule out small, slowly creeping faults in this region based on the small sample of events.

3.6 Conclusions

We identify portions of the San Andreas, southern Calaveras-Paicines, and Quien Sabe fault zones as actively slipping at depth between 1 March 1984 and 1 May 2005 based on the identification of 150 RE sequences (Figure 3.2A). Of these three faults, only the San Andreas and southern Calaveras-Paicines faults are known to be also actively creeping at the surface. Although several fault structures are seismically active in the general location of the southern Calaveras fault zone, RE sequences clearly delineate one actively creeping fault plane (Figure 3.2A). Since REs did not occur in the center of our study area over the transition between the southern Calaveras and Paicines faults, it is unclear if this portion of the fault is locked, creeping at a slower rate than can be imaged, or if this portion is simply unable to nucleate RE sequences.

The recurrence intervals of REs are seen to be both quasi-periodic and aperiodic, indicating that portions of the fault were creeping steadily over the observation period while other portions had a variable creep rate, possibly influenced by stress changes induced by nearby larger earthquakes. Quasi-periodic recurrence intervals are observed for RE sequences on the southwestern segment of the Quien Sabe fault zone as well as on portions of the San Andreas and southern Calaveras-Paicines faults, suggesting that creep surrounding these RE sequences is occurring steadily at depth. Evidence of triggered creep is seen on the northwestern segment of the Quien Sabe fault zone, after the Mw5.5 1986 Tres Piños earthquake (Sequences 1-7 in Figure 3.4), and on the San Andreas fault after both the Mw6.9 1989 Loma Prieta earthquake (Section 1 in Figure 3.6) and the Mw5.1 San Juan Bautista event (Section

II in Figure 3.6). Discrete episodic creep events, not caused by larger nearby earthquakes, are also identified on the San Andreas and southern Calaveras-Paicines faults from an increase in frequency of events within certain RE sequences (for example Sequence 23 in Figure 3.5).

Of the sequences identified, 24 were burst type REs and occurred both near the southern Calaveras and Quien Sabe fault zones and also along portions of the San Andreas fault. Interestingly, the majority of these bursts occurred around the time of the Mw5.1 1998 San Juan Bautista event and subsequent slow earthquake. Further research into this intriguing phenomenon is necessary to better illuminate the mechanism causing these burst REs.

We compare the spatial and temporal behavior of REs identified on the San Andreas and southern Calaveras-Paicines fault juncture area (Box A in Figure 3.1) with the behavior of REs identified on the southern Coast Ranges fault system west of the creeping section of the San Andreas fault (Box B in Figure 3.1). Only six burst type REs are identified within the granitic and metamorphic Salinian block (Figure 3.2B). Non-burst type REs were not found in this area, even within the sliver of the coastal Franciscan which is thought to have nucleated the Mw6.5 2003 San Simeon earthquake and aftershock sequence (Hauksson et al., 2004).

The reason why some faults creep aseismically while others do not is an area of active scientific interest. The identification of RE sequences and the determination of the amount of slip at individual sequence locations have been shown to be a convenient proxy to the location and magnitude of fault creep. Two caveats must be added. The first being that burst type REs have been identified both on and off major

107

fault planes, but may not be indicative of a general background creep rate. The second

caveat is that the lack of REs along a fault plane does not necessarily indicate that

creep is not occurring. Additionally, the identification of RE sequences along the

Quien Sabe fault zone shows that faults do not need to be mature or have streaks of

seismicity for creep to occur on them. The lack of non-burst type REs on the fault

structures within the Salinian block of the southern Coast Ranges west of the creeping

section of the San Andreas fault, suggests that perhaps the production of REs, and thus

creep, is hindered in environments where granitic rocks occur on both sides of the

fault zone.

3.7 Data Sources

The Northern California Seismic Network (NCSN) phase and waveform data

used in this study was collected by the U.S. Geological Survey, Menlo Park and is

freely available from the Northern California Earthquake Data Center

(www.ncedc.org).

Chapter 4

Subsurface Creep on the Calaveras Fault, California, Following the 1984 M6.2 Morgan Hill Earthquake

4.1 Introduction

The ability to accurately determine the magnitude and location of postseismic slip after a large earthquake is essential when identifying regions that are releasing elastic strain through aseismic slip and locked areas that this slip may be further loading. This is especially important in hazard assessment studies on faults that are known to have locked and creeping sections, such as the Calaveras, Hayward and San Andreas faults. Transient postseismic slip could both relieve strain over a broader area than just that which ruptured during the earthquake, as well as increase the stress on nearby asperities, thereby promoting their future coseismic rupture.

Although not necessarily typical, on both the central Calaveras and creeping section of the San Andreas fault, the amount of postseismic afterslip following larger earthquakes can be on the same order as the coseismic slip [Prescott et al., 1984 ; Langbein et al., 2006]. The extent to which these creeping patches can influence the timing of rupture of nearby locked patches is currently under question. An

investigation of a sequence of three northward progressing earthquakes on the Calaveras fault, the 1979 M5.9 Coyote Lake earthquake, the 1984 M6.2 Morgan Hill earthquake, and the 1988 M5.1 Alum Rock earthquake, deduced that coseismic shear stress increases alone could not be wholly responsible for the sequence occurrence [Du and Aydin, 1993].

An analysis of microseismicity with respect to probable rupture areas of historic earthquakes greater than M5 along the central Calaveras fault illustrates that large earthquakes tend to rupture in deep relatively aseismic areas, suggesting that these aseismic holes are locked [Oppenheimer et al., 1990]. An independent assessment using surface geodetic data to identify regions with interseismic subsurface slip deficits reinforces the inference that these aseismic holes are locked [Manaker et al., 2003]. Similar behavior has also been observed on the Parkfield segment of the San Andreas fault where a previously identified deep section of the fault lacking REs [Nadeau and McEvilly, 1999] later ruptured as the northwest slip patch of the 2004 $M_w6.0$ Parkfield earthquake [Dreger et al., 2005]. The Morgan Hill earthquake was located within a deep, presumably locked, aseismic portion of the fault [Schaff et al., 2002].

Due to a lack of near fault surface displacement measurements prior to the Morgan Hill earthquake, it is not well known if the surface trace of the fault up-dip from the rupture area was locked or creeping [Manaker et al., 2003]. After the earthquake, a small-aperture alignment array installed four kilometers southeast of the epicenter and above the rupture zone did not reveal significant amounts of slip above the projected errors for at least two months after the mainshock [Brown, 1984].

However, early electronic distance meter (EDM) modeling by Prescott et al. [1984] showed a large 335 mm subsurface creep signal in the 4 months following the earthquake, at least a portion of which must have occurred shallower than ~4 km.

In an attempt to resolve this apparent discrepancy, we investigate the evolution of postseismic subsurface slip after the 1984 Morgan Hill earthquake using repeating earthquake (RE) data from 1984 to 2005. We image both the accelerated slip transients due to the earthquake as well as the return to interseismic background rates. RE data are used to develop a dislocation model of the first 6 and 18 months of surface deformation, which we compare with a compilation of available surface EDM line-length changes of stations near the Morgan Hill earthquake. The modeling shows that additional creep is required to match observed line-length rates, most likely below the rupture and seismogenic zone or outside our fault model boundaries.

4.2 Repeating Earthquake Identification

REs are sequences of events that are thought to rupture the same asperity on the fault surface and thus produce nearly identical earthquake records [Nadeau and McEvilly, 1999]. In this study, we identify RE sequences on the Calaveras fault using a combination of cross-correlation techniques and phase and amplitude spectra coherence measures, which we will summarize below. Further descriptions of this method can be found in Nadeau and McEvilly [2004, supplemental online material] and Templeton et al. [2007, in review].

To identify RE sequences, we cross-correlate all pairs of events within our study area with epicentral separations of up to 10 km (Figure 1A). Vertical
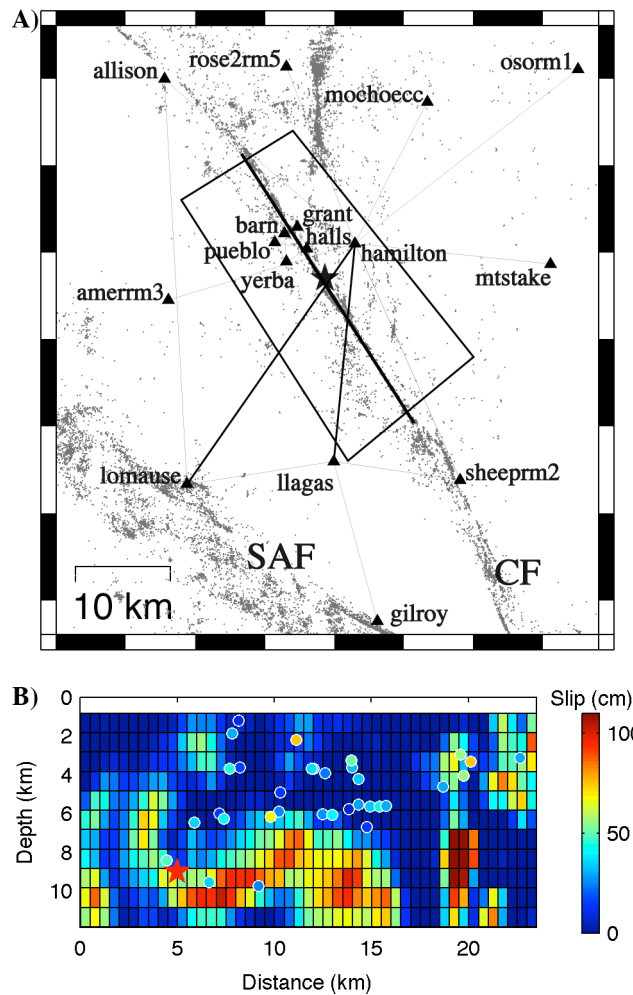
Figure 4.1: A) Location map with EDM stations as black inverted triangles, surface fault traces as thick grey lines, relocated background seismicity [Ellsworth et al., 2000] as small grey dots. Fault model as thick black line. Study area indicated by black box and Morgan Hill epicenter by black star. B) Locations of REs included in forward model in cross-section as circles color coded by total slip over the observation period. Beroza and Spudich (1988) coseismic rupture model is shown in the background. We realign the depth of the hypocenter of the rupture model to match that found by the earthquake relocations of Schaff et al. (2002).

component, short-period Northern California Seismic Network (NCSN) waveforms

from stations up to 50 km away from the center of our study area are used in this

analysis. A master-pair of events is selected for further consideration if their average

cross-correlation coefficient across all stations is greater then 0.98 as determined by

using a 5-second time window beginning with the P-phase arrival. We then calculate

the phase and amplitude coherence for this master-pair of events between 8-20 Hz. If

the average of the phase and amplitude coherence assessments is greater than 0.85, the

master-pair is identified as a RE. To identify additional members of the RE sequence,

phase and amplitude coherence assessments are then performed on all events with

average cross-correlation coefficients greater then 0.85 with at least one master-pair

event. Individual events are included if their average spectral coherence is greater than

0.85.

Using this methodology, we identify 85 RE sequences on the central Calaveras

fault (Figure 1B; Table S1). This number is slightly less than half the number of RE

sequences that other authors have identified in this region. However Peng et al. [2005]

and Schaff et al. [2002] used a selection criteria based on magnitude, relocated

hypocenter similarities, and circular rupture dimensions based on an assumed stress

drop to identify REs, while this study uses a more conservative method which relies

on waveform similarities.

4.3 Subsurface Slip

RE seismological data has several advantages when investigating postseismic

deformation at depth after a large earthquake, the most important of which is the

ability to gain subsurface slip information over the entire post-seismic period with pre-

existing instruments. The limitation of this method is that it is restricted to areas on the

fault that also produce REs. On this section of the Calaveras fault, seismicity generally

1	37.4221	-121.7690	7.32	1.60	11.2	0.51	
	1990.008.222628	37.4237	-121.7687	7.25	1.53		
	1991.213.135922	37.4210	-121.7695	7.32	1.59		
	2005.245.174336	37.4217	-121.7688	7.38	1.66		
2	37.4171	-121.7684	5.79	1.62	28.2	1.29	
	1986.196.175834	37.4185	-121.7692	6.09	1.65		
	1989.354.145729	37.4167	-121.7668	5.62	1.49		
	1993.316.225516	37.4170	-121.7685	5.76	1.56		
	1998.114.131427	37.4175	-121.7685	5.53	1.56		
	2002.084.142828	37.4173	-121.7690	6.10	1.70		
	2005.350.204128	37.4158	-121.7685	5.62	1.69		
3	37.4120	-121.7626	5.78	1.53	16.1	0.74	
	1985.091.171618	37.4120	-121.7622	5.60	1.46		
	1994.152.064034	37.4117	-121.7622	5.76	1.49		
	1998.129.121335	37.4115	-121.7627	5.85	1.55		
	2004.183.193535	37.4127	-121.7632	5.92	1.60		
4	37.4129	-121.7628	7.10	2.33	17.1	0.79	
	1987.047.011104	37.4128	-121.7630	7.04	2.29		
	1997.344.134514	37.4127	-121.7623	7.01	2.26		
	2004.346.133227	37.4133	-121.7630	7.26	2.42		
5	37.4108	-121.7604	6.93	1.93	6.8	0.31	
	1993.164.143724	37.4117	-121.7607	6.81	1.98		
	1998.048.110053	37.4098	-121.7602	7.06	1.86		
6	37.3992	-121.7652	3.58	2.24	24.4	1.12	
	1986.038.171527	37.3998	-121.7660	3.46	2.40		
	1992.117.191709	37.3988	-121.7655	3.34	2.13		
	1998.159.001759	37.3992	-121.7640	3.67	2.17		
	2004.114.050348	37.3990	-121.7655	3.87	2.17		

Table 4.S1A: First line within each row indicates the sequence label number, average sequence latitude, average sequence longitude, average sequence depth, average sequence magnitude, total amount of slip (cm), and slip rate (mm/yr) at sequence location. Following lines indicate earthquake time, earthquake latitude, earthquake longitude, earthquake depth, and earthquake magnitude for each individual event within a repeating earthquake sequence.

7	37.3755	-121.7665	2.58	2.00	14.1	0.65	
	1984.229.233953	37.3768	-121.7668	1.37	1.99		
	1995.213.092913	37.3743	-121.7660	2.92	1.98		
	2003.193.122751	37.3755	-121.7668	3.46	2.04		
8	37.3874	-121.7431	6.17	1.99	21.1	0.96	
	1987.313.123958	37.3888	-121.7438	5.44	1.92		
	1991.008.113318	37.3865	-121.7430	6.43	1.98		
	1995.068.035619	37.3870	-121.7423	6.42	2.05		
	1999.215.154412	37.3872	-121.7433	6.39	2.01		
9	37.3757	-121.7322	8.45	1.80	50.2	2.30	
	1984.151.074333	37.3748	-121.7305	8.57	2.08		
	1986.186.090059	37.3750	-121.7320	8.52	1.86		
	1991.030.045325	37.3755	-121.7327	8.21	1.47		
	1994.181.124315	37.3762	-121.7328	8.25	1.84		
	1996.232.085444	37.3758	-121.7322	8.17	1.56		
	1996.286.093208	37.3758	-121.7323	8.47	1.69		
	1998.285.224448	37.3753	-121.7317	8.48	1.91		
	2002.352.043902	37.3765	-121.7328	8.86	1.63		
	2002.352.050847	37.3760	-121.7330	8.49	1.47		
10	37.3715	-121.7288	8.53	1.38	29.4	1.35	
	1984.355.063628	37.3713	-121.7287	8.66	1.20		
	1988.318.193144	37.3717	-121.7293	8.58	1.58		
	1989.255.162218	37.3723	-121.7283	8.41	1.52		
	1990.290.095415	37.3708	-121.7275	8.67	1.32		
	1995.092.074401	37.3713	-121.7278	8.85	0.87		
	1997.306.163412	37.3727	-121.7315	8.75	1.48		
	2003.310.073347	37.3703	-121.7283	7.77	1.01		

Table 4.S1B: First line within each row indicates the sequence label number, average sequence latitude, average sequence longitude, average sequence depth, average sequence magnitude, total amount of slip (cm), and slip rate (mm/yr) at sequence location. Following lines indicate earthquake time, earthquake latitude, earthquake longitude, earthquake depth, and earthquake magnitude for each individual event within a repeating earthquake sequence.

11	37.3739	-121.7336	6.65	1.48	20.8	0.95
	1988.122.140753	37.3732	-121.7338	6.61	1.36	
	1989.266.230235	37.3753	-121.7358	6.54	1.41	
	1998.272.053016	37.3733	-121.7333	6.78	1.56	
	2002.181.055808	37.3732	-121.7318	6.23	1.49	
	2004.323.193616	37.3743	-121.7330	7.11	1.55	
12	37.3609	-121.7369	2.04	1.48	10.4	0.48
	1987.112.150227	37.3612	-121.7367	1.86	1.49	
	1992.313.213727	37.3608	-121.7358	2.04	1.49	
	2000.192.052232	37.3607	-121.7383	2.22	1.47	
13	37.3588	-121.7255	6.64	2.50	28.4	1.30
	1986.218.185924	37.3580	-121.7258	6.50	2.50	
	1989.233.202357	37.3587	-121.7252	6.60	2.49	
	1996.245.143447	37.3592	-121.7252	6.56	2.51	
	2000.272.084406	37.3593	-121.7260	6.91	2.48	
14	37.3539	-121.7208	5.99	2.11	15.1	0.69
	1993.104.121635	37.3538	-121.7215	5.81	1.96	
	1995.133.132338	37.3540	-121.7207	6.06	2.16	
	1998.224.053333	37.3540	-121.7202	6.11	2.16	
15	37.3528	-121.7200	5.83	1.67	40.7	1.86
	1986.282.231459	37.3523	-121.7202	5.70	1.49	
	1988.135.205134	37.3520	-121.7198	5.93	1.74	
	1990.018.032441	37.3520	-121.7197	5.95	1.71	
	1991.341.111502	37.3527	-121.7205	5.81	1.79	
	1996.247.041356	37.3533	-121.7210	6.07	1.57	
	1998.224.055803	37.3537	-121.7192	5.98	1.63	
	2002.320.085155	37.3542	-121.7202	5.89	1.64	
	2005.204.112204	37.3522	-121.7198	5.32	1.64	

Table 4.S1C: First line within each row indicates the sequence label number, average sequence latitude, average sequence longitude, average sequence depth, average sequence magnitude, total amount of slip (cm), and slip rate (mm/yr) at sequence location. Following lines indicate earthquake time, earthquake latitude, earthquake longitude, earthquake depth, and earthquake magnitude for each individual event within a repeating earthquake sequence.

16	37.3534	-121.7226	4.65	1.33	42.9	1.96	
1985.017.062909	37.3527	-121.7237	4.68	1.19			
1986.127.141013	37.3533	-121.7227	4.60	1.31			
1987.326.095712	37.3535	-121.7232	4.61	1.09			
1988.301.121341	37.3540	-121.7223	4.84	1.12			
1992.285.053208	37.3535	-121.7238	4.80	1.13			
1995.336.211714	37.3530	-121.7222	4.56	1.45			
1998.174.150554	37.3540	-121.7217	4.45	1.47			
2001.079.173135	37.3533	-121.7220	4.51	1.36			
2003.016.123107	37.3533	-121.7225	4.40	1.38			
2005.205.132315	37.3533	-121.7217	5.06	1.43			
17	37.3574	-121.7215	8.27	1.97	6.9	0.32	
1994.203.043558	37.3575	-121.7207	8.16	1.86			
1996.214.052454	37.3573	-121.7223	8.38	2.05			
18	37.3427	-121.7173	1.24	1.59	27.7	1.27	
1987.128.155242	37.3418	-121.7185	1.22	1.73			
1989.131.001611	37.3440	-121.7190	2.58	0.96			
1993.161.160641	37.3417	-121.7163	0.33	1.77			
1997.202.164657	37.3408	-121.7178	1.01	1.69			
2000.306.173349	37.3447	-121.7167	0.93	1.26			
2003.044.170339	37.3432	-121.7155	1.38	1.47			
19	37.3385	-121.7049	7.64	1.57	21.9	1.00	
1986.305.145338	37.3383	-121.7055	7.10	1.73			
1988.048.065645	37.3380	-121.7057	7.80	1.51			
1996.191.005458	37.3390	-121.7045	7.83	1.24			
2000.185.222135	37.3380	-121.7043	7.73	1.51			
2001.360.175120	37.3392	-121.7047	7.73	1.64			

Table 4.S1D: First line within each row indicates the sequence label number, average sequence latitude, average sequence longitude, average sequence depth, average sequence magnitude, total amount of slip (cm), and slip rate (mm/yr) at sequence location. Following lines indicate earthquake time, earthquake latitude, earthquake longitude, earthquake depth, and earthquake magnitude for each individual event within a repeating earthquake sequence.

20	37.3320	-121.6995	7.56	1.52	42.6	1.95
	1984.169.151248	37.3317	-121.6988	7.46	1.51	
	1987.322.054535	37.3318	-121.7000	7.38	1.45	
	1988.134.072908	37.3318	-121.6997	7.50	1.37	
	1990.134.160910	37.3320	-121.6988	7.21	1.43	
	1990.310.173912	37.3323	-121.7002	7.79	1.57	
	1997.157.035026	37.3323	-121.6992	7.77	1.63	
	2001.057.060653	37.3330	-121.7008	8.12	1.47	
	2003.059.151613	37.3317	-121.6983	7.25	1.51	
	2005.334.002059	37.3310	-121.6993	7.60	1.63	
21	37.3269	-121.6955	7.10	1.76	18.4	0.84
	1988.024.173657	37.3278	-121.6975	6.79	1.59	
	1995.083.192743	37.3255	-121.6948	7.27	0.98	
	2000.047.052425	37.3275	-121.6958	7.14	1.84	
	2005.046.211433	37.3268	-121.6937	7.19	1.95	
22	37.3221	-121.6936	5.19	1.56	54.5	2.50
	1984.260.060614	37.3213	-121.6930	4.74	1.59	
	1986.137.234321	37.3210	-121.6937	5.17	1.42	
	1987.148.005948	37.3218	-121.6943	5.11	1.51	
	1988.267.153608	37.3218	-121.6933	4.85	1.57	
	1990.045.013657	37.3222	-121.6942	5.13	1.62	
	1991.316.161115	37.3218	-121.6943	5.32	1.55	
	1994.015.055354	37.3223	-121.6935	5.26	1.49	
	1996.030.001520	37.3218	-121.6942	5.41	1.51	
	1998.007.202308	37.3225	-121.6938	5.13	1.51	
	2002.232.065848	37.3242	-121.6923	5.15	1.69	
	2005.098.054640	37.3218	-121.6925	5.78	1.58	

Table 4.S1E: First line within each row indicates the sequence label number, average sequence latitude, average sequence longitude, average sequence depth, average sequence magnitude, total amount of slip (cm), and slip rate (mm/yr) at sequence location. Following lines indicate earthquake time, earthquake latitude, earthquake longitude, earthquake depth, and earthquake magnitude for each individual event within a repeating earthquake sequence.

23	37.3210	-121.6904	7.85	1.59	38.8	1.78	
	1984.167.020741	37.3213	-121.6912	7.69	1.77		
	1984.205.042704	37.3215	-121.6907	7.98	1.47		
	1984.257.154253	37.3208	-121.6902	7.25	1.70		
	1984.303.232820	37.3200	-121.6890	8.02	1.23		
	1984.358.213926	37.3213	-121.6910	7.87	1.59		
	1985.067.080327	37.3210	-121.6902	7.91	1.76		
	1985.277.221809	37.3215	-121.6907	7.96	1.28		
	1986.205.193519	37.3202	-121.6902	8.14	1.28		
24	37.3205	-121.6900	7.50	1.35	9.6	0.44	
	1984.161.125705	37.3210	-121.6907	7.89	1.38		
	1984.219.210703	37.3197	-121.6878	6.39	1.42		
	1984.249.160104	37.3207	-121.6915	8.23	1.18		
25	37.3149	-121.6892	2.76	1.29	23.3	1.07	
	1984.310.004114	37.3133	-121.6913	3.03	1.19		
	1985.303.012612	37.3218	-121.6843	0.31	0.00		
	1986.327.220617	37.3127	-121.6907	3.09	1.30		
	1995.204.043507	37.3133	-121.6890	3.09	1.33		
	2001.058.120442	37.3147	-121.6902	2.86	1.39		
	2005.323.100420	37.3133	-121.6898	4.19	1.42		
26	37.3099	-121.6820	6.48	1.48	52.0	2.38	
	1984.127.143748	37.3098	-121.6810	6.35	1.58		
	1984.157.040122	37.3102	-121.6837	6.40	1.43		
	1984.327.145022	37.3093	-121.6818	6.14	1.46		
	1985.158.140942	37.3100	-121.6832	6.20	1.48		
	1986.049.030330	37.3103	-121.6830	5.97	1.55		
	1987.014.222731	37.3098	-121.6830	6.45	1.49		
	1988.036.180459	37.3102	-121.6818	6.20	1.36		
	1989.159.185749	37.3102	-121.6832	6.35	1.33		
	1993.174.054010	37.3098	-121.6825	6.20	1.53		
	1998.190.093415	37.3107	-121.6828	6.79	1.47		
	2001.214.120020	37.3090	-121.6758	8.23	1.53		

Table 4.S1F: First line within each row indicates the sequence label number, average sequence latitude, average sequence longitude, average sequence depth, average sequence magnitude, total amount of slip (cm), and slip rate (mm/yr) at sequence location. Following lines indicate earthquake time, earthquake latitude, earthquake longitude, earthquake depth, and earthquake magnitude for each individual event within a repeating earthquake sequence.

27	37.3042	-121.6751	9.04	1.48	10.4	0.48	
	1984.127.124456	37.3035	-121.6748	9.14	1.56		
	1984.150.013559	37.3050	-121.6745	8.47	1.61		
	1984.189.045333	37.3040	-121.6760	9.52	0.80		
28	37.3022	-121.6761	6.53	1.85	12.9	0.59	
	1989.267.152501	37.3020	-121.6753	6.69	1.76		
	1996.131.224353	37.3022	-121.6763	6.34	1.88		
	2003.292.182910	37.3025	-121.6765	6.55	1.88		
29	37.3002	-121.6750	5.70	1.81	31.6	1.45	
	1984.143.033003	37.2998	-121.6733	5.91	1.66		
	1984.172.031831	37.2997	-121.6752	5.54	1.83		
	1984.328.150602	37.2998	-121.6750	5.62	1.89		
	1985.106.233935	37.3003	-121.6750	5.59	1.78		
	1985.308.195835	37.3002	-121.6753	5.60	1.87		
	2000.158.034820	37.3013	-121.6760	5.92	1.79		
30	37.2996	-121.6733	6.23	1.39	24.7	1.13	
	1984.232.073437	37.2995	-121.6733	6.09	1.50		
	1986.160.041518	37.2995	-121.6730	6.16	1.53		
	1988.059.225227	37.2998	-121.6735	6.40	1.34		
	1989.316.120001	37.2997	-121.6743	6.45	1.30		
	1992.087.005413	37.2992	-121.6728	6.08	1.27		
	1995.030.045148	37.2997	-121.6727	6.18	1.24		

Table 4.S1G: First line within each row indicates the sequence label number, average sequence latitude, average sequence longitude, average sequence depth, average sequence magnitude, total amount of slip (cm), and slip rate (mm/yr) at sequence location. Following lines indicate earthquake time, earthquake latitude, earthquake longitude, earthquake depth, and earthquake magnitude for each individual event within a repeating earthquake sequence.

31	37.2997	-121.6736	6.60	1.33	66.7	3.05	
	1984.115.225824	37.2985	-121.6723	5.83	1.53		
	1984.116.120403	37.3023	-121.6760	7.30	0.00		
	1984.117.144908	37.2977	-121.6718	5.86	1.53		
	1984.124.155900	37.2985	-121.6725	5.98	1.27		
	1984.142.172746	37.3093	-121.6775	10.32	1.32		
	1984.206.202408	37.2982	-121.6730	6.02	1.28		
	1984.299.122500	37.2990	-121.6732	6.46	1.12		
	1985.170.062933	37.2988	-121.6740	6.14	1.39		
	1986.150.224121	37.2985	-121.6727	6.61	1.34		
	1988.253.133738	37.2987	-121.6742	6.26	1.35		
	1990.264.225958	37.2995	-121.6748	6.25	1.30		
	1992.009.083923	37.2987	-121.6723	6.24	0.97		
	1993.127.102055	37.2985	-121.6738	6.43	0.88		
	1994.077.082506	37.2993	-121.6728	6.28	1.34		
	2004.223.044802	37.2993	-121.6735	6.98	1.48		
32	37.2977	-121.6699	6.18	1.44	15.2	0.70	
	1986.194.022853	37.2968	-121.6717	6.23	1.11		
	1993.096.233803	37.2977	-121.6718	6.64	1.53		
	1996.267.142306	37.2985	-121.6698	5.52	1.41		
	2002.163.151422	37.2977	-121.6663	6.34	1.54		
33	37.2898	-121.6744	0.66	1.43	30.3	1.39	
	1984.116.033945	37.2902	-121.6710	0.03	1.47		
	1984.302.092104	37.2902	-121.6775	0.03	1.27		
	1986.082.022915	37.2897	-121.6762	0.04	1.33		
	1989.144.193734	37.2893	-121.6745	0.26	1.36		
	1993.229.150743	37.2900	-121.6755	0.24	1.48		
	1997.277.051310	37.2890	-121.6743	1.11	1.43		
	2005.143.115232	37.2902	-121.6720	2.90	1.57		

Table 4.S1H: First line within each row indicates the sequence label number, average sequence latitude, average sequence longitude, average sequence depth, average sequence magnitude, total amount of slip (cm), and slip rate (mm/yr) at sequence location. Following lines indicate earthquake time, earthquake latitude, earthquake longitude, earthquake depth, and earthquake magnitude for each individual event within a repeating earthquake sequence.

34	37.2940	-121.6766	2.01	1.71	35.7	1.64	
	1985.012.075917	37.2935	-121.6767	2.05	1.84		
	1986.066.084827	37.2940	-121.6765	1.61	1.68		
	1987.334.081605	37.2943	-121.6773	2.13	1.74		
	1991.364.022142	37.2935	-121.6757	2.03	1.52		
	1994.153.154911	37.2942	-121.6765	1.95	1.70		
	2000.193.093900	37.2943	-121.6763	2.11	1.69		
	2004.216.153357	37.2942	-121.6770	2.20	1.70		
35	26.6953	-113.3927	1.87	1.36	67.9	3.11	
	1984.119.210830	37.2943	-121.6773	1.65	1.46		
	1984.209.231924	37.2932	-121.6743	1.78	0.97		
	1985.322.080228	37.2940	-121.6775	1.78	1.50		
	1987.145.203232	37.2940	-121.6783	1.96	1.52		
	1988.306.194625	37.2935	-121.6770	1.73	1.38		
	1989.353.200807	37.2940	-121.6760	1.80	1.31		
	1991.084.232228	37.2943	-121.6765	1.68	1.46		
	1993.027.112241	37.2935	-121.6763	2.08	1.39		
	1994.301.080639	37.2938	-121.6765	1.91	1.00		
	1995.255.110338	37.2937	-121.6768	2.00	1.42		
	1997.171.201650	37.2830	-121.6792	4.23	1.16		
	1998.304.004156	37.2932	-121.6745	2.16	1.17		
	2000.230.224428	37.2972	-121.6778	1.82	1.43		
	2004.217.044111	37.2947	-121.6770	2.58	1.49		
36	37.2942	-121.6763	2.12	1.78	62.0	2.84	
	1985.012.224242	37.2940	-121.6772	1.96	1.82		
	1986.079.200720	37.2938	-121.6772	2.15	1.85		
	1987.122.060003	37.2937	-121.6773	2.04	1.64		
	1987.318.101436	37.2940	-121.6772	1.98	1.54		
	1988.318.183716	37.2938	-121.6767	2.13	1.75		
	1991.056.153534	37.2943	-121.6760	2.18	2.07		
	1993.297.110655	37.2937	-121.6760	2.31	1.75		
	1997.233.050240	37.2945	-121.6758	2.17	1.71		
	2000.137.012217	37.2968	-121.6782	1.44	1.74		
	2003.112.004444	37.2942	-121.6755	2.17	1.69		
	2004.324.114133	37.2932	-121.6725	2.75	1.54		

Table 4.S1I: First line within each row indicates the sequence label number, average sequence latitude, average sequence longitude, average sequence depth, average sequence magnitude, total amount of slip (cm), and slip rate (mm/yr) at sequence location. Following lines indicate earthquake time, earthquake latitude, earthquake longitude, earthquake depth, and earthquake magnitude for each individual event within a repeating earthquake sequence.

37	37.2936	-121.6763	1.74	1.83	44.7	2.05	
	1984.221.001704	37.2932	-121.6762	1.44	1.85		
	1985.321.191308	37.2938	-121.6755	1.75	1.83		
	1986.157.123245	37.2927	-121.6752	1.95	1.36		
	1987.174.233033	37.2935	-121.6768	1.76	1.81		
	1991.085.014938	37.2930	-121.6775	1.45	1.82		
	1993.157.095712	37.2933	-121.6763	1.98	1.85		
	1995.258.121500	37.2937	-121.6762	1.89	1.80		
	2000.134.021909	37.2957	-121.6767	1.70	2.00		
38	37.2939	-121.6760	1.74	1.38	39.2	1.80	
	1988.108.104206	37.2928	-121.6758	1.82	1.39		
	1990.029.013959	37.2933	-121.6758	1.89	1.34		
	1991.193.113814	37.2933	-121.6758	2.11	1.23		
	1993.067.183803	37.2932	-121.6758	1.96	1.35		
	1995.040.022444	37.2932	-121.6750	1.78	1.29		
	1997.033.010612	37.2942	-121.6727	1.08	1.47		
	2000.129.042440	37.2955	-121.6747	1.28	1.46		
	2003.160.044248	37.2925	-121.6753	2.43	1.46		
	2005.364.175812	37.2970	-121.6828	1.33	1.35		
39	37.2932	-121.6753	1.97	1.41	49.9	2.29	
	1984.225.012051	37.2933	-121.6775	1.66	1.27		
	1985.161.215752	37.2928	-121.6750	1.97	1.43		
	1986.201.021848	37.2957	-121.6785	1.57	1.40		
	1990.212.104647	37.2927	-121.6752	2.27	1.41		
	1993.153.103257	37.2927	-121.6762	2.08	1.43		
	1995.062.141822	37.2927	-121.6755	1.93	1.26		
	1997.005.061042	37.2923	-121.6747	2.00	1.35		
	1998.214.095058	37.2933	-121.6745	1.74	1.49		
	2001.074.122020	37.2942	-121.6735	1.79	1.49		
	2003.165.135828	37.2927	-121.6750	2.02	1.36		
	2005.334.095356	37.2927	-121.6732	2.62	1.48		

Table 4.S1J: First line within each row indicates the sequence label number, average sequence latitude, average sequence longitude, average sequence depth, average sequence magnitude, total amount of slip (cm), and slip rate (mm/yr) at sequence location. Following lines indicate earthquake time, earthquake latitude, earthquake longitude, earthquake depth, and earthquake magnitude for each individual event within a repeating earthquake sequence.

40	34.5229	-112.3130	1.70	1.30	56.2	2.57
	1985.112.203709	37.2898	-121.6715	1.90	1.27	
	1986.012.013343	37.2905	-121.6743	1.75	1.20	
	1986.334.181950	37.2897	-121.6728	1.98	1.34	
	1988.015.152317	37.2907	-121.6747	1.48	1.33	
	1989.040.234327	37.2903	-121.6740	1.84	1.31	
	1990.232.104757	37.2905	-121.6728	1.92	1.40	
	1992.085.125515	37.2890	-121.6728	1.81	1.26	
	1993.343.014441	37.2905	-121.6743	1.89	1.25	
	1995.179.091357	37.2902	-121.6733	1.92	1.45	
	1998.258.054806	37.2900	-121.6732	1.73	1.32	
	2001.023.171236	37.2932	-121.6673	0.06	1.31	
	2002.234.153718	37.2932	-121.6713	3.15	1.21	
	2004.309.081609	37.2898	-121.6700	1.66	1.37	

41	37.2894	-121.6722	1.86	1.60	50.2	2.30
	1984.145.072840	37.2893	-121.6722	1.66	1.53	
	1985.118.125532	37.2887	-121.6727	2.08	1.69	
	1987.296.052821	37.2895	-121.6728	1.95	1.56	
	1989.043.224212	37.2897	-121.6745	1.88	1.60	
	1990.246.000917	37.2898	-121.6735	1.81	1.57	
	1992.085.180019	37.2890	-121.6718	1.68	1.46	
	1994.166.193253	37.2892	-121.6722	1.70	1.59	
	1997.271.020915	37.2893	-121.6718	2.00	1.64	
	2001.309.121551	37.2903	-121.6695	1.82	1.64	
	2005.329.221521	37.2893	-121.6708	2.06	1.64	

42	37.2886	-121.6723	1.94	1.92	60.6	2.78
	1984.144.183558	37.2882	-121.6757	0.70	1.96	
	1985.031.074614	37.2882	-121.6723	1.90	1.93	
	1988.189.102418	37.2883	-121.6732	1.76	1.95	
	1990.221.085352	37.2883	-121.6723	2.15	1.94	
	1992.213.005340	37.2883	-121.6717	1.84	1.91	
	1995.072.140831	37.2885	-121.6727	1.83	2.00	
	1997.206.054908	37.2882	-121.6722	2.24	1.84	
	2000.008.044431	37.2893	-121.6717	2.95	1.82	
	2002.075.221338	37.2913	-121.6703	1.79	1.84	
	2005.329.230015	37.2875	-121.6705	2.25	1.92	

Table 4.S1K: First line within each row indicates the sequence label number, average sequence latitude, average sequence longitude, average sequence depth, average sequence magnitude, total amount of slip (cm), and slip rate (mm/yr) at sequence location. Following lines indicate earthquake time, earthquake latitude, earthquake longitude, earthquake depth, and earthquake magnitude for each individual event within a repeating earthquake sequence.

43	37.2866	-121.6691	2.19	1.45	86.9	3.98
	1985.065.102542	37.2853	-121.6683	1.99	1.68	
	1986.067.095637	37.2868	-121.6705	1.68	1.20	
	1986.067.095652	37.2863	-121.6708	1.21	1.53	
	1987.012.165240	37.2862	-121.6680	1.87	1.27	
	1987.035.072810	37.2870	-121.6702	1.91	1.29	
	1987.350.221524	37.2873	-121.6715	1.75	1.35	
	1988.225.001024	37.2843	-121.6698	2.12	1.60	
	1990.103.022113	37.2860	-121.6695	2.02	1.51	
	1991.201.064806	37.2867	-121.6688	1.74	1.08	
	1994.039.021608	37.2858	-121.6697	2.17	1.60	
	1996.026.023018	37.2863	-121.6697	1.93	1.38	
	1996.309.075825	37.2863	-121.6677	2.80	1.61	
	1998.330.071329	37.2880	-121.6695	2.75	1.29	
	1999.341.034252	37.2858	-121.6693	2.06	1.60	
	2002.101.180720	37.2883	-121.6650	1.39	1.23	
	2002.101.195706	37.2893	-121.6708	6.07	1.48	
	2004.073.014909	37.2868	-121.6675	1.91	1.40	
	2005.343.064625	37.2853	-121.6668	2.03	1.05	
44	37.2956	-121.6773	3.14	2.02	42.9	1.96
	1984.116.014441	37.2950	-121.6768	2.73	2.00	
	1988.056.100359	37.2953	-121.6775	2.59	1.30	
	1988.056.100819	37.2955	-121.6778	2.78	1.40	
	1990.114.120854	37.2957	-121.6777	2.85	2.20	
	1994.341.073418	37.2953	-121.6768	3.23	2.15	
	2000.343.031749	37.2967	-121.6768	3.12	2.21	
	2004.219.090130	37.2957	-121.6773	4.69	1.78	

Table 4.S1L: First line within each row indicates the sequence label number, average sequence latitude, average sequence longitude, average sequence depth, average sequence magnitude, total amount of slip (cm), and slip rate (mm/yr) at sequence location. Following lines indicate earthquake time, earthquake latitude, earthquake longitude, earthquake depth, and earthquake magnitude for each individual event within a repeating earthquake sequence.

45	37.2947	-121.6762	2.67	1.77	74.0	3.39	
	1984.187.030550	37.2943	-121.6753	2.45	1.41		
	1985.081.204855	37.2943	-121.6755	2.51	1.84		
	1986.012.113719	37.2942	-121.6778	2.48	1.51		
	1988.179.224709	37.2948	-121.6758	2.45	1.83		
	1989.278.073820	37.2935	-121.6798	2.23	1.57		
	1991.131.095630	37.2943	-121.6765	2.59	1.75		
	1992.287.061018	37.2940	-121.6767	2.63	1.61		
	1994.177.172537	37.2943	-121.6757	2.68	1.82		
	1997.136.085427	37.2950	-121.6757	3.20	1.92		
	1999.263.030713	37.2958	-121.6763	2.70	1.79		
	2002.134.011209	37.2978	-121.6762	2.55	1.96		
	2003.199.074827	37.2947	-121.6735	3.31	0.96		
	2005.357.033841	37.2942	-121.6753	2.96	1.93		
46	37.2880	-121.6699	3.20	1.37	14.6	0.67	
	1990.225.124835	37.2857	-121.6695	2.47	1.27		
	1995.145.120957	37.2872	-121.6668	2.41	1.30		
	1999.105.201644	37.2895	-121.6715	2.06	1.45		
	2002.218.040549	37.2898	-121.6718	5.85	1.43		
47	37.2958	-121.6758	3.56	1.85	12.9	0.59	
	1985.316.205336	37.2955	-121.6757	3.34	1.86		
	1991.184.000838	37.2958	-121.6760	3.82	1.85		
	2003.242.180026	37.2962	-121.6757	3.53	1.85		
48	37.2946	-121.6750	3.98	2.16	62.0	2.84	
	1984.148.202345	37.2950	-121.6755	3.26	2.00		
	1985.236.130957	37.2940	-121.6753	3.96	2.29		
	1987.119.031505	37.2942	-121.6760	3.88	2.19		
	1989.130.101906	37.2943	-121.6753	3.79	2.07		
	1991.183.230010	37.2943	-121.6752	4.18	2.20		
	1994.244.230210	37.2942	-121.6743	3.83	2.21		
	1996.251.064134	37.2950	-121.6732	4.06	1.95		
	2000.160.055327	37.2957	-121.6752	5.02	2.20		
	2004.168.181909	37.2952	-121.6752	3.82	2.17		

Table 4.S1M: First line within each row indicates the sequence label number, average sequence latitude, average sequence longitude, average sequence depth, average sequence magnitude, total amount of slip (cm), and slip rate (mm/yr) at sequence location. Following lines indicate earthquake time, earthquake latitude, earthquake longitude, earthquake depth, and earthquake magnitude for each individual event within a repeating earthquake sequence.

49	37.2909	-121.6699	3.53	1.54	32.3	1.48	
	1984.179.145038	37.2913	-121.6708	3.61	1.59		
	1984.357.044344	37.2908	-121.6708	3.71	1.60		
	1986.067.103204	37.2917	-121.6707	3.59	1.63		
	1986.268.120152	37.2907	-121.6700	3.60	1.36		
	1988.205.104221	37.2907	-121.6717	3.67	1.53		
	1992.242.170429	37.2893	-121.6670	3.37	1.64		
	2004.102.073836	37.2917	-121.6685	3.17	1.20		
50	37.2890	-121.6695	3.68	1.79	68.6	3.14	
	1984.323.002855	37.2890	-121.6703	3.42	1.69		
	1985.365.155052	37.2888	-121.6695	3.40	1.74		
	1987.154.065851	37.2887	-121.6702	3.79	1.74		
	1988.308.013004	37.2888	-121.6697	3.64	1.71		
	1989.347.053346	37.2875	-121.6682	3.81	1.60		
	1991.149.094522	37.2885	-121.6700	3.82	1.83		
	1991.338.000849	37.2892	-121.6698	3.77	1.89		
	1993.354.223507	37.2892	-121.6690	3.48	1.77		
	1995.349.185339	37.2890	-121.6693	3.71	1.82		
	1997.301.120144	37.2893	-121.6692	3.68	1.61		
	2002.062.110702	37.2910	-121.6690	3.70	1.79		
	2004.303.092939	37.2892	-121.6698	3.94	2.02		
51	37.2907	-121.6717	4.69	2.65	20.7	0.95	
	1984.189.001709	37.2907	-121.6722	3.91	2.67		
	1995.185.112049	37.2910	-121.6713	5.47	2.65		
	2004.102.073806	37.2905	-121.6715	4.70	2.63		
52	37.2887	-121.6661	6.32	2.30	16.8	0.77	
	1990.070.115234	37.2882	-121.6660	6.04	2.34		
	1996.307.122252	37.2883	-121.6660	6.35	2.29		
	2000.167.133213	37.2895	-121.6662	6.58	2.25		
53	37.2892	-121.6648	6.42	1.73	12.1	0.55	
	1985.044.235225	37.2887	-121.6650	6.49	1.70		
	1988.120.072957	37.2897	-121.6647	6.15	1.68		
	1989.053.141028	37.2892	-121.6648	6.61	1.79		

Table 4.S1N: First line within each row indicates the sequence label number, average sequence latitude, average sequence longitude, average sequence depth, average sequence magnitude, total amount of slip (cm), and slip rate (mm/yr) at sequence location. Following lines indicate earthquake time, earthquake latitude, earthquake longitude, earthquake depth, and earthquake magnitude for each individual event within a repeating earthquake sequence.

54	37.2865	-121.6581	9.22	1.42	25.1	1.15	
	1984.116.213817	37.2860	-121.6585	9.07	1.59		
	1984.126.024117	37.2848	-121.6567	9.18	1.12		
	1984.136.200128	37.2867	-121.6597	9.01	1.51		
	1984.149.200500	37.2870	-121.6582	8.99	1.54		
	1984.183.133614	37.2872	-121.6572	9.57	1.27		
	1984.258.235100	37.2872	-121.6583	9.53	1.06		
55	37.2805	-121.6586	5.87	1.72	77.9	3.57	
	1984.134.151749	37.2800	-121.6590	5.60	1.78		
	1984.159.102642	37.2805	-121.6583	5.81	1.76		
	1984.200.024516	37.2808	-121.6588	5.81	1.73		
	1984.270.031415	37.2798	-121.6582	5.93	1.74		
	1985.009.070017	37.2807	-121.6592	6.00	1.73		
	1985.184.022934	37.2807	-121.6588	5.79	1.78		
	1986.093.230306	37.2807	-121.6583	5.89	1.75		
	1987.022.181459	37.2803	-121.6585	6.30	1.68		
	1988.057.145146	37.2805	-121.6588	6.19	1.60		
	1989.186.104406	37.2805	-121.6588	6.25	1.71		
	1990.288.213245	37.2805	-121.6590	5.65	1.73		
	1992.190.042831	37.2807	-121.6595	6.08	1.64		
	1994.284.153355	37.2805	-121.6578	5.61	1.69		
	2003.351.165530	37.2807	-121.6572	5.25	1.72		
56	37.2773	-121.6554	5.56	1.57	43.9	2.01	
	1984.115.234934	37.2760	-121.6548	5.36	1.63		
	1984.125.111000	37.2773	-121.6562	5.62	1.45		
	1984.158.074620	37.2777	-121.6555	5.25	1.61		
	1984.212.040156	37.2763	-121.6548	5.51	1.55		
	1984.359.072203	37.2770	-121.6565	5.73	1.62		
	1987.013.195954	37.2775	-121.6570	5.87	1.54		
	1988.278.064133	37.2775	-121.6568	5.78	1.46		
	1991.121.225844	37.2772	-121.6562	5.66	1.55		
	2002.323.035426	37.2793	-121.6505	5.24	1.63		

Table 4.S1O: First line within each row indicates the sequence label number, average sequence latitude, average sequence longitude, average sequence depth, average sequence magnitude, total amount of slip (cm), and slip rate (mm/yr) at sequence location. Following lines indicate earthquake time, earthquake latitude, earthquake longitude, earthquake depth, and earthquake magnitude for each individual event within a repeating earthquake sequence.

57	37.2758	-121.6570	4.79	1.86	19.5	0.89	
	1984.125.095521	37.2760	-121.6568	4.51	1.94		
	1984.212.161244	37.2760	-121.6570	4.57	1.89		
	1985.046.111123	37.2752	-121.6577	4.92	1.77		
	1989.086.073710	37.2758	-121.6565	5.16	1.83		
58	37.2762	-121.6528	6.85	1.47	20.7	0.95	
	1986.049.122948	37.2778	-121.6508	6.76	1.67		
	1991.314.061439	37.2748	-121.6547	6.75	1.45		
	1993.310.000757	37.2748	-121.6532	6.81	1.36		
	1999.327.022405	37.2775	-121.6532	7.09	1.48		
	2004.110.032516	37.2760	-121.6523	6.83	1.17		
59	37.2687	-121.6552	2.35	1.92	74.1	3.39	
	1984.315.124731	37.2680	-121.6550	2.38	2.04		
	1985.161.020515	37.2692	-121.6552	2.15	1.82		
	1986.074.184759	37.2690	-121.6558	2.04	2.00		
	1987.026.171826	37.2687	-121.6552	2.23	1.76		
	1988.212.004234	37.2682	-121.6563	2.39	1.94		
	1990.067.004652	37.2683	-121.6548	2.19	1.89		
	1991.251.192939	37.2690	-121.6558	2.09	1.83		
	1993.350.184235	37.2687	-121.6550	2.20	1.93		
	1995.260.011626	37.2680	-121.6550	2.29	1.78		
	1998.120.103758	37.2683	-121.6548	3.42	1.97		
	2001.223.121049	37.2703	-121.6545	2.68	1.96		
	2004.285.080816	37.2682	-121.6548	2.20	1.93		
60	37.2636	-121.6485	3.67	2.01	42.6	1.95	
	1984.204.121908	37.2632	-121.6480	3.59	2.00		
	1985.045.182114	37.2638	-121.6488	3.47	2.05		
	1985.300.144223	37.2638	-121.6487	3.65	2.00		
	1987.138.115929	37.2632	-121.6487	3.64	2.00		
	1989.242.131201	37.2638	-121.6492	3.83	2.05		
	1991.081.223437	37.2635	-121.6485	3.83	1.92		
	1998.014.092337	37.2637	-121.6477	3.71	2.04		

Table 4.S1P: First line within each row indicates the sequence label number, average sequence latitude, average sequence longitude, average sequence depth, average sequence magnitude, total amount of slip (cm), and slip rate (mm/yr) at sequence location. Following lines indicate earthquake time, earthquake latitude, earthquake longitude, earthquake depth, and earthquake magnitude for each individual event within a repeating earthquake sequence.

61	37.2623	-121.6477	3.74	2.05	29.1	1.33	
	1984.194.104818	37.2622	-121.6470	3.64	2.03		
	1985.073.023300	37.2622	-121.6472	3.72	2.12		
	1986.005.234508	37.2627	-121.6477	3.59	1.94		
	1987.300.102327	37.2620	-121.6480	3.74	2.06		
	1991.082.020046	37.2627	-121.6487	4.01	2.08		
62	37.2586	-121.6426	3.89	1.38	39.2	1.80	
	1984.117.112923	37.2573	-121.6412	3.91	1.43		
	1984.223.161442	37.2587	-121.6427	3.68	1.32		
	1985.011.052600	37.2587	-121.6433	3.88	1.34		
	1985.240.210112	37.2582	-121.6435	3.64	1.33		
	1986.174.172614	37.2583	-121.6432	3.65	1.38		
	1988.203.134306	37.2583	-121.6438	4.24	1.35		
	1991.190.131120	37.2582	-121.6428	4.15	1.36		
	1995.233.204416	37.2580	-121.6430	3.61	1.35		
	2001.340.222654	37.2613	-121.6402	4.28	1.49		
63	37.2604	-121.6428	5.65	1.41	44.9	2.06	
	1984.118.072130	37.2607	-121.6410	5.17	1.41		
	1984.166.173542	37.2602	-121.6427	5.71	1.37		
	1984.218.105319	37.2603	-121.6440	5.64	1.43		
	1984.262.164254	37.2597	-121.6428	5.81	1.43		
	1985.047.061756	37.2602	-121.6430	5.53	1.33		
	1985.187.231530	37.2608	-121.6427	5.48	1.32		
	1986.059.033713	37.2603	-121.6427	5.73	1.41		
	1987.264.221445	37.2605	-121.6428	6.40	1.26		
	1995.205.222132	37.2600	-121.6437	5.51	1.53		
	2004.041.135047	37.2613	-121.6430	5.49	1.51		

Table 4.S1Q: First line within each row indicates the sequence label number, average sequence latitude, average sequence longitude, average sequence depth, average sequence magnitude, total amount of slip (cm), and slip rate (mm/yr) at sequence location. Following lines indicate earthquake time, earthquake latitude, earthquake longitude, earthquake depth, and earthquake magnitude for each individual event within a repeating earthquake sequence.

64	37.2568	-121.6398	5.84	1.50	57.9	2.65	
	1984.116.040036	37.2558	-121.6392	5.87	1.54		
	1984.149.191451	37.2570	-121.6402	5.33	1.57		
	1984.198.052542	37.2557	-121.6382	5.23	1.49		
	1984.257.194644	37.2573	-121.6403	5.95	1.56		
	1985.008.104125	37.2577	-121.6398	5.72	1.53		
	1985.209.141401	37.2567	-121.6405	6.05	1.53		
	1986.210.234936	37.2563	-121.6393	5.67	1.53		
	1988.052.201418	37.2563	-121.6397	6.07	1.44		
	1989.181.102217	37.2562	-121.6400	6.11	1.42		
	1992.247.121530	37.2567	-121.6422	5.59	1.50		
	1995.118.165352	37.2572	-121.6388	5.82	1.43		
	2000.072.104926	37.2585	-121.6400	6.68	1.45		
65	37.2539	-121.6388	5.79	2.58	59.5	2.73	
	1986.005.051848	37.2535	-121.6395	5.46	2.66		
	1988.086.210525	37.2535	-121.6388	5.77	2.57		
	1990.197.065856	37.2535	-121.6380	5.42	2.53		
	1993.132.030854	37.2543	-121.6395	5.98	2.60		
	1996.264.100227	37.2537	-121.6387	5.87	2.56		
	1999.191.112030	37.2542	-121.6385	5.93	2.64		
	2003.109.100044	37.2543	-121.6388	6.07	2.46		
66	37.2501	-121.6348	5.73	1.36	9.7	0.44	
	1984.130.124238	37.2503	-121.6343	5.67	1.43		
	1985.189.141328	37.2497	-121.6350	5.54	1.29		
	1987.190.223004	37.2503	-121.6350	5.98	1.34		
67	37.2462	-121.6322	5.12	1.53	42.9	1.96	
	1984.149.060533	37.2460	-121.6313	4.72	1.54		
	1984.192.044608	37.2453	-121.6317	4.69	0.92		
	1984.250.111640	37.2467	-121.6335	4.99	1.65		
	1985.059.125117	37.2467	-121.6323	4.86	1.67		
	1985.323.001012	37.2453	-121.6312	5.43	1.05		
	1986.226.135451	37.2470	-121.6330	5.08	1.58		
	1988.037.112606	37.2463	-121.6317	5.43	1.18		
	1995.197.021035	37.2462	-121.6332	5.14	1.64		
	1998.182.164946	37.2465	-121.6317	5.75	1.64		

Table 4.S1R: First line within each row indicates the sequence label number, average sequence latitude, average sequence longitude, average sequence depth, average sequence magnitude, total amount of slip (cm), and slip rate (mm/yr) at sequence location. Following lines indicate earthquake time, earthquake latitude, earthquake longitude, earthquake depth, and earthquake magnitude for each individual event within a repeating earthquake sequence.

68	37.2415	-121.6296	5.29	2.23	56.6	2.59	
	1984.116.005200	37.2407	-121.6297	4.76	2.20		
	1984.231.115427	37.2410	-121.6295	4.91	2.26		
	1985.101.103459	37.2415	-121.6300	5.15	2.26		
	1987.057.144435	37.2415	-121.6307	5.53	2.26		
	1990.007.150309	37.2418	-121.6288	5.33	2.19		
	1993.313.191734	37.2430	-121.6308	5.06	2.22		
	1999.016.101201	37.2420	-121.6290	5.98	2.21		
	2004.292.181842	37.2408	-121.6287	5.61	2.19		
69	37.2375	-121.6253	5.27	1.37	48.8	2.23	
	1984.140.153933	37.2380	-121.6247	4.51	1.62		
	1984.201.174143	37.2378	-121.6268	4.77	1.64		
	1984.265.085858	37.2373	-121.6248	5.09	1.30		
	1984.353.095645	37.2377	-121.6262	5.54	1.32		
	1985.110.232544	37.2368	-121.6245	4.99	1.30		
	1985.303.215433	37.2370	-121.6255	5.71	1.28		
	1986.218.154019	37.2370	-121.6260	5.73	1.24		
	1987.240.234010	37.2377	-121.6253	5.71	1.27		
	1988.262.021147	37.2373	-121.6243	5.92	0.83		
	1990.120.014309	37.2383	-121.6263	4.92	1.31		
	1992.102.114322	37.2375	-121.6240	5.12	1.14		
70	37.2345	-121.6242	5.51	2.88	59.2	2.71	
	1984.190.065629	37.2342	-121.6233	5.32	2.96		
	1984.315.095409	37.2345	-121.6235	6.02	2.88		
	1985.228.170405	37.2342	-121.6245	5.31	2.82		
	1988.241.225551	37.2347	-121.6255	5.36	2.90		
	1993.069.194213	37.2352	-121.6247	5.63	2.81		
	2004.323.142146	37.2342	-121.6235	5.41	2.86		

Table 4.S1S: First line within each row indicates the sequence label number, average sequence latitude, average sequence longitude, average sequence depth, average sequence magnitude, total amount of slip (cm), and slip rate (mm/yr) at sequence location. Following lines indicate earthquake time, earthquake latitude, earthquake longitude, earthquake depth, and earthquake magnitude for each individual event within a repeating earthquake sequence.

71	37.2450	-121.6305	5.84	1.42	30.1	1.38	
	1984.118.102425	37.2447	-121.6308	5.95	1.43		
	1984.131.162938	37.2453	-121.6302	5.80	1.51		
	1984.143.224128	37.2448	-121.6292	5.69	1.32		
	1984.179.165307	37.2455	-121.6308	6.12	1.48		
	1984.227.142151	37.2455	-121.6297	5.53	1.39		
	1984.301.111929	37.2442	-121.6312	6.21	1.34		
	1988.078.231838	37.2452	-121.6318	5.57	1.42		
72	37.2437	-121.6278	6.09	1.71	29.8	1.36	
	1986.122.182831	37.2432	-121.6283	6.21	1.74		
	1990.049.104716	37.2428	-121.6283	5.80	1.74		
	1993.206.200618	37.2438	-121.6277	5.83	1.75		
	1997.211.130643	37.2433	-121.6268	5.98	1.67		
	2000.120.020617	37.2448	-121.6283	6.04	1.62		
	2003.029.102056	37.2445	-121.6273	6.66	1.71		
73	37.2428	-121.6275	6.59	1.39	14.8	0.68	
	1984.122.031633	37.2427	-121.6273	6.46	1.37		
	1984.135.210436	37.2418	-121.6248	6.90	1.49		
	1984.168.022944	37.2438	-121.6295	6.66	1.32		
	1984.230.014851	37.2428	-121.6282	6.35	1.36		
74	37.2414	-121.6249	6.74	1.39	29.6	1.36	
	1984.361.043349	37.2400	-121.6255	6.11	1.37		
	1985.362.092731	37.2415	-121.6270	6.26	1.43		
	1987.018.233049	37.2403	-121.6232	7.49	1.25		
	1988.170.010945	37.2418	-121.6255	6.98	1.45		
	1990.139.202340	37.2423	-121.6255	6.51	1.43		
	1992.350.232623	37.2420	-121.6235	6.53	1.44		
	2001.163.195014	37.2418	-121.6245	7.28	1.29		

Table 4.S1T: First line within each row indicates the sequence label number, average sequence latitude, average sequence longitude, average sequence depth, average sequence magnitude, total amount of slip (cm), and slip rate (mm/yr) at sequence location. Following lines indicate earthquake time, earthquake latitude, earthquake longitude, earthquake depth, and earthquake magnitude for each individual event within a repeating earthquake sequence.

75	37.2482	-121.6359	3.04	1.46	66.8	3.06	
	1984.119.174845	37.2465	-121.6332	2.22	1.17		
	1984.119.175208	37.2488	-121.6355	2.98	1.20		
	1984.200.195751	37.2477	-121.6347	2.86	1.47		
	1984.360.114652	37.2482	-121.6367	3.12	1.64		
	1985.156.021752	37.2488	-121.6375	3.13	1.60		
	1985.354.010716	37.2483	-121.6363	3.18	1.55		
	1986.346.141812	37.2482	-121.6352	2.83	0.82		
	1986.346.141846	37.2482	-121.6367	3.21	1.43		
	1988.037.191020	37.2483	-121.6352	2.95	0.80		
	1988.037.194448	37.2487	-121.6368	3.08	1.40		
	1990.357.193252	37.2477	-121.6373	2.94	1.55		
	1993.273.180200	37.2483	-121.6360	4.22	1.35		
	1995.308.165427	37.2480	-121.6362	2.85	1.65		
	1999.045.115002	37.2488	-121.6362	2.93	1.50		
76	37.2472	-121.6362	4.06	2.73	32.5	1.49	
	1984.192.230115	37.2468	-121.6355	3.86	2.80		
	1985.274.044552	37.2470	-121.6363	4.01	2.76		
	1987.286.141429	37.2472	-121.6367	4.27	2.69		
	1990.355.070949	37.2477	-121.6362	4.11	2.64		
77	37.2463	-121.6347	3.96	2.17	46.8	2.14	
	1984.193.002534	37.2465	-121.6342	3.41	2.30		
	1985.279.232736	37.2458	-121.6350	3.64	2.22		
	1987.256.091137	37.2460	-121.6352	3.92	2.16		
	1989.223.043753	37.2460	-121.6352	4.03	2.10		
	1992.175.230507	37.2463	-121.6352	3.41	2.09		
	1995.340.002916	37.2457	-121.6345	3.19	2.16		
	2002.002.073832	37.2477	-121.6340	6.15	2.09		

Table 4.S1U: First line within each row indicates the sequence label number, average sequence latitude, average sequence longitude, average sequence depth, average sequence magnitude, total amount of slip (cm), and slip rate (mm/yr) at sequence location. Following lines indicate earthquake time, earthquake latitude, earthquake longitude, earthquake depth, and earthquake magnitude for each individual event within a repeating earthquake sequence.

78	37.2486	-121.6358	4.33	1.40	59.6	2.73	
	1985.189.072520	37.2478	-121.6358	4.27	1.19		
	1985.310.025657	37.2490	-121.6360	3.70	1.59		
	1986.339.074502	37.2482	-121.6355	3.73	1.41		
	1987.242.110731	37.2475	-121.6352	5.39	1.35		
	1988.063.020338	37.2487	-121.6368	3.76	1.44		
	1988.231.065921	37.2472	-121.6340	4.40	1.13		
	1991.006.010302	37.2477	-121.6365	3.64	1.40		
	1993.318.022219	37.2488	-121.6352	3.36	1.39		
	1997.191.155939	37.2483	-121.6348	4.63	1.35		
	1998.295.115217	37.2493	-121.6358	4.72	1.34		
	2001.100.013612	37.2507	-121.6378	4.74	1.45		
	2002.256.044727	37.2513	-121.6360	5.48	1.45		
	2004.236.123027	37.2478	-121.6355	4.47	1.43		
79	37.2457	-121.6326	4.13	1.70	53.3	2.44	
	1984.115.235322	37.2443	-121.6318	4.34	1.76		
	1984.224.012316	37.2448	-121.6325	4.60	1.65		
	1985.001.071254	37.2452	-121.6328	3.84	1.71		
	1985.198.235639	37.2465	-121.6320	3.24	1.70		
	1987.199.143510	37.2462	-121.6338	4.25	1.67		
	1988.310.133136	37.2457	-121.6332	4.49	1.65		
	1990.331.193819	37.2457	-121.6318	3.65	1.63		
	1993.318.080315	37.2463	-121.6327	3.80	1.70		
	1998.305.023024	37.2460	-121.6332	4.63	1.75		
	2005.199.114204	37.2460	-121.6323	4.47	1.74		
80	37.2209	-121.6129	4.04	1.49	5.2	0.24	
	1984.234.074704	37.2207	-121.6128	3.92	1.47		
	1984.356.002014	37.2212	-121.6130	4.16	1.50		

Table 4.S1V: First line within each row indicates the sequence label number, average sequence latitude, average sequence longitude, average sequence depth, average sequence magnitude, total amount of slip (cm), and slip rate (mm/yr) at sequence location. Following lines indicate earthquake time, earthquake latitude, earthquake longitude, earthquake depth, and earthquake magnitude for each individual event within a repeating earthquake sequence.

81	37.2124	-121.6067	4.57	1.54	32.3	1.48
	1984.119.011656	37.2138	-121.6057	4.13	1.62	
	1984.127.185235	37.2110	-121.6045	3.96	1.60	
	1984.149.034229	37.2135	-121.6123	5.35	1.63	
	1984.181.191851	37.2127	-121.6075	4.40	1.60	
	1984.229.211624	37.2127	-121.6038	4.01	1.35	
	1985.033.083245	37.2107	-121.6073	4.41	1.14	
	1986.017.231212	37.2127	-121.6060	5.72	1.57	
82	37.2039	-121.6018	3.08	1.45	71.5	3.28
	1984.116.100913	37.2032	-121.6005	3.08	1.70	
	1984.149.182315	37.2028	-121.6007	2.85	1.48	
	1984.309.024929	37.2025	-121.6013	2.31	1.24	
	1985.066.201519	37.2037	-121.6025	3.07	1.47	
	1986.079.021103	37.2035	-121.6032	3.15	1.40	
	1986.287.202818	37.2033	-121.6032	3.32	1.43	
	1987.105.143919	37.2032	-121.6000	2.74	1.24	
	1988.034.211056	37.2050	-121.6012	1.95	1.36	
	1988.349.105323	37.2037	-121.6012	3.44	1.40	
	1990.046.111852	37.2042	-121.6017	3.26	1.52	
	1991.330.142702	37.2042	-121.6015	2.90	1.36	
	1992.288.063219	37.2040	-121.6027	3.07	0.92	
	1994.121.205202	37.2047	-121.6017	3.01	1.52	
	1999.358.113410	37.2050	-121.6023	3.65	1.50	
	2001.103.132304	37.2052	-121.6028	4.41	1.50	

Table 4.S1W: First line within each row indicates the sequence label number, average sequence latitude, average sequence longitude, average sequence depth, average sequence magnitude, total amount of slip (cm), and slip rate (mm/yr) at sequence location. Following lines indicate earthquake time, earthquake latitude, earthquake longitude, earthquake depth, and earthquake magnitude for each individual event within a repeating earthquake sequence.

83	37.1996	-121.5994	3.82	1.38	98.1	4.49	
	1984.116.195349	37.1973	-121.5973	3.25	1.52		
	1984.144.035618	37.1993	-121.6007	3.48	1.27		
	1984.188.120010	37.1948	-121.5920	11.28	1.40		
	1985.034.145941	37.2002	-121.5985	3.27	1.49		
	1985.198.190500	37.2000	-121.6000	2.60	1.38		
	1986.023.100916	37.1995	-121.5993	3.84	1.40		
	1986.271.041738	37.1995	-121.6002	3.75	1.50		
	1987.225.145411	37.1983	-121.6005	2.79	1.44		
	1988.105.190900	37.2003	-121.6008	3.52	1.24		
	1989.033.123434	37.1995	-121.6008	3.74	1.34		
	1990.049.052910	37.2003	-121.5995	3.50	1.40		
	1991.093.180716	37.1997	-121.5983	3.22	1.39		
	1992.208.180521	37.2002	-121.6000	3.37	1.45		
	1994.029.135050	37.2002	-121.5997	3.20	1.34		
	1995.197.125116	37.2005	-121.6005	2.98	1.39		
	1996.291.195915	37.1990	-121.5995	3.20	1.36		
	1997.355.174150	37.2002	-121.6005	3.60	1.20		
	1999.126.055809	37.2018	-121.5995	3.25	1.20		
	2001.007.005149	37.2018	-121.6007	3.13	1.38		
	2002.213.042307	37.1993	-121.5988	6.16	1.28		
	2004.175.233928	37.2008	-121.5998	3.18	1.38		

Table 4.S1X: First line within each row indicates the sequence label number, average sequence latitude, average sequence longitude, average sequence depth, average sequence magnitude, total amount of slip (cm), and slip rate (mm/yr) at sequence location. Following lines indicate earthquake time, earthquake latitude, earthquake longitude, earthquake depth, and earthquake magnitude for each individual event within a repeating earthquake sequence.

84	37.2029	-121.5999	4.08	1.43	75.8	3.47	
	1984.117.191039	37.2015	-121.5995	4.17	1.44		
	1984.147.232034	37.2015	-121.5997	4.37	1.51		
	1984.231.061210	37.2025	-121.5993	3.82	1.45		
	1984.321.071952	37.2020	-121.5997	4.63	1.47		
	1985.063.124447	37.2018	-121.5988	3.93	1.43		
	1985.263.032118	37.2030	-121.6005	4.15	1.44		
	1986.168.053026	37.2038	-121.6010	3.04	1.47		
	1987.007.073537	37.2028	-121.5983	4.14	1.29		
	1988.178.144004	37.2023	-121.5988	4.24	1.24		
	1990.172.212244	37.2030	-121.5998	4.24	1.34		
	1991.213.212234	37.2027	-121.5993	4.19	1.30		
	1993.351.011226	37.2028	-121.6005	4.16	1.41		
	1995.168.034530	37.2052	-121.5998	3.85	1.27		
	1996.353.192529	37.2022	-121.6007	4.16	1.35		
	2000.312.153401	37.2050	-121.6020	4.25	1.58		
	2003.305.181055	37.2045	-121.6010	3.89	1.54		
85	37.1807	-121.5826	3.49	2.39	44.4	2.03	
	1984.200.130402	37.1805	-121.5832	3.13	2.47		
	1985.327.122810	37.1810	-121.5832	3.30	2.32		
	1987.199.025705	37.1807	-121.5825	3.48	2.42		
	1991.132.122231	37.1807	-121.5825	3.58	2.39		
	1996.294.193402	37.1807	-121.5825	3.34	2.29		
	2002.021.095302	37.1807	-121.5817	4.11	2.42		

Table 4.S1Y: First line within each row indicates the sequence label number, average sequence latitude, average sequence longitude, average sequence depth, average sequence magnitude, total amount of slip (cm), and slip rate (mm/yr) at sequence location. Following lines indicate earthquake time, earthquake latitude, earthquake longitude, earthquake depth, and earthquake magnitude for each individual event within a repeating earthquake sequence.

occurs between 2 - 10 km. Additionally, from RE data alone, it is unknown if holes within the seismicity are creeping aseismically or are locked and accumulating elastic strain.

We use the empirical method of Nadeau and McEvilly [1999] to estimate the amount of slip around a RE location using the average moment of the RE sequence and the number of times the earthquake repeated. Although this relationship was calibrated on the Parkfield segment of the San Andreas fault, it has proven to be consistent with geodetically determined values of creep on other transform, reverse and subduction faults [Igarashi et al., 2003 ; Chen and Rau, 2003 ; Bürgmann et al., 2000]. Slip rates can be determined by dividing the total amount of slip over the time interval in question.

In general, the locations of the REs occur in the region adjacent to the fault patches inferred to have ruptured from the Beroza and Spudich [1988] coseismic slip model (Figure 1B). Additionally, the REs with the highest amounts of postseismic slip were seen to be near the mainshock hypocenter and directly above a large deep coseismic slip patch located approximately 0 – 10 km southeast of the hypocenter. Lower values of afterslip are observed in the shallowest portions of the fault above ~4 km as well as to the northwest of the main coseismic rupture area (Figure 1B). The Beroza and Spudich [1988] model has a high slip patch ~15 km to the southeast of the hypocenter with slip in excess of 200 cm, whereas the coseismic slip within the deep rupture area directly beneath the majority of the REs did not exceed 110 cm. For comparison, the average amount of total slip determined from RE data for the first 6 months after the mainshock was 9.4 cm with a range of 0.1 - 29.0 cm, corresponding

to amounts calculated from different individual REs. The average RE-derived slip rate

for this time period was 168 mm/yr with a range between 2 – 520 mm/yr.

Another coseismic rupture model of the Morgan Hill earthquake by Hartzell

and Heaton [1986] did not show a similar relationship between areas inferred to have

ruptured coseismically and the locations of the RE. Here, REs occurred both away

from and within areas that are thought to have ruptured coseismically. It is important

to note however, that different input data were used when computing the coseismic

rupture models. The Beroza and Spudich [1988] model used near-source strong

motion records bandpass filtered between 0.2 – 4.0 Hz while the Hartzell and Heaton

[1986] model used both near-source strong motion records and teleseismic short-

period P waveforms filtered between 0.2 – 2.0 Hz. Additionally, even if the data had

been the same, the authors could have produced different coseismic models since

finite source models are known to be non-unique. This is due in part to the

uncertainties involved when choosing the model parameters, when assigning values to

the fixed seismological input parameters (such as rupture speed, slip duration, fault

geometry, or crustal structure), when linearizing and stabilizing the inverse problem,

and when discretizing an inherently continuous signal [Beresnev, 2003]. In synthetic

tests, it has even been shown that results providing an exact match between the

original and calculated seismograms can produce significantly different coseismic

rupture models due to the fact that different source parameterizations may fit the data

equally well [Beresnev, 2003].

We also compare slip rates between different periods after the mainshock to

determine when the Morgan Hill earthquake no longer appears to influence the creep

rate on the fault. Between 1985 and 1988 the average RE-derived slip rate at individual RE locations was 36.8 mm/yr with a range of 3.7 – 84.3 mm/yr. The average slip rate between 1989 – 1997 was 17.0 mm/yr with a range of 0.4 – 41.3 mm/yr while the average slip rate between 1998 – 2005 was 10.9 mm/yr with a range of 0.2 – 35.0 mm/yr. Thus, it appears that the mainshock influenced the timing of REs even beyond 1989. One possible reason for the long duration of creep-rate decay would be that the Mw6.9 1989 Loma Prieta earthquake, which occurred on the nearby San Andreas fault, influenced the REs by changing the stress on this portion of the Calaveras fault. However, individual RE sequences which were active over the entire time interval do not reveal a clear influence of the Loma Prieta earthquake. Interestingly, a handful of REs that had high slip rates directly after the Morgan Hill earthquake failed to repeat after a few years. It is unclear if these asperities became locked or were destroyed due to the accelerated creep.

4.4 Subsurface Slip Model

4.4.1 Repeating Earthquake Data

We determine the amount of total slip at RE locations for the 6 and 18 month periods directly following the 1984 Morgan Hill earthquake. To best include the amount of slip that occurred between the Morgan Hill mainshock and the first occurrence of a RE within a sequence, we model RE slip as

$$S = a * \log\left(1 + \frac{T}{\tau}\right) + b$$

where S is slip at time T for a particular RE, τ is the relaxation time in years, and a and b are the regression constants. We use the above form since rate and state variable friction laws applied to afterslip suggest that slip decays logarithmically [Marone et al., 1991]. We find a median τ value of 0.2100 yrs over the fault using the first 5 years of RE data for sequences that have at least 3 events within this early time period. One of these events must also have occurred within the first 6 mo. Of the 85 RE sequences originally identified, 33 match this criterion and are used to model the EDM data.

4.4.2 EDM Data

In our modeling of post-Morgan Hill subsurface slip, we use EDM data collected by the United States Geological Survey (USGS, http://quake.wr.usgs.gov/research/deformation/gps/geodolite/index.html) to study the postseismic surface deformation following the mainshock. Only baselines measured starting 0-2 days after the mainshock are used in this study. Eighteen baselines near the Morgan Hill earthquake are included.

4.4.3 Model Parameterization

To relate RE-derived afterslip estimates to the EDM data we develop elastic half-space models that forward model surface deformation using slip on rectangular dislocations patches around RE events on the Calaveras fault as input. Relocated seismicity indicates that this portion of the central Calaveras fault at depth is steeply dipping between 90° to 85° to the northeast and that the up-dip extension of the

142

seismically illuminated fault plane does not always meet the more complicated surface

trace [Schaff et al., 2002]. Taking this into consideration, we orient our fault plane to

328°, the same azimuth as that of the relocated seismicity of Ellsworth et al. [2000],

and fix its dip to 90°. We discretize the fault into 2 x 2 km subfaults and average RE-

derived total slip values within subfaults. We isolate the transient afterslip component

by subtracting average RE interseismic creep rates inferred from the 1998-2005 time

interval. EDM baseline changes are corrected for their average rates established in the

~10-year interval prior to the Morgan Hill earthquake [Manaker et al., 2003]. Our

model predicts EDM line-length changes due to slip on the subfaults at depth within a

homogenous, isotropic, elastic half-space.

It has been shown, however, that coseismic slip inversions for strike-slip

earthquakes in layered Earth models that account for depth dependent elasticity

recover larger amounts of seismic moment and greater amounts of deeper slip than

elastic half-space models which use the same observed surface deformation data

[Hearn and Bürgmann, 2005]. The implications for our forward models would be that

identical RE-derived slip patches would produce more surface deformation in an

elastic half-space model than in a layered elastic Earth model.

4.5 Model Results and Discussion

In general, RE-derived slip models underpredict the observed line-length

distance changes. A comparison between observed and calculated line-length changes

as a function of time for two baselines that cross the fault can be seen in Figure 2. We
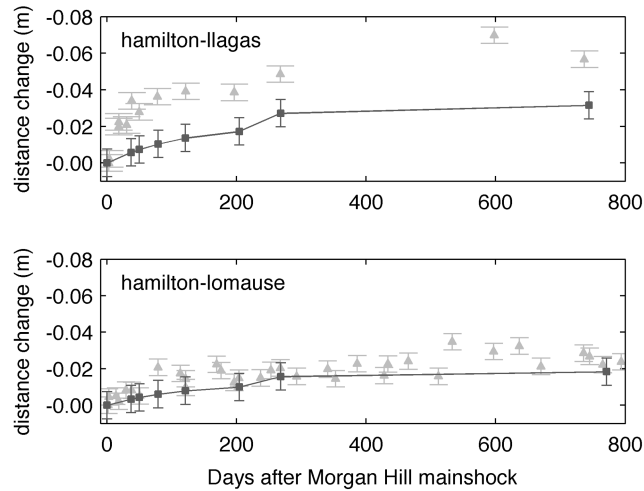
Figure 4.2: Comparison of predicted and observed line-length changes at two EDM lines. Observed data as grey triangles and predicted values as black circles. A) hamil ec to llagas and B) hamilton to loma use.

also compare surface displacements calculated from RE-derived afterslip models for the first 6 and 18 months with displacements inverted from the observed line-length change measurements using a model-coordinate solution [Segall and Matthews, 1988] (Figures S1 and S2). We see that the 6-month RE-model generally predicts less than 80% of the magnitude of individual baseline changes, while the 18-month slip model typically predicts less than 65%.

A number of factors may lead to the observed underprediction. One possible reason is that afterslip occurred on two or more parallel sub-faults near the primary fault. Mapping across the Calaveras fault in this area determined that the fault zone includes several shorter sub-parallel fault strands at the surface [Page, 1984]; however, at depth precisely relocated microseismicity suggest a much simpler and continuous fault surface [Schaff et al., 2002]. If we had failed to identify all REs along all portions of the fault zone, it is also possible that areas of the fault that we infer to be locked are

in fact creeping. REs determined by Peng et al. [2005] for example, cover more areas

of the fault especially above ~4 km and directly below one portion of the coseismic

rupture zone. Unmodeled afterslip may also be occurring on sections of the fault

lacking seismicity, either deeper or along strike, where REs cannot nucleate. Finally, it

is possible that the RE-derived slip estimates underpredict true slip. The RE-derived

estimates of interseismic creep rates along the Calaveras fault (averaging 10.9 mm/yr

during 1998-2005) agree to first order with those inferred geodetically [Manaker et al.,

2003]. However, recent rate-state-friction model investigations propose that RE-rates

may systematically underestimate true slip during times of accelerated postseismic slip

as some slip is accommodated by slow slip events [Ariyoshi et al., 2007].

To determine if additional aseismic slip below the rupture zone is the cause of

this discrepancy, we add deep slip between 10-18 km, decreasing downward from 25

cm to 10 cm, to our RE-derived 6 mo slip model. We chose the maximum value of

deep slip to be approximately the same as that closer to the rupture as measured by the

RE data. We display the model results at all stations together with displacements

inverted from the observed EDM data in Figure 3.

The model with the additional deep afterslip leads to a significantly improved

fit to the EDM data (χ^2 sum reduced from 81 to 55). This is especially due to the

improved fit to the baselines spanning longer distances across the rupture (hamilton to

llagas and lomause). None of the models we tested that involve slip near the rupture

are able to match the observed shortening between allison and lomause and lack of

shortening between hamilton and sheeprm2. This may be due to errors in these

measurements or indicate that additional creep occurred beyond the fault model we

145

Figure 4.3: Map view of 6 mo model predicted displacement field. Grey arrows determined from observed EDM data and black arrows from calculated subsurface slip model. Stations show a 95% confidence line if only one baseline pair is used to constrain the solution.

considered.

We performed a similar comparison for 18 mo of observed and predicted surface baseline changes, with added deep slip between 41 cm – 15 cm, and found essentially the same result, although the amount of discrepancy was still proportionally larger (Figures S2 and S3).

To test if underprediction of the RE-derived slip values could be the cause of the baseline discrepancy, we quadrupled our 6 mo calculated slip values and found
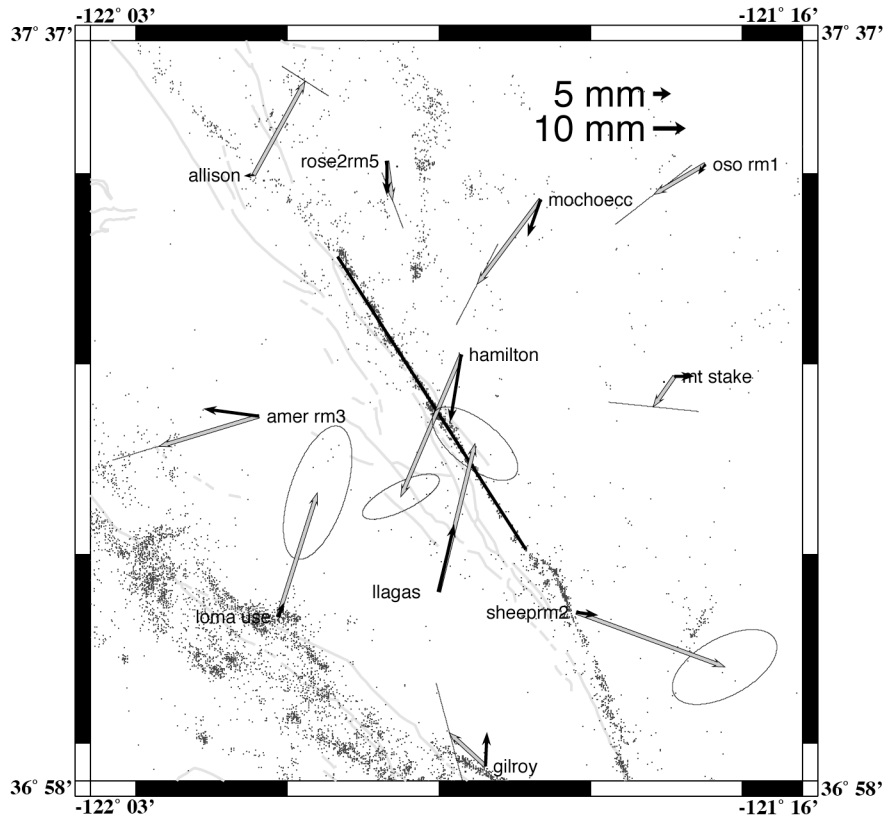
Figure 4.S1: Map view of 6 mo model predicted displacement field. RE data only above 10 km and no deep slip in subsurface slip model. Grey arrows determined from observed EDM data and black arrows from calculated subsurface slip model. Stations show a 95% confidence line if only one baseline pair is used to constrain the solution.

that the long baseline data was still underpredicted while the agreement between the

observed and calculated shorter baseline data was worse than that for the above model

which added deep slip (Figure S4). The χ^2 sum for this model was also higher than

that of the original model, 149 compared to 81.

4.6 Conclusions

A comparison between the regions of the fault that ruptured coseismically and

the locations of the REs show that the REs preferentially occur in areas adjacent to the
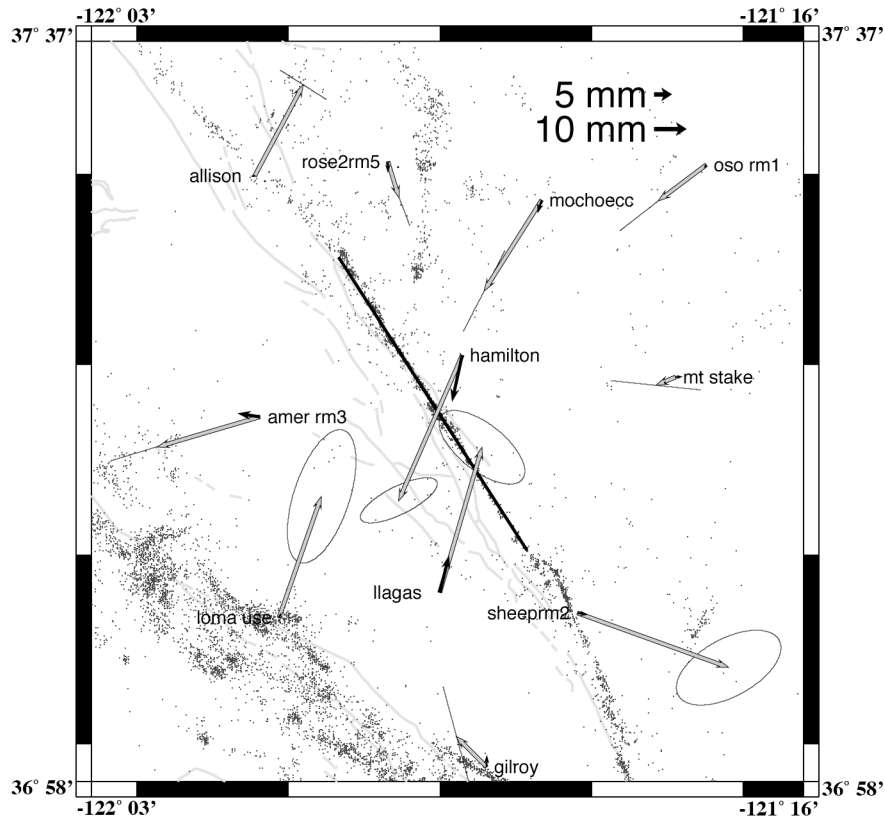
Figure 4.S2: Map view of 18 mo model predicted displacement field. RE data only above 10 km and no deep slip in subsurface slip model. Grey arrows determined from observed EDM data and black arrows from calculated subsurface slip model. Stations show a 95% confidence line if only one baseline pair is used to constrain the solution.

coseismic rupture (Figure 1B). Taking into account the fact that the average slip rate at RE locations over the observation period always exceeded or was close to the long-term rate of 15 +/- 3 mm/yr [WG99, 1999], we infer that these regions are actively slipping and loading the deeper asperities which rupture as infrequent larger earthquakes.

Interestingly, the slow decrease of slip rates through time over the study area shows that the 1984 Morgan Hill earthquake influenced the recurrence times of REs until at least 1989. This extraordinarily long apparent decay of the slip rates was not

Figure 4.S3: Map view of 18 mo model predicted displacement field. RE data above 10 km and inferred deep slip between 10 – 18 km in subsurface slip model. Grey arrows determined from observed EDM data and black arrows from calculated subsurface slip model. Stations show a 95% confidence line if only one baseline pair is used to constrain the solution.

obviously due to the influence of the 1989 Loma Prieta earthquake, although it cannot

be ruled out completely [Bürgmann et al., 1997].

When comparing the observed and predicted EDM data, our model

consistently underpredicted the observed long baseline data. The reason for this

discrepancy may be due to the fact that our method is limited to areas where

earthquakes can nucleate. If afterslip were to occur deeper than ~10 km, RE data alone

cannot constrain it. A significant amount of afterslip deeper than the Morgan Hill

rupture is possible and a modified model with such deeper afterslip fits the EDM data

149
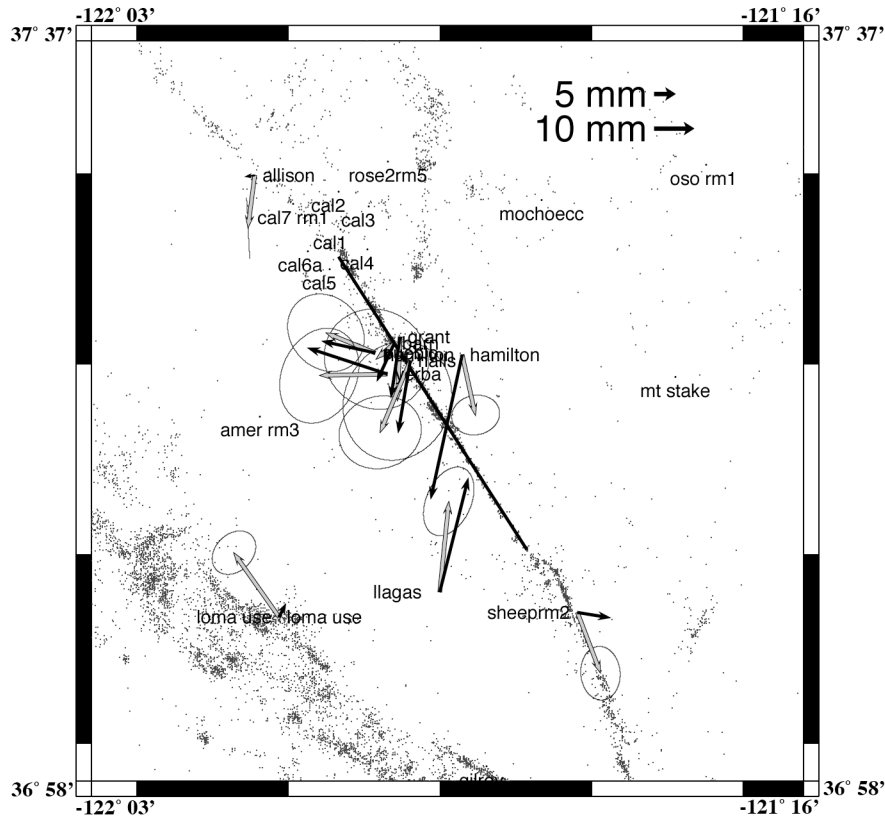
Figure 4.S4: Map view of 6 mo model predicted displacement field. Subsurface slip model determined using 4 times the calculated RE data above 10 km and no inferred deep slip. Grey arrows determined from observed EDM data and black arrows from calculated subsurface slip model. Stations show a 95% confidence line if only one baseline pair is used to constrain the solution.

better. On the creeping section of the San Andreas fault, coseismic stress changes have

been shown to be able to drive accelerated slip on deeper velocity strengthening

portions of the fault zone [Johnson et al., 2006]. The inferred deeper relaxation

beneath the Morgan Hill rupture area may even have had an added contribution from

the previous nearby 1979 M5.9 Coyote Lake earthquake. These results show that

when investigating fault interactions beyond coseismic static stress increases, as

observed by Du and Aydin (1993), and also when determining the slip budget on the

150
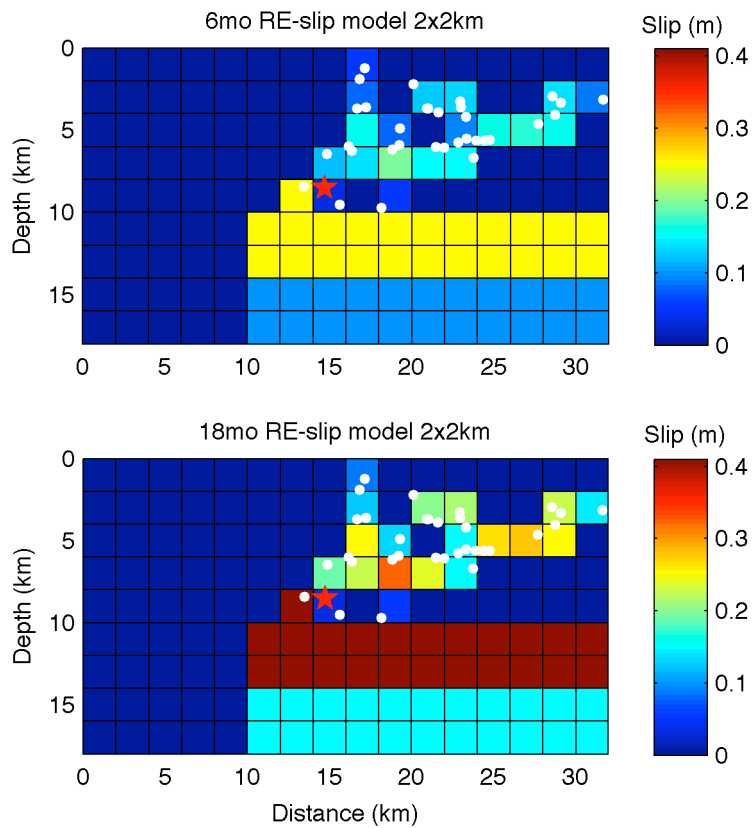
Figure 4.S5: 6 mo and 18 mo RE-derived subsurface slip models used in forward modeling. White dots indicate locations of REs used to derive model. Red star indicates location of Morgan Hill hypocenter.
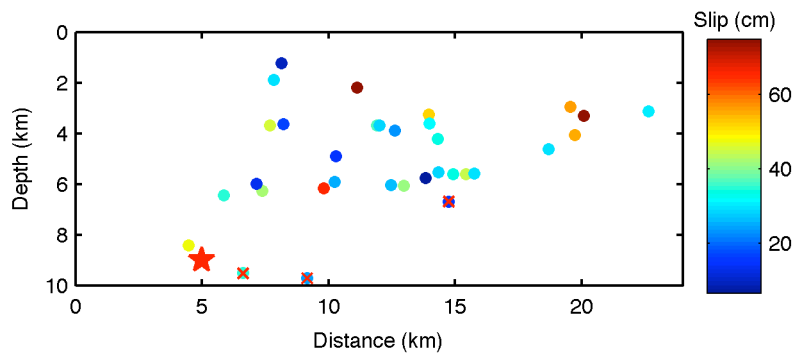
Figure 4.S6: Cumulative slip observed between 1984 – 2005 at RE locations used in 6 mo and 18 mo forward models. Crossed out REs indicated sequences that were active directly after the Morgan Hill earthquake but became aseismic post-1984. Red star indicates location of Morgan Hill hypocenter.
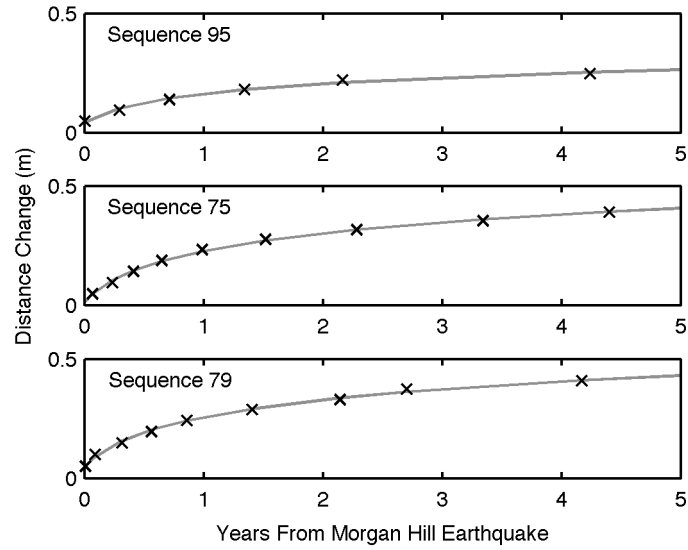
Figure 4.S7: Comparison between observed RE cumulative slip data points through time and functional logarithmic form, with a constant 10.9 mm/yr interseismic rate removed, which is used to infer slip over discrete time intervals for use in forward models. A constant τ of 0.2100yrs is used for all sequences.

fault, it is important to consider the effects due to afterslip on creeping shallow fault

patches as well as slip beneath the seismogenic zone.

Station 1	Station 2	Observed Data	Calculated Data
barn	halls	1.23E-02	1.87E-03
barn	pueblo	7.50E-03	6.18E-04
barn	yerba	-5.20E-03	-3.32E-03
grant	halls	-1.30E-03	7.77E-04
grant	pueblo	-1.50E-03	-9.85E-05
halls	pueblo	4.90E-03	3.82E-03
halls	yerba	2.60E-03	4.13E-04
pueblo	yerba	5.70E-03	-1.69E-03
allison	loma use	-3.18E-02	-9.02E-04
hamilton	loma use	-1.86E-02	-9.96E-03
hamilton	llagas	-3.97E-02	-1.72E-02
hamilton	sheeprm2	8.00E-04	-6.62E-03
llagas	sheeprm2	9.50E-03	1.44E-03

Table 4.S2: Comparison of observed and predicted EDM line-length distance changes for 6 mo model of only RE data above 10 km and no deep slip.

Station 1	Station 2	Observed Data	Calculated Data
barn	halls	1.23E-02	2.20E-03
barn	pueblo	7.50E-03	9.67E-04
barn	yerba	-5.20E-03	-4.76E-03
grant	halls	-1.30E-03	2.97E-04
grant	pueblo	-1.50E-03	-1.53E-04
halls	pueblo	4.90E-03	5.61E-03
halls	yerba	2.60E-03	5.43E-04
pueblo	yerba	5.70E-03	-1.71E-03
allison	loma use	-3.18E-02	-2.72E-03
hamilton	loma use	-1.86E-02	-1.57E-02
hamilton	llagas	-3.97E-02	-2.80E-02
hamilton	sheeprm2	8.00E-04	-9.50E-03
llagas	sheeprm2	9.50E-03	3.32E-03

Table 4.S3: Comparison of observed and predicted EDM line-length distance changes for 6 mo model with both RE data above 10 km and deep slip between 10 – 18 km decreasing downward from 0.25 m to 0.10 m.

Station 1	Station 2	Observed Data	Calculated Data
allison	hamilton	2.28E-02	7.97E-03
amer rm3	hamilton	1.30E-03	-1.06E-03
gilroy	llagas	3.03E-02	6.96E-03
hamilton	sheeprm2	1.80E-03	-1.05E-02
llagas	loma use	7.00E-04	3.82E-03
llagas	sheeprm2	4.60E-02	2.26E-03
allison	loma use	-1.03E-02	-1.42E-03
hamilton	rose2rm5	2.43E-02	9.71E-03
hamilton	oso rm1	2.56E-02	1.09E-02
hamilton	mochoecc	1.68E-02	1.07E-02
hamilton	mt stake	9.70E-03	3.83E-03
hamilton	llagas	-9.88E-02	-2.72E-02
hamilton	loma use	-9.17E-02	-1.58E-02

Table 4.S4: Comparison of observed and predicted EDM line-length distance changes for 18 mo model of only RE data above 10 km and no deep slip.

Station 1	Station 2	Observed Data	Calculated Data
allison	hamilton	2.28E-02	1.39E-02
amer rm3	hamilton	1.30E-03	6.17E-03
gilroy	llagas	3.03E-02	8.80E-03
hamilton	sheeprm2	1.80E-03	-1.51E-02
llagas	loma use	7.00E-04	5.67E-03
llagas	sheeprm2	4.60E-02	5.29E-03
allison	loma use	-1.03E-02	-4.34E-03
hamilton	rose2rm5	2.43E-02	9.56E-03
hamilton	oso rm1	2.56E-02	1.30E-02
hamilton	mochoecc	1.68E-02	8.73E-03
hamilton	mt stake	9.70E-03	7.57E-03
hamilton	llagas	-9.88E-02	-4.46E-02
hamilton	loma use	-9.17E-02	-2.50E-02

Table 4.S5: Comparison of observed and predicted EDM line-length distance changes for 18 mo model with both RE data above 10 km and deep slip between 10 – 18 km decreasing downward from 0.41 m to 0.15 m.

Station 1	Station 2	Observed Data	Calculated Data
barn	halls	1.23E-02	7.48E-03
barn	pueblo	7.50E-03	2.46E-03
barn	yerba	-5.20E-03	-1.32E-02
grant	halls	-1.30E-03	3.13E-03
grant	pueblo	-1.50E-03	-3.91E-04
halls	pueblo	4.90E-03	1.52E-02
halls	yerba	2.60E-03	1.65E-03
pueblo	yerba	5.70E-03	-6.76E-03
allison	loma use	-3.18E-02	-3.59E-03
hamilton	loma use	-1.86E-02	-3.98E-02
hamilton	llagas	-3.97E-02	-6.89E-02
hamilton	sheeprm2	8.00E-04	-2.66E-02
llagas	sheeprm2	9.50E-03	5.74E-03

Table 4.S6: Comparison of observed and predicted EDM line-length distance changes for 6 mo model of 4 times the observed RE data above 10 km and no deep slip.

Chapter 5

Bibliography

Anooshehpoor, A. and J. N. Brune (2001). Quasi-static slip-rate shielding by locked and creeping zones as an explanation for small repeating earthquakes at Parkfield, *Bull. Seismol. Soc. Am.,* **91**, 401-403.

Bailey, R.A. (1989). Geologic map of the Long Valley Caldera, Mono-Inyo Craters volcanic chain, and vicinity, Eastern California, Map I-1933, *U.S. Geol. Surv. Misc. Invest. Series*.

Beroza, G. C. (1988), Linearized Inversion for fault rupture behavior: application to the 1984 Morgan Hill, California, earthquake, *J. Geophys. Res*., 93, 6275-6296.

Bos, A. G., and W. Spakman (2003). The resolving power of coseismic surface displacement data for fault slip distribution at depth, *Geophys. Res. Lett.*, 30(21), **2110**, doi:10.1029/2003GL017946.

Beeler, N. M., D. L. Lockner and S. H. Hickman (2001). A simple stick-slip and creep-slip model for repeating earthquakes and its implication for microearthquakes at Parkfield, *Bull. Seismol. Soc. Am.,* **91**, 1797-1804.

Breckenridge, K. S. and R. W. Simpson (1997). Response of U.S. Geological Survey creepmeters to the Loma Prieta earthquake, in Reasenberg, ed., The Loma Prieta, California, earthquake of October 17, 1989-Aftershocks and Postseismic effects, *U.S. Geological Survey Professional Paper 1550-D,* 143-178.

Brown, B. D. (1984), Alignment-array measurements in the San Felipe Valley, California, in Hoose, S. N., ed., *The Morgan Hill, California, earthquake of April 24, 1984*, U. S. Geological Survey Bulletin Report 1639, 117-118.

Bryant, W. A. (1985). Faults in the southern Hollister area, San Benito counties, California, *California Division of Mines and Geology Fault Evaluation Report 164*.

Bürgmann R., D. Schmidt, R. M. Nadeau, M. d'Alessio, E. Fielding, D. Manaker, T. V. McEvilly, M. H. Murray (2000) Earthquake potential along the northern Hayward Fault, California, *Science,* **289**, 1178-1182.

Bürgmann, R., P. Segall, M. Lisowski, and J. Svarc (1997), Postseismic strain following the 1989 Loma Prieta earthquake from GPS and leveling measurements, J. Geophys. Res., 102, 4933-4955.

Clark, D. G., D. B. Slemmons, S. J. Caskey, and D. M. dePolo (1994). Seismotectonic framework of coastal central California, in Alterman, I. B., R. B. McMullen, L. S. Cluff, and D. B. Slemmons, eds., Seismotectonics of the Central California Coast Ranges: Boulder, Colorado, Geological Society of America Special Paper 292.

Dibblee, T. W. (1972), Preliminary geologic maps of three quadrangles, Santa Clara County, California, U. S. Geol. Surv. Open-File Report 72-90.

Dreger, D. S., L. Gee, P. Lombard, M. H. Murray, and B. Romanowicz (2005). Rapid finite-source analysis and near-fault strong ground motions: Application to the 2003 Mw 6.5 San Simeon and 2004 Mw 6.0 Parkfield earthquakes, *Seismol. Res. Lett., 76*, 40-48.

Dreger, D. S., and D. V. Helmberger (1993). Determination of source parameters at regional distances with three-component sparse network data, *J. Geophys. Res., 98*, 8107-8125.

Dreger, D. S., H. Tkalčić, and M. Johnston (2000). Dilational processes accompanying earthquakes in the Long Valley Caldera, *Science, 288*, 122-125.

Dreger, D. S., and B. Woods (2002). Regional distance seismic moment tensors of nuclear explosions, *Tectonophysics, 356*, 139-156.

Du, Y, and A. Aydin (1993), Stress transfer during three sequential moderate earthquakes along the central Calaveras fault, California, *J. Geophys. Res., 98*, 9947-9962.

Ellsworth, W. L., G. C. Beroza, B. R. Julian, F. Klein, A. J. Michael, D. H. Oppenheimer, S. G. Prejean, K. Richards-Dinger, S. L. Ross, D. P. Schaff, and F. Waldhauser (2000). Seismicity of the San Andreas Fault system in central California: Application of the double-difference location algorithm on a regional scale, *Eos Trans. AGU*, **81,** 919.

Ernst, W. G. (1971). Metamorphic zonations on presumably subducted lithospheric slabs from Japan, California, and the Alps, *Contributions to Mineralogy and Petrology*, **34**, 43-59.

Finke, j. C. and M. D. Zoback (2000). Structure-related and stress-induced shear-wave velocity anisotropy: Observations from Microearthquakes near the Calaveras Fault in Central California, *Bull. Seismol. Soc. Am.,* **90**, 1305-1312.

Foulger, G. R., B. R. Julian, D. P. Hill, A. M. Pitt, P. E. Malin, and E. Shalev (2004). Non-double-couple microearthquakes at Long Valley caldera, California, provide evidence for hydraulic fracturing, *J. Volcanol. Geothermal Res., 132*, 45-71.

Galehouse, J. S., and J. J. Lienkaemper (2003). Inferences drawn from two decades of alignment array measurements of creep on faults in the San Francisco bay region, *Bull. Seismol. Soc. Am.,* **93**, 2415-2433.

Guidarelli, M., A. Saraò, and G. F. Panza (2002). Surface wave tomography and seismic source studies at Campi Flegrei (Italy), *Phys. Earth Planet. Int., 134*, 157-173.

Gwyther, R. L., C. H. Thurber, M. T. Gladwin, and M. Mee (2000). Seismic and aseismic observations of the 12th August 1998 San Juan Bautista, California M5.3 earthquake, paper presented at 3rd San Andreas Fault Conference, Stanford Univ., Stanford, Calif.

Hauksson, E., D. Oppenheimer, and T. M. Brocher (2004). Imaging the source region of the 2003 San Simeon earthquake within the weak Franciscan subduction complex, central California, Geophys. Res. Lett., 31, L20607, doi:10.1029/2004GL021049.

Hearn, E. H., and R. Bürgmann (2005), The effect of elastic layering on inversions of GPS data for coseismic slip and resulting stress changes: Strike-slip earthquakes, *Bull. Seismol. Soc. Am., 95*, 1637-1653.

Hill, D. P., R. A. Bailey, and A. S. Ryall (1985). Active tectonic and magmatic processes beneath Long Valley caldera, eastern California: An overview, *J. Geophys. Res., 90*, 11,111-11,120.

Hill, D. P., J. O. Langbein, and S. Prejean (2003). Relations between seismicity and deformation during unrest in the Long Valley Caldera, California, from 1995 through 1999, *J. Volcanol. Geothermal Res., 127*, 175-193.

Hopson, C. A., J. M. Mattinson, and E. A. Pessagno (1981). Coast Range ophiolite, western California in Ernst, W. G., ed., The geotectonic development of California, 418-510.

Hough, S. E., R. S. Dollar, and P. Johnson (2000). The 1998 Earthquake Sequence South of Long Valley Caldera, California: Hints of Magmatic Involvement, *Bull. Seism. Soc. Am., 90*, 752-763.

Igarashi, T., T. Matsuzawa, and A. Hasegawa (2003). Repeating earthquakes and interplate aseismic slip in the northeastern Japan subduction zone, *J. Geophys. Res., 108*, **2249**, doi:10.1029/2002JB001920, 2003.

Irwin, W. P., and I. Barnes (1975). Effect of geologic structure and metamorphic fluids on seismic behavior of the San Andreas fault system in central and northern California, *Geology*, **3**, 713-716.

Johanson and Bürgmann (2005). Creep and quakes on the northern transition zone of the San Andreas fault from GPS and InSAR data, *Geophys. Res. Lett.*, **32**, L14306, doi:10.1029/2005GL023150.

Johnson, K. M., R. Bürgmann, and K. Larson (2006), Frictional properties on the San Andreas fault near Parkfield, California, inferred from models of afterslip following the 2004 earthquake, Bull. Seis. Soc. Am., 96, S321-S338.

Johnston, M. J. S., R. Gwyther, A. T. Linde, M. Gladwin, G. D. Myren, and R. J. Mueller (1996). Another slow earthquake on the San Andreas fault triggered by a M4.7 earthquake on April 19, 1996, *Eos Trans. AGU*, **77**, 515.

Julian, B. R., A. D. Miller, and G. R. Foulger (1998). Non-double-couple earthquakes, 2, Theory, *Rev. Geophys., 36*, 525-549.

Julian, B. R., and S. A. Sipkin (1985). Earthquake processes in the Long Valley Caldera area, California, *J. Geophys. Res., 90*, 11,155-11,169.

Kelson, K. I., W. R. Lettis, and M. Lisowski (1992). Distribution of geologic slip and creep along faults in the San Francisco Bay region, in Borchardt, Glenn, and others, eds., Proceedings of the Second Conference on Earthquake Hazards in the Eastern San Francisco Bay Area: California Department of Conservation, *Division of Mines and Geology Special Publication 113*, 31-38.

Kimura, H., K. Kasahara, T. Igarashi, and N. Hirata (2006). Repeating earthquake activities associated with the Philippine Sea plate subduction in the Kanto district, central Japan: A new plate configuration revealed by interplate aseismic slips, *Tectonophysics*, **417**, 101-118.

Langbein, J. O. (2003). Deformation of the Long Valley Caldera, California: Inferences From Measurements From 1988 to 2001, *J. Volcanol. Geothermal Res., 127*, 247-267.

Langbein, J., J. R. Murray, and H. A. Snyder (2006), Coseismic and initial postseismic deformation from the 2004 Parkfield, California, earthquake, observed by global positioning system, electronic distance meter, creepmeters, and borehole strainmeters, *Bull. Seis. Soc. Am., 96*, S304-S320.

Legrand, D., S. Kaneshima, and H. Kawakatsu (2000). Moment tensor analysis of near-field broadband waveforms observed at Aso Volcano, Japan, *J. Volcanol. Geothermal Res., 101*, 155-169.

Linde A. T., M. T. Gladwin, M. J. S. Johnston, R. L. Gwyther, and R. G. Bilham (1996). A slow earthquake sequence on the San Andreas fault, *Nature*, **383**, 65-68.

Lisowski, M., and W. H. Prescott (1981). Short-range distance measurements along the San Andreas fault system in central California, 1975 to 1979, *Bull. Seismol. Soc. Am.*, **71**, 1607-1624.

Manaker, D. M., R. Bürgmann, W. H. Prescott, and J. Langbein (2003). Distribution of interseismic slip rates and the potential for significant earthquakes on the Calaveras fault, central California, *J. Geophys. Res.*, **108**(B6), 2287,doi:10.1029/2002JB001749.

Marone C. J., C. H. Scholz, and R. Bilham (1991), On the mechanics of earthquake afterslip, *J. Geophys. Res., 96*, 8441-8452.

Massé, R. P. (1981). Review of seismic source models for underground nuclear explosions, *Bull. Seismol. Soc. Am., 71*, 1249-1268.

Matsuzawa, T, T. Igarashi, and A. Hasegawa (2002). Characteristic small-earthquake sequence off Sanriku, northeastern Honshu, Japan, *Geophys. Res. Lett.*, **29**(11), 1543, doi:10.1029/2001GL014632.

McLauglin, R. J., S. A. Kling, R. Z. Poore, K. McDougall, E. C. Beutner (1982). Post-middle Miocene accretion of Franciscan rocks, northwest California, *Geol. Soc. Am. Bull.*, **93**, 595-605.

Menke, W. (1989). Geophysical data analysis: discrete inverse theory, Academic Press, San Diego, Ca.

Minson, S. E., and D. S. Dreger (in prep.). Improved Full Moment Tensor Inversions, to be submitted to Geophys. J. Int..

Moore, D. E., and J. Byerlee (1992). Relationships between sliding behavior and internal geometry of laboratory fault zones and some creeping and locked strike-slip faults of California, *Tectonophysics*, **211,** 305-316.

Moore, D. E., D. A. Lockner, M. Shengli, R. Summers, and J. D. Byerlee (1997). Strengths of serpentinite gouges at elevated temperatures, J. Geophys. Res., 102, 14,787-14,801.

Nadeau, R. M., W. Foxall, and T. V. McEvilly (1995). Clustering and periodic recurrence of microearthquakes on the San Andreas fault at Parkfield, California, *Science*, **267**, 503-507.

Nadeau, R. M. and T. V. McEvilly (1999). Fault slip rates at depth from recurrence intervals of repeating microearthquakes, *Science,* **285**, 718-721.

Nadeau, R. M. and T. V. McEvilly (2004). Periodic pulsing of characteristic microearthquakes on the San Andreas fault, *Science*, **303**, 220-222.

Oppenheimer, D. H., W. H. Bakun, and A. G. Lindh (1990). Slip partitioning of the Calaveras fault, California, and prospects for future earthquakes, *J. Geophys. Res.*, **95**, 8483-8498.

Page, B. (1984), The Calaveras fault zone of California, an active plate boundary element, in Bennett, J. H and R. W. Sherburne, eds., *The 1984 Morgan Hill, California earthquake*, California Division of Mines and Geology Special Publication 68, 109-122.

Panning, M., D. Dreger, and H. Tkalčić (2001). Near-source velocity structure and isotropic moment tensors: a case study of the Long Valley Caldera, *Geophys. Res. Lett., 28*, 1815-1818.

Panza, G. F., and A. Saraò (2000). Monitoring volcanic and geothermal areas by full seismic moment tensor inversion: are non-double-couple components always artefacts of modeling?, *Geophys. J. Int., 143*, 353-364.

Platt, J. P. (1986). Dynamics of orogenic wedges and the uplift of high-pressure metamorphic rocks, *Geol. Soc. Am. Bull.*, **97**, 1037-1053.

Prejean, S. G. (2002a). The interaction of tectonic and magmatic processes in the Long Valley caldera, California, Ph.D. thesis, Stanford University, Stanford,California, 131 pp.

Prejean, S., W. Ellsworth, M. Zoback, and F. Waldhauser (2002b). Fault structure and kinematics of the Long Valley Caldera Region, California, revealed by high-accuracy earthquake hypocenters and focal mechanism stress inversions, *J. Geophys. Res., 107*, 2355, doi:10.1029/2001JB001168.

Prescott W. H., N. E. King, G. Guohua (1984), Preseismic, coseismic, and postseismic deformation associated with the 1984 Morgan Hill, California, earthquake, in Bennett, J. H and R. W. Sherburne, eds., *The 1984 Morgan Hill, California earthquake*, California Division of Mines and Geology Special Publication 68, 137-148.

Prescott W. H., M. Lisowski, and J. C. Savage (1981), Geodetic measurement of crustal deformation on the San Andreas, Hayward, and Calaveras faults near San Francisco, California, J. Geophys. Res., 86, 10,853-10,869.

Reinen, L. A., J. D. Weeks, and T. E. Tullis (1991). The frictional behavior of serpentinite: Implications for aseismic creep on shallow crustal faults, *Geophys. Res. Lett., 18*, 1921-1924.

Ring, U., and M. T. Brandon (1994). Kinematic data for the Coast Range fault and implications for exhumation of the Franciscan subduction complex, Geology, 22, 735-738.

Roeloffs, E. A. (2001). Creep rate changes at Parkfield, California, 1966-1999: seasonal, precipitation induced, and tectonic, *J. Geophys. Res.*, **106**, 16,525-16,547.

Roeloffs, E., M. Sneed, D. L. Galloway, M. L. Sorey, C. D. Farrar, J. F. Howle, and J. Hughes (2003). Water level changes induced by local and distant earthquakes at Long Valley Caldera, California, *J. Volcanol. Geothermal Res., 127*, 269-303.

Ryall, A. S., and F. D. Ryall (1984). Shallow magma bodies related to lithospheric extension in the western Great Basin, western Nevada and eastern California, *Earthquake Notes, 55*, 11-12.

Sammis C. G. and J. R. Rice (2001) Repeating earthquakes as low-stress-drop events at a border between locked and creeping fault patches, *Bull. Seismol. Soc. Am.*, **91**, 532-537.

Sanders, C. O., and L. D. Nixon (1995). S wave attenuation structure in Long Valley caldera, California from three-component S to P amplitude ratio data, *J. Geophys. Res., 100*, 12,395-12,404.

Saraò, A., G. F. Panza, E. Privitera, and O. Cocina (2001). Non-double-couple mechanisms in the seismicity preceding the 1991-1993 volcano eruption, *Geophys. J. Int., 145*, 319-335.

Savage, J. C., and M. M. Clark (1982). Magmatic resurgence in Long Valley caldera, California: possible cause of the 1980 Mammoth Lakes earthquakes, *Science, 271*, 531-533.

Schaff, D. P., G. C. Beroza, and B. E. Shaw (1998). Postseismic response of repeating aftershocks, *Geophys. Res. Lett.*, **25**, 4549-4552.

Schaff, D. P., G. H. R. Bokelmann, G. C. Beroza, F. Waldhauser, and W. L. Ellsworth (2002), High-resolution image of Calaveras Fault seismicity, *J. Geophys. Res., 107*(B9), 2186, doi:10.1029/2001JB000633.

Schmidt, D.A., R. Bürgmann, R. M. Nadeau, and M. d'Alessio (2005). Distribution of aseismic slip rate on the Hayward fault inferred from seismic and geodetic data, J. Geophys. Res., 110, B08406, doi:10.1029/2004JB003397.

Segall, P., and M. V. Mathews (1988), Displacement calculations from geodetic data and the testing of geophysical deformation models, *J. Geophys. Res., 93*, 14954-14966.

Sieh, K. E. (1984). Most recent eruptions of the Mono Craters, eastern California, *U.S. Geol. Survey Open-File Report 84-939, Proceedings of Workshop XIX: Active tectonic and magmatic processes beneath Long Valley Caldera, eastern California*, 96-129.

Šílený, J., P. Campus, and G. F. Panza (1996). Seismic moment tensor resolution by waveform inversion of a few local noisy records-I. Synthetic tests, *Geophys. J. Int., 126*, 605-619.

Simpson, R. W., S. S. Schulz, L. D. Dietz, and R. O. Burford (1988). The response of creeping parts of the San Andreas fault to earthquakes on nearby faults: Two examples, Pageoph., 126, 665-685.

Steck, L. K., and W. A. Prothero (1994). Crustal structure beneath Long Valley caldera from modeling of teleseismic P-wave polarizations and PS converted waves, *J. Geophys. Res., 99*, 6881-6898.

Templeton, D., R. Nadeau, and R. Bürgmann (2007, in review), Behavior of Repeating Earthquake Sequences in Central California and the Implications for Subsurface Fault Creep, *Bull. Seismol. Soc. Am*.

Uchida, N., T. Matsuzawa, A. Hasegawa, and T. Igarashi (2003). Interplate quasi-static slip off Sanriku, NE Japan, estimated from repeating earthquakes, *Geophys. Res. Lett.*, **30**, doi:10.1029/2003GL017452.

Uhrhammer, R., L. S. Gee, M. Murray, D. Dreger, and B. Romanowicz (1999). The

Mw5.1 San Juan Bautista, California earthquake of 12 August 1998, Seismol. Res.

Lett., 70, 10-18.

Vidale, J. E., W. L. Ellsworth, A. Cole, and C. Marone (1994). Variations in rupture

process with recurrence interval in a repeated small earthquake, *Nature*, **368**, 624-629.

Wallace, T.C. (1985). A reexamination of the moment tensor solutions of the 1980

Mammoth Lakes earthquakes, *J. Geophys. Res., 90*, 11,171-11,176.

Wallace, R. E., ed. (1990). The San Andreas fault system, California, *U. S. Geological

Survey Professional paper 1515*, 283p.

Working Group on California Earthquake Probabilities (WG99) (1999). Earthquake

probabilities in the San Francisco Bay region: 2000 to 2030-A summary of findings,

U. S. Geol. Surv. Open File Rep., 99-517, 36p.